Investigation of the effects of nonlinear soil-structure interaction for a jacket-founded offshore wind turbine

TU Delft Delft University of Technology

Martin Dirkzwager

SIEMENS Gamesa RENEWABLE ENERGY

Investigation of the effects of nonlinear soil-structure interaction for a jacket-founded offshore wind turbine

Author:

Martin Dirkzwager

Student number: 5420148

Committee Members:

Dr. Ir. Apostolos Tsouvalas	TU Delft - Chairman
Dr. Ir. Vagelis Kementzetzidis	TU Delft
Ir. Stavros Panagoulias	TU Delft - SGRE
Ir. Corine de Winter	SGRE
Ir. Valentijn van den Bosch	SGRE

TU Delft Delft University of Technology

SIEMENS Gamesa RENEWABLE ENERGY

Cover page background figure source: Lori Valigra - Spectrum News [1]

March 21, 2024

Abstract

Offshore wind energy is expanding rapidly as governments aim for net-zero emissions, with monopiles and jackets being the primary foundation methods for offshore wind turbines (OWTs). Supply chains, heavier turbines and deeper waters influence the efficiency of jacket foundations. This research considers a jacket-founded OWT. The development of OWTs has sparked its expansion to building sites with a proclivity to earthquakes. Such loading involves soil-structure interaction of which more needs to be known to improve accurate computational modelling.

Current practice of Siemens Gamesa Renewable Energy (SGRE) is to perform aeroelastic simulations in their computational tool BHawC. The Foundation Designer delivers a foundation Superelement to maintain secrecy. The equation of motion for the jacket foundation can then be solved linearly with a reduced amount of unknowns. However, prevalence of nonlinearity in soil raises the question to what degree a linear model adequately captures the response.

This study investigates the impact of soil nonlinearity on OWT dynamic behavior under seismic loads by comparing linear and nonlinear soil models. The analysis involves performing seismic simulations using multiple earthquakes. Another distinction is made through soil models with different characteristics. Nonlinearity is introduced to the soil stiffness and energy dissipation mechanism under cyclic loading. The investigated variations are a linear (elastic), geometrically nonlinear (nonlinear elastic) or both geometrically and physically nonlinear soil model (nonlinear plastic).

The numerical model consists of a Rotor Nacelle Assembly (RNA), tower, transition piece, jacket, piles and soil springs. Beam elements are used for the tower, jacket and piles. The transition piece is simulated by stiffening the top jacket braces. The RNA is modelled using a lumped mass with rotational inertia. It is vertically eccentric to the tower top and connected with a rigid link. The earthquake is applied uniform over depth and only horizontal movements are considered.

The findings underscore a difference in results between the linear and nonlinear models. The evaluated results from simulations consist of forces, displacements and dynamic characteristics of the structure. Also noted should be that the computational time of the linear model is significantly lower. The results found in models can differ greatly due to the loading spectrum with highly varying frequency peaks. Another factor is softening of the stiffness. The frequency domain of the elastic model results consists of narrow peaks at the system's natural frequencies. The peaks for the nonlinear elastic model are wider due to softening of the stiffness. For the structure used in this research, softening introduces coupled modes with greater displacements along the height of the structure. This makes it possible for the evaluated results to have higher values, even with less energy put into the system. The plastic models' peaks are of a width in between the elastic and nonlinear elastic model due to the combined use of isotropic hardening and nonlinear stiffness. When the model falls back on its initial stiffness upon unloading, the eigenfrequencies related to that stiffness become more pronounced. To match the occupancy of wider frequency peaks, loading and unloading should both happen nonlinearly. This can be achieved by using kinematic hardening instead of isotropic hardening. Plasticity generally reduces peak displacement and sectional moment values and nonlinear stiffness broadens the response frequency spectrum. Careful consideration of cyclic material behaviour, eigenfrequencies and loading characteristics are essential for a realistic model.

Acknowledgements

As I conclude my Master's Thesis, I am filled with anticipation as I near the completion of my studies at TU Delft's Faculty of Civil Engineering. It was a privilege to be able to complete my dream of getting a Masters degree. I could not have made a better decision than to take this route, it has changed my life. The two-year journey through the Structural Engineer master track has provided me with invaluable insights in structural engineering that will shape my future endeavors.

I am deeply grateful to my supervisors Apostolos Tsouvalas, Vagelis Kementzetzidis and Stavros Panagoulias for their guidance and scientific support throughout this journey. Their mentorship has been essential in overcoming academic challenges. I also want to extend my sincere appreciation to Corine de Winter and Valentijn van den Bosch from Siemens Gamesa Renewable Energy for their guidance and consistent support on the more practical side of my research. This greatly enriched my research experience and gave me new goals for skills I want to develop.

Lastly, I want to express my heartfelt gratitude to my family and close friends, who have been unwavering pillars of support, joy and distraction throughout this journey. Especially my mother and father who always believe in me, my friend Uri Peker who set an incredible academic example for me, my friend Carlo Salsbach who shared my ups and downs with me on the badminton court, my friend Khalil Akchikchi who always checked up on me and pushed me to never give up and many more talented, kind people who I wish only the best for.

Contents

List of Figures

List of Tables

Nomenclature

- SGRE: Siemens Gamesa Renewable Energy
- ULS: Ultimate Limit State
- FT: Fourier Transform
- IFT: Inverse Fourier Transform
- OWT: Offshore Wind Turbine
- RNA: Rotor Nacelle Assembly
- DoF: Degrees Of Freedom
- SSI: Soil-Structure Interaction

1 Introduction

1.1 Background information offshore wind

1.1.1 Wind industry

Wind energy is seen by many governments as an efficient tool to fulfill sustainable energy goals. After a period of subsidization for the development of the technology, independent economic viability has been achieved. This is made possible by the increase in the size of the wind turbines. Larger turbines increase the power output greatly and the installation time and material is relatively more efficient. The trend for offshore wind turbines is that they are still becoming larger. Countries all over the world are pursuing the use of wind energy. This leads to varying building sites with different design loads, geometry and soil characteristics.

1.1.2 Jacket foundations

The two most popular foundations of the offshore wind turbines include monopiles and jacket foundations. Monopiles are large diameter steel piles that are driven into the ground using high impact hammers. Jackets are steel frame structures which are usually fabricated on land by welding tubular sections together [2]. About 81% of all offshore foundations have a monopile foundation and 9% are jacket founded by 2019 [3]. Factors that determine the design choice between the two are the size of the turbine, the water depth, the supply chain. The jacket foundations are desirable for deeper water and larger wind turbines due to their stability and strength.

1.1.3 Involved parties

Siemens Gamesa Renewable Energy (SGRE) is a designer of the offshore wind turbine tower, blades and nacelle and works with load simulations of the entire structure. SGRE calculates/designs the structure using a reduced foundation model to be able to run the many simulations required with less computation time. The models used are an approximation due to nonlinearities in the soil that may not be accounted for. More knowledge about the soil-structure interaction mechanism may help to be able to predict the response of the structure more accurately. That is the reason for this research in collaboration with TU Delft. More questions have risen about accurately modelling the wind turbines. The offshore engineering department of the university has been occupied with such questions to partake in the development of the offshore wind sector.

1.1.4 Jacket founded offshore wind turbine structure

The structure in question consists of the following parts from top to bottom. The RNA (Rotor-Nacelle Assembly), where the nacelle has the components gearbox, generator, brakes, yaw actuators, etc. and the rotor has the components hub, blades, pitch actuators, etc.. Below is the tower, which consists of the cylindrical and conal sections with at times flanges for connections. Then there is a transition piece that connects the tower to the jacket. Both of these are constructed using steel tubular sections. The top of the jacket is supposed to rise above the water level and connects to piles at the sea bed. Jackets typically have three or four legs and braces are used to connect the legs.

1.2 Computational Modeling

Wind turbines are subjected to dynamic loads that are constantly present like wind and waves or less often present like earthquakes. The design life of the wind turbine is dependent on the amount of load cycles it is subjected to, because

this eventually results in fatigue and failure. The amplitude and the frequency of the loads matter, because they have a connection with those of the response of the structure.

Finite element methods are employed to solve the equations behind the motion numerically. Describing the structure with finite elements means to split it up into small parts that are called elements. Elements consist of two or more nodes that are connected in space. Depending on the knowledge that you want to gain, there is a choice to be made for the type of element. Based on the mathematical formulation, some elements account for axial deformation, while others also have displacements in other directions or rotations. There are many dimensions for which there are elements. Computationally the difference is the amount of degrees of freedom. A degree of freedom is a displacement or rotation of a node. The dimension of the elements has a great effect on the computational power required to solve the equation. To achieve accurate results there is a certain size of the elements that suits the demand. Building the model can be done using a program with a user interface to visualize the elements, but is not necessary to solve the equation and find the unknowns.

Offshore wind turbines are computationally modelled efficiently by means of simplifications and reductions. There are many choices to be made when modelling a structure that affect the run-time of simulations and the accuracy of the model. This is why in some cases the model is simplified or reduced to create an approximation of the larger model. SGRE uses BHawC to execute simulations [4]. This is done with aeroelastic calculations. A lot of analyses are done in time domain, because this gives insight into the behaviour of the system. Accurate computational modelling is important for the design life of the structure and the efficiency of the design of the parts.

To design jacket-founded offshore wind turbines (jacket-founded OWTs) there is the need for thousands of simulations of wind, wave and earthquake load combinations. To make this feasible it is necessary to have a model of the tower, jacket and ground that is as small as possible, but large enough to maintain a reasonably accurate and realistic response. One way to reduce the model is by means of a superelement formulation. This is only possible for linear model, because it is a summation of modes. Modes are the shapes in which a structure oscillates if it is loaded by a harmonic load at a specific frequency. It is possible to find the modes that are more dominant in the response of the structure by looking at the frequency content of the expected loading and comparing this with the frequency response function of the structure. One manner to reduce the model is with the Craig Bampton method which reduces the amount of degrees of freedom by multiplication with a transformation matrix which size depends on the amount of modes that are included. The degrees of freedom can decrease by tenfold from this reduction. It takes less effort to solve the equation of motion in this modal domain. Afterwards there is a transformation back to the time domain and the results are extrapolated to the degrees of freedom that were affected by the reduction before, leading to an approximation of the motion. Important for the research is the underlying thought that a linear model would be preferable to work with for SGRE in case the nonlinear SSI effects have to be approximated.

Due to the expansion of the offshore wind industry to earthquake prone regions, there is more need than ever to include the influence of the soil-structure interaction (SSI) to the response. The regions are also more likely to have deeper water depths, which is relevant for inclination towards jacket foundations. The more accurate modelling is desirable for being able to predict the structural integrity. Soil-structure interaction is a huge factor for the dynamic response of the structure to earthquakes. Thus the computational modelling of it is extremely important. The behaviour of soil is complex and can be modelled in many ways, some methods are more realistic than others. As the complexity increases it can become more computationally expensive. There are for example 3D models of solid brick elements

with many degrees of freedom and considerations of the fluids and water pore pressure. A way to simplify the soil is to use distributed springs along the pile called the spring-dashpot method [5]. In any case the first step towards a more realistic soil model is to use a nonlinear stiffness. Of second importance is the soil damping, which can be related to the materials' plasticity or radiation damping.

1.3 Thesis Outline

To guide the reader in this thesis paper an overview is given of each chapter according to the research plan structure.

Chapter one is the introduction to the thesis topic with the background information of the subjects that are recurrent in each chapter with the goal to indicate the challenges at hand and how it is executed in this research.

Chapter two contains the problem statement. The contents of this chapter evaluate the introduction and background information to find the problem to be addressed. The chapter formulates the main research question and is compartmentalized by subquestions with a description of their respective objective.

Chapter three contains the literature review. This chapter aims to touch upon the subjects that are essential to the research with the goal of giving an overview of the academic space and state of the art. The subjects are elected by following the subquestions from the problem statement chapter.

Chapter four contains the methodology. This chapter describes how the research is performed, for what reason the steps are taken and how it is verified. It describes the specific parts from the subjects discussed in the literature review chapter that are used and the reasoning behind it.

Chapter five contains the results. This chapter brings forward the results obtained from the execution of the research methodology. The observed results are put on display and the findings are evaluated.

Chapter six contains the conclusions. This discusses in short the used methodology and then elaborates the conclusions that can be made from the research. The outcome of the results are coupled to the research questions to see if the goal that was set out has been completed and what knowledge it has provided and what knowledge can be gained from it.

Chapter seven contains the recommendations. The shortcomings, alternative approaches and continuations of the research are laid out.

2 Problem Statement

As can be found in the introduction, the harnessing of offshore wind energy has emerged as a critical component of global efforts to transition towards cleaner energy sources. Offshore wind turbines (OWTs) are a vital component of this transition. Their structural design affects their performance and thus their efficiency. The more accurate the computational model resembles reality, the more reliable the design becomes. Soil-structure interaction (SSI) assumptions play a significant role in the accuracy of the response of the system found from simulations. Soil is a complex entity that can be modelled in many ways. Nonlinear soil models may be more desirable to use in order to find more accurate behaviour descriptions and design values for the loads on the structure. The influence of nonlinear soil models compared to linear models is unknown. To address this problem, this research aims to add to the knowledge about the influence of nonlinear soil models to the structure interaction in OWTs.

2.1 Research questions and objectives

In response to the problem statement, the main research question of this thesis is as follows:
"How can a jacket-founded OWT be modelled, taking into account the soil-structure interaction and what are the advantages of such a model compared to a linear reduced model?"

To answer the main research question, the research will be guided by a set of sub-questions with their respective objective:

Sub-question 1. What are the current approaches for modeling representative OWTs?
This sub-question seeks to create an overview of the existing methodologies and techniques that are used for the modeling of offshore wind turbines, highlighting the limitations and shortcomings of current practices.

Objective 1: Find a modeling method for an offshore wind turbine with nonlinear soil.
Identify a modelling approach that provides a realistic representative model with different soil-structure interaction variants and accurate results. Its characteristics shall be verified by comparing the built model to reference models.

Sub-question 2. How can a representative OWT be modeled with nonlinear soil?
Here, the focus will shift towards the computational modelling of an offshore wind turbine with the incorporation of nonlinear soil behavior. This aims to capture the dynamic and complex interactions of the OWT with surrounding soil.

Objective 2: Substantiate the modelling assumptions for the OWT model.
The modelling assumptions have to be brought forward, justified, tested and integrated. For the numerical model this includes the RNA, tower, transition piece, jacket, piles, and soil. For the analysis process, this includes boundary conditions, loading types, element types, and damping coefficients, meshing and solving the equation.

Sub-question 3. What is the difference in response between a jacket-founded OWT model with a linear and nonlinear soil model?
This sub-question will uncover the key distinctions in the response of the system. Relevant variables are evaluated for the different models. The behavior of linear and nonlinear soil-structure interaction models are compared to understand the effect of increasing the complexity of a model.

Objective 3: Evaluate simulation results and compare with previous models and expectations
Conduct simulations using the built model with variation in linear and nonlinear soil models. Analyze the output data and assess the impact of the soil-structure interaction design choice to the response of the structure and sought after variables.

3 Literature Review

Chapter 3 contains the literature review. This chapter aims to touch upon the subjects that are essential to the research with the goal of giving an overview of the academic space and state of the art. The subjects are elected by following the sub-questions from the problem statement chapter.

Sub-questions 1 and 2 bring forward the subjects: current modelling approaches and modelling a representative OWT with nonlinear soil. Much work has been done already in the scientific field regarding these subjects.

To elaborate the first subject of current modelling approaches, this chapter seeks to create an overview of the existing methodologies and techniques that are used for the modelling of offshore wind turbines. The limitations and shortcomings of current practices are highlighted. In order to elaborate the background of this question, the current practice of the offshore wind turbine modelling field is discussed. This considers modelling methods with its pros and cons for both the overarching methodology and modelling simplifications.

For the second subject, the focus shifts towards the computational modelling of an offshore wind turbine with the incorporation of nonlinear soil behavior. This aims to elaborate interactions of the OWT with surrounding soil under seismic loading conditions. The complexity of soil is discussed and the modelling possibilities and practices are elaborated.

Jacket-founded OWTs generally consist of the parts shown in Figure 1. The jacket can have three or four legs. The Rotor Nacelle Assembly (RNA) consists of the blades and the nacelle with its mechanisms.

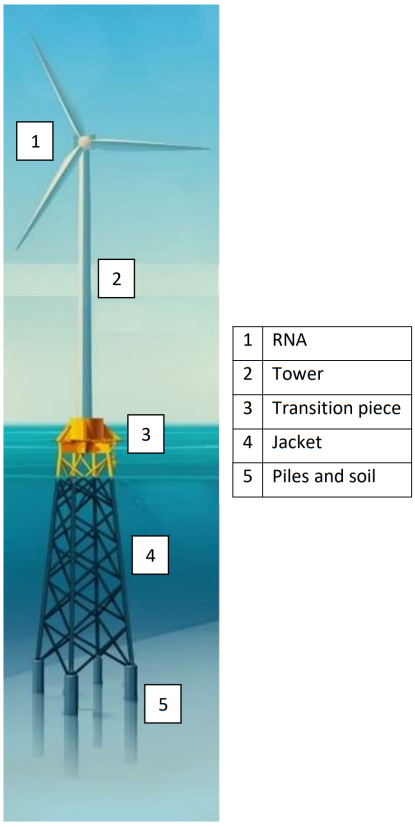

Figure 1: Jacket-founded OWT [6]

3.1 Modelling methods

Two types of modelling that are currently used can be considered for the purpose of finding design values and dynamic responses of the system due to earthquakes and other loads. There is the ”Fully integrated analysis approach” and the ”Superelement approach”. Since the first one is an extreme, variations on the spectrum of complexity can still yield desirable results by approximation. The Superelement method is not necessarily the design choice that has the most influence on the physics of the system. The structural models from the foundation designer contains a lot of degrees of freedom which increases the computational demand, so they are not used in the aero-elastic simulations directly [7]. To overcome this problem in the practical field the foundation model is reduced instead. There are different kinds of reduction strategies. In this research there is no aero-elastic simulation done as the scope is limited to earthquakes. To investigate the soil-structure interaction effects there is no need for a reduced model. However, there is a purpose for discussing the reduction methods. To be able to use the information of the nonlinear model, a linearization has to be done. The linear foundation model can be combined with the tower and used in the aero-elastic simulations. The computation of offshore wind turbines is preferably done in time domain, because the response of the system is interesting for the most dominant factor for the design life which is fatigue.

The OWT can be divised into two parts using the jacket-tower interface, which is standard due to the foundation designer and the tower designer working separately [8]. Above the interface is the superstructure and below is the substructure.

3.1.1 Fully integrated analysis approach

In a fully integrated approach the model as much of the physics is maintained as possible [9]. The description of such an analysis is all encompassing and considers the following aspects. The analysis is performed in the time domain. All the parts of offshore wind turbine with its geometrical configuration can be explicitly modelled. The RNA including the blades, tower, jacket piles are modelled with finite elements. The controller behaviour is also included. Then there is the soil as springs with damping characteristics that should be nonlinear if possible and the earthquake loading is depth-varying. Also wind and wave loads are included. In the fully integrated modelling approach the model is completely modelled in a 3D finite elements space, using a combination of 2D and 3D elements for the structure and the foundation. This type of analysis takes a significant amount of computational power and time, but can capture many complex physics that may be more realistic.

For seismic analysis, the ground motion can consist of depth-varying earthquake motion signals that come from site specific response analysis. These signals may vary significantly over depth depending on how far the jacket piles penetrate the soil [9], which is a more extensive method. The ground motion includes two horizontal directions and one vertical. It is possible to have a uniform ground motion over depth, in case the foundation is shallow. The depth-varying motion depends on the soil layer properties. They lead to more realistic soil-structure interaction results, because the motions are physically more accurate.

3.1.2 BHawC

SGRE uses an in-house software BHawC, which specializes in aeroelastic time-domain analysis for wind turbines [10]. It offers extensive capabilities for dynamic time-domain analysis under various environmental conditions like wind, waves and earthquakes. Despite its accuracy, BHawC entails a high computational demand, averaging around 30 minutes for a single seismic analysis calculation. In response, this study seeks to give insight about the influence of using linear soil models to the representativity of the computational model.

3.1.3 Superelement approach

The foundation comprises ground, tubular steel piles, and a steel jacket structure. In SGRE's load calculations [4] document which describes the load calculation process for complex foundations, the BHawC program plays an important role. The program is used to find the governing loads from all different operating regimes of the OWT. Due to the number of simulations, it is important to reduce the number of DoFs to manage the computational load. A typical number of DoFs for the BHawC model is 300-400. Employing the Superelement method reduces the equation of motion to fewer modes and nodes. The frequency ranges of interest determine the inclusion of which modes and specific modes can be added in case of spatially dependent forcing using modal truncation augmentation (MTA). The use of such reduction method assumes that parts of the model can be represented by a linear model. The study's significance for SGRE lies in validating the current use of linear foundation models and more importantly the foundation dynamics. Most of the knowledge on foundations lies on the side of the foundation designer. Collaboration with a foundation designer involves iterative adjustments to the foundation Superelement formulation to match the integral design instead of one with a reference tower.

Normal Superelement approach The normal superelement approach for the case of earthquakes considers a reduced foundation model with a single interface node at the tower-jacket interface. The response to seismic loads is included in the right hand side of the formulation when it is reduced. When creating the superelement the seismic load that is embedded can be an equivalent signal at the bottom of the substructure or along the embedded piles or it can be depth-varying along the piles [9].

The normal superelement approach is an approximation of the fully integrated model and reality. It is an approximation because there is a reduction of the model by taking part of the structure as linear and reducing its degrees of freedom to only include those that can capture the most dominant mode shapes. Therefore the response is not exact [11], but it has been proven to be good practice for engineering purposes.

Seismic Superelement approach The seismic superelement approach for the case of earthquakes includes the possibility to have many attachment nodes at the soil. These degrees of freedom can be used for the earthquake motion signature.

3.1.4 Superelement formulation

There are multiple methods for substructuring. For static or quasi-static problems the Guyan formulation can be used. The Craig-Bampton method also takes vibrational modes into account. This can be enriched by MTA (modal truncation augmentation) to take into account modes that are spatially load dependent. The most common superelement formulation that is used for dynamic problems is the Craig-Bampton one. The Craig-Bampton (CB) method is a technique used in structural dynamics and finite element analysis to reduce the degrees of freedom of a large structure by replacing a substructure with a superelement. This reduces computational costs while maintaining accuracy. They are used for linear systems.

The way these formulations work is to use a reduction matrix based on the amount of modes that will be included for the approximation of the response of the system.

Consider a structure divided into two parts: the master structure and the slave structure. The slave structure is the part of the system for which the reduced degrees of freedom are desired. The modes that are included consider a fixed interface. This creates the need for another formulation for the motion at the interface.

To model a superelement, the motions of a structural component can be formulated. Damping is not present here, but can be included through other means [11].

$$\boldsymbol{M}\ddot{\boldsymbol{u}}(t) + \boldsymbol{K}\boldsymbol{u}(t) = \boldsymbol{f}(t) \tag{1}$$

$$\begin{bmatrix} \boldsymbol{M}_{bb} & \boldsymbol{M}_{bi} \\ \boldsymbol{M}_{ib} & \boldsymbol{M}_{ii} \end{bmatrix} \begin{bmatrix} \ddot{\boldsymbol{u}}_b \\ \ddot{\boldsymbol{u}}_i \end{bmatrix} + \begin{bmatrix} \boldsymbol{K}_{bb} & \boldsymbol{K}_{bi} \\ \boldsymbol{K}_{ib} & \boldsymbol{K}_{ii} \end{bmatrix} \begin{bmatrix} \boldsymbol{u}_b \\ \boldsymbol{u}_i \end{bmatrix} = \begin{bmatrix} \boldsymbol{f}_b \\ \boldsymbol{f}_i \end{bmatrix} \tag{2}$$

The response of the system can be given by summation of a static and a dynamic part.

$$u_i = u_{i,\text{stat}} + u_{i,\text{dyn}} \tag{3}$$

The static part can be obtained from the assumption that there is no excitation on the internal DoF. That way $\boldsymbol{u}_i$ can be condensed into $\boldsymbol{u}_b$ to find the static constraint modes Ψ_C.

$$u_{i,\text{stat}} = -K_{ii}^{-1} K_{ib} u_b = \Psi_C u_b \tag{4}$$

Now the static response is described exactly for forces applied at the boundary DoF. The dynamic response can be approximated by looking at the internal vibration modes which can be found by fixing the boundary. An eigenvalue problem is solved with $\boldsymbol{u}_b = 0$.

$$(\boldsymbol{K}_{ii} - \omega_i^2 \boldsymbol{M}_{ii})\boldsymbol{\phi}_i = \boldsymbol{0} \tag{5}$$

The reduction happens here. A subset of the mode shapes $\boldsymbol{\Phi}_i$ which are mass normalized is retained.

$$\boldsymbol{\Phi}_i = \begin{bmatrix} \phi_{i,1} & \phi_{i,2} & \dots & \phi_{i,m} \end{bmatrix} \tag{6}$$

$$\boldsymbol{\Phi}_i^T \boldsymbol{M}_{ii} \boldsymbol{\Phi}_i = \boldsymbol{I} \tag{7}$$

$$\boldsymbol{\Phi}_i^T \boldsymbol{K}_{ii} \boldsymbol{\Phi}_i = \text{diag}(\omega_{i,1}^2, \dots, \omega_{i,m}^2) = \boldsymbol{\Omega}_i^2 \tag{8}$$

The total set of internal DoFs is then approximated by the exact static part and reduced vibrational part.

$$u_i = \Psi_C u_b + \Phi_i \eta_i \tag{9}$$

Here η_i are the internal node modal amplitudes. To find the Craig-Bampton reduction matrix, the equation can be put into the following format.

$$\begin{bmatrix} \boldsymbol{u}_b \\ \boldsymbol{u}_i \end{bmatrix} = \begin{bmatrix} \boldsymbol{u}_b \\ \Psi_C \boldsymbol{u}_b + \Phi_i \boldsymbol{\eta}_i \end{bmatrix} = \begin{bmatrix} \boldsymbol{I} & \boldsymbol{0} \\ \Psi_C & \Phi_i \end{bmatrix} \begin{bmatrix} \boldsymbol{u}_b \\ \boldsymbol{\eta}_i \end{bmatrix} = \boldsymbol{Rq} \tag{10}$$

Here:

- $\boldsymbol{u}_b$: Boundary DoF vector
- $\boldsymbol{u}_i$: Internal DoF vector
- $\boldsymbol{\Psi}_c$: Static constraint mode vector
- $\boldsymbol{\Phi}_i$: Selected internal vibration mode matrix
- $\boldsymbol{I}$: Identity matrix
- $\boldsymbol{\eta}_i$: Modal domain interior DoF vector
- $\boldsymbol{R}$: Craig-Bampton reduction matrix
- $\boldsymbol{q}$: Modal coordinate of the DoFs

The set of component DoFs are reduced to the modal coordinates by substitution into the original set of equations.

$$\boldsymbol{MR\ddot{q}} + \boldsymbol{KRq} = \boldsymbol{f} + \boldsymbol{r} \tag{11}$$

There is a residual force $\boldsymbol{r}$ represents the difference between the exact solution and the approximation. It can be eliminated by pre-multiplication.

$$\boldsymbol{R}^T\boldsymbol{MR\ddot{q}} + \boldsymbol{R}^T\boldsymbol{KRq} = \boldsymbol{R}^T\boldsymbol{f} \tag{12}$$

The reduced mass and stiffness matrix and force vector are then defined as follows.

$$\tilde{\boldsymbol{K}} = \boldsymbol{R}^T\boldsymbol{KR} \quad \tilde{\boldsymbol{M}} = \boldsymbol{R}^T\boldsymbol{MR} \quad \tilde{\boldsymbol{f}} = \boldsymbol{R}^T\boldsymbol{f} \tag{13}$$

When the modal DoFs $\boldsymbol{q}$ are found, the original DoFs $\boldsymbol{u}$ can be found through the previously mentioned relation of $\boldsymbol{u} = \boldsymbol{Rq}$.

The Craig-Bampton method is a powerful tool for reducing the complexity of large structural models, making them computationally more efficient while maintaining accuracy in dynamic analyses. Thanks to the retained interface nodes, the reduced matrix can easily be added to another set of equations that may represent another part of the structure.

3.2 Superstructure

The superstructure part of the OWT consists of everything above the transition piece. This comes down to the tower and the RNA. This is shown in figure 1 in section 3.

3.2.1 Tower

In the field of structural modelling for offshore wind turbine tower designs, various approaches are employed in research and in practice to capture the complex behaviour of these structures. The choice for the modelling method has impact on nonlinear behaviour and computational efficiency. Multiple methods are available do investigate these subjects.

Shotaro et al. [10] aims to create a simple calculation model that includes higher vibration modes for the blade-tower coupling effects. The goal is to develop a clustering strategy to optimize the design of the RNA and the support structure for monopile founded OWT farms under seismic conditions. Timoshenko beam elements are chosen for the tower to maintain applicability for a range of structural geometries and soil conditions. These effects may be interesting for further research with a more complex model.

Bouman et al. [12] explored a variety of modelling complexities for a prototype wind turbine steel tower. The goal of this research is to compare the load capacity and the dynamic behaviour for different refined finite element models and simplified models prescribed by building codes. The most extensive model is a 3D model FEM tower model with quadrilateral shell elements resulting in 69186 DoFs. This model is used for detecting local buckling or the influence of local geometrical anomalies. Another 3D model used consists of 1D beam elements resulting in 108 DoFs. Both models are used in a fixed-base analysis and including dynamic SSI effects. The two 3D models share the same eigenfrequencies, but since there is no shear in the beam elements, the torsional mode is not detected. When analysing more local failure modes in seismic analysis, such modelling approach proves to be useful.

Bouman et al. [13] analyzed a prototype steel wind turbine tower by subjecting it to static and seismic analysis. This helps achieve the goal of understanding the tower's response to various loading conditions. Two models are used for the analysis. The first model consists of a complete FE model of the tower and its foundation. The tower consists of 2D shell elements and the foundation is modelled using 3D brick elements. They are connected using unilateral contact elements which introduces the need for non-linear algorithms. The second model is a simplified model with 1D beam elements used for reliability and accuracy of the results obtained with the complete FE model. The similarity between the behaviour of the models shows that global behaviour does not necessarily require an extensive model.

In summary, two types of models are used between which there is a significant difference in computational requirement. Sophisticated FEM models may include knowledge about failure types like local or global buckling, nonlinear deformations and effects of local stiffening [14]. Sophisticated models of the tower can be created with shell or solid finite elements. However, analysis with such a model requires a lot of computational power. If the interest is not so much in the local behaviour a simplified model using beam elements can be adopted instead. The simplified model is shown to be similar to the sophisticated model when it comes to global dynamic behaviour.

3.2.2 RNA

Computational modelling choices for the Rotor Nacelle Assembly (RNA) for seismic analysis are lead by many parameters. Common considerations are done for the rotary inertia, blade flexibility and eccentricity and mass discretization can increase the complexity of the model and the accuracy to real physics. The choice can be made depending on the research goals.

Gentils et al. [15] tried to create a parametric model with multiple design constraints. The optimal foundation design takes into account vibrations, stress, deformation, buckling and fatigue. The goal of this research is to optimize the steel usage in the foundation. The RNA is modelled as a lumped mass with rotary inertia to capture the influence of the global dynamic behaviour of the superstructure to the local behaviour of the foundation.

Ali et al. [16] investigated the significance of the influence of higher modes and forces higher up in the tower. The goal is to enhance the accuracy of estimating failure probabilities under pulse-like ground motions. The RNA is modelled as a lumped mass with and without rotary inertia to demonstrate the difference. It is found that adding inertia has influence on the higher modes and leads to more accurate estimations of the forces in the structure.

Ali et al. [17] investigated the effects of rotary inertia of the blades and the rotor eccentricity on the nonlinear structural response and failure probably of OWTs. The goal is to examine how crucial the RNA numerical modelling is. Increased complexity in RNA modelling helps to examine the seismic fragility of OWTs due to the influence of the blades on their local modes and deformability. The rotor and the nacelle are modelled as masses eccentric to each other and to the tower yaw axis. The difference between the conventional rigid body lumped mass approach and refined turbine blade modelling differ most when rotational inertia is excluded and this can result in dangerous consequences.

De Sanctis et al. [18] compares the response of a monopile-founded OWT for different types of natural earthquakes. To capture the global response of the RNA, the Rotor is modelled separately from the Nacelle and both are eccentric to the tower yaw axis. They are modelled as lumped masses with the inertia of the blades added to the rotor mass.

Prowell et al. [19] compared the experimental and numerical seismic response of a physical wind turbine. The goal is to investigate the differences in the results between those of numerical models with different complexity and the experiment. The first model is a vertical column with a lumped mass at the top to represent the RNA. The second model explicitly represents the geometric configuration of the RNA with additional beam-column elements for the blades. The outcome of the comparison is that the first mode is similar for all models, but higher modes are different for the first model.

To conclude the overview, different levels of modelling are used to represent the RNA. The complexity increases from a lumped mass only approach [20], to a mass that is eccentric or with inertia [21] [18]. Adding inertia to the lumped mass adds value for dynamic response of higher tower bending modes [17] [19] and gives a better estimation of the loads in the structure. Instead of the lumped mass of the blades, they can also be explicitly modelled with beam elements for insight into the dynamic coupling with the tower. For the internal dynamics of the blades, shell elements can be used.

3.3 Substructure

The substructure considers the part of the structure below the tower. This comes down to the transition piece, jacket, piles and soil. This is shown in figure 1 in section 3.

3.3.1 Jacket

In the field of structural modelling for offshore jacket designs, various approaches are employed to capture the complex behaviour of these structures. Modelling choices are made to better fit the goal of the question at hand. The choice of modelling the elements plays a crucial role in giving insight to mass reduction, joint representation and dynamic analysis. Research for these objectives has been done using diverse modelling strategies.

Chew et al. [22] compared four-legged and three-legged jacket designs. The goal of this investigation is to look at mass reduction and weld joint optimization which can lead to more efficient jacket production. Beam elements are chosen for a computationally efficient representation of the structure that leads to the global stresses in the jacket elements that guide the optimization.

Argyriadis et al. [23] aimed to present the structural behaviour of an integrated analysis for an offshore wind turbine with a complex support structure. The goal of an integrated load analysis is to reveal the global elastic behaviour. Beam elements are used to ensure a balance between modelling precision and computational efficiency.

Dubois et al. [24] introduced a novel approach for modelling joints in jacket structures for dynamic analysis. The goal of this approach is to give insight to the influence of fatigue on structural response which can lead to lighter jacket structures or improved fatigue performance. To achieve this, local Superelements with Guyan reduction are used in combination with beam elements. The Superelements represent the joints while the beam elements represent the rest of the jacket geometry.

In summary, the state of art of the modelling of jackets is influenced by the questions at hand. The interest of the field is directed towards global dynamic behaviour, local fatigue and optimization for strength and production. Research with local interests like joints are more prone to use sub-models that increase the complexity of the computation [25]. Research with global interests lean heavily towards the use of beam elements.

3.3.2 Transition piece

In the study conducted by Lee et al. [26] the design of a transition piece is optimized for weight, fatigue life, buckling resistance, natural frequencies and most importantly stiffness. The research states that the main purpose of a transition piece is to be stiff to connect the tower and the jacket foundation. The piece is modelled as a box made out of beams when it comes to capturing global dynamic behaviour. This choice is made while the geometry is significantly more complex. This indicates that any model which has significant stiffness can suffice for global analysis.

3.3.3 Piles

Problems with the use of beam elements to represent piles in seismic analysis models only arise when the piles are not slender. Piles with a large diameter to depth ratio induce 3D soil effects which are difficult to capture with beam elements combined with only lateral soil springs [27]. Piles used in jacket OWTs are slender.

3.4 Soil

Soil is a material that has mechanical properties which can be found through laboratory and field testing for static and dynamic situations. In dynamic situations, soil properties are dependent on the strain level [28]. Soil shows a linear stiffness for very small strains and as the strain increases the stiffness decays. Larger strains result in the rearrangement of the soil particles, leading to looser soil, increased void ratios, and a weaker soil skeleton. This behaviour induces soil degradation and hydromechanical effects like pore pressure build-up during cyclic loading. The dynamic stiffness of soil is governed by the shear modulus, which is influenced by the confining pressure. The plasticity index of a soil is the numerical difference between its liquid limit and its plastic limit. It can be derived from the Atterberg limits, which are a basic measure of the critical water contents of a fine-grained soil. The relationship between plasticity index, shear modulus, and overconsolidation influences the soil's stiffness and damping characteristics. Higher plasticity correlates with a decreased shear modulus and increased damping ratio [29]. The overview of the strain levels with the cyclic behaviour of the stress-strain can be found in figure 2. The damping ratio depends on the strain level and the frequency of the loading, but the stiffness behaviour is more straight forward as can be seen in figure 3.

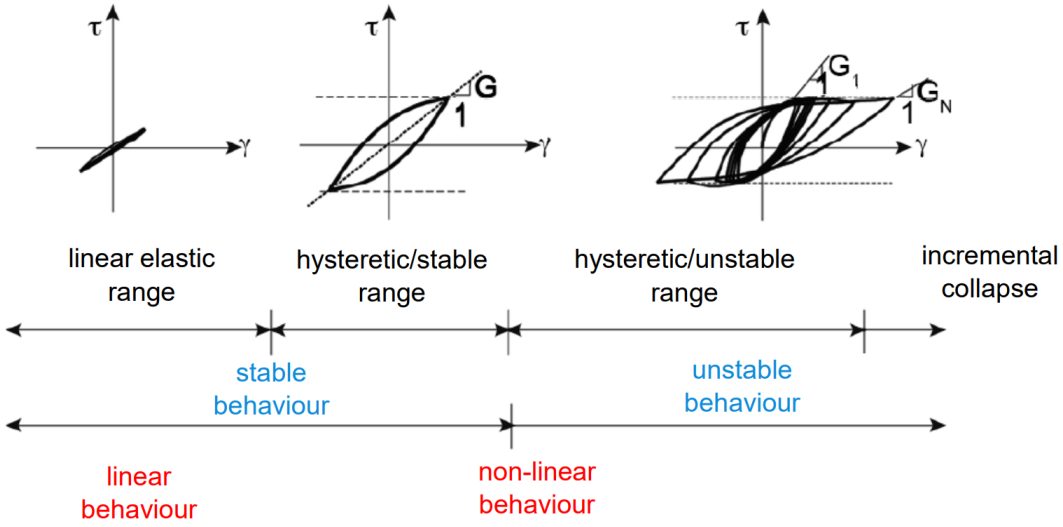

Figure 2: Soil strain characteristics [29]

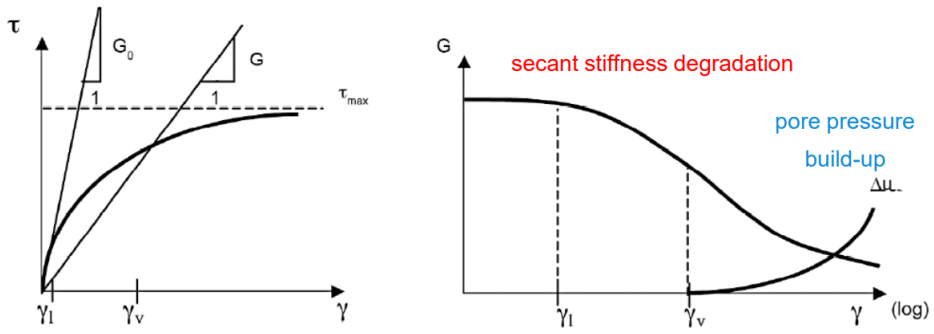

Figure 3: Soil strain characteristics [29]

The soil model complexity increases with the strain level. Depending on the load, the soil behaviour is different. The soil behaviour can be categorized by three strain levels. Stiffness and damping are the characteristics that govern the dynamic soil behaviour. For small strains, the soil can be represented in an idealized manner by a model with a single stiffness and a frequency dependent damping ratio. For small strains the frequency dependence can be found in figure 5, where it is noted at which frequency the Cyclic Torsional Shear (CTS) and Resonant Column (RC) test operate.

The behaviour of the stiffness and damping ratio with the idealized model for small strains can be found in figure 4. With the frequency dependence of the damping ratio shown in figure 5.

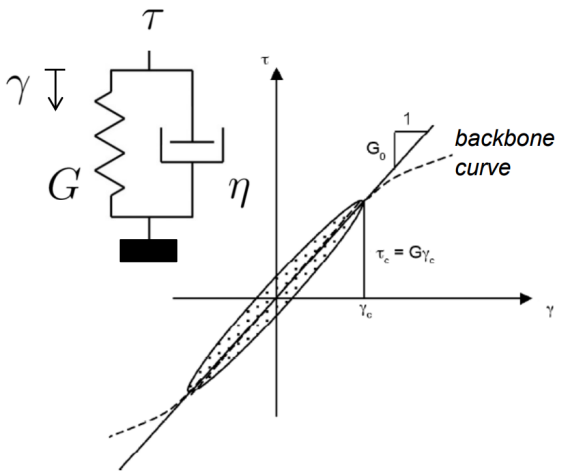

Figure 4: Small strain damping [29]

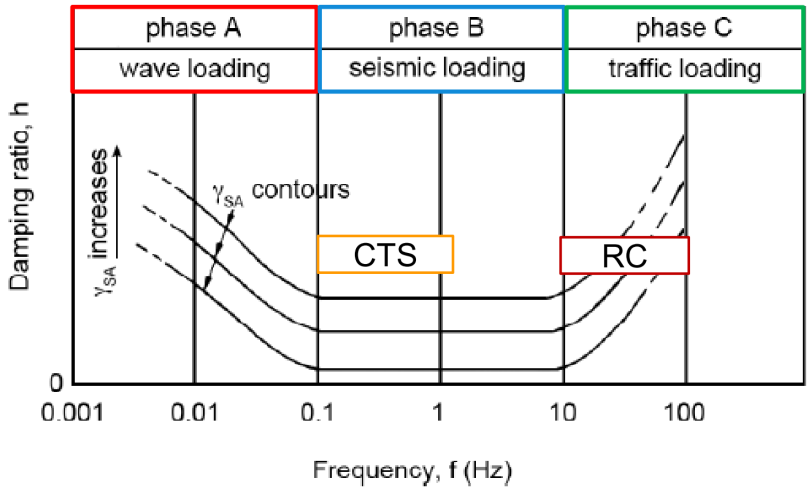

Figure 5: Small strain frequency dependence [29]

Fine grained soils (clay) and course grained soils (sand) properties depend on the confinement pressure, overconsolidation ratio (OCR) and plasticity index (PI). Tests for properties of medium strain cyclic loading are highly dependent on the confining pressure, but not so much on the void ratio.

Toyoura sand is a coarse-grained soil of which the properties have been tested under cyclic loading. The results of which can be found in figures 6 and 7.

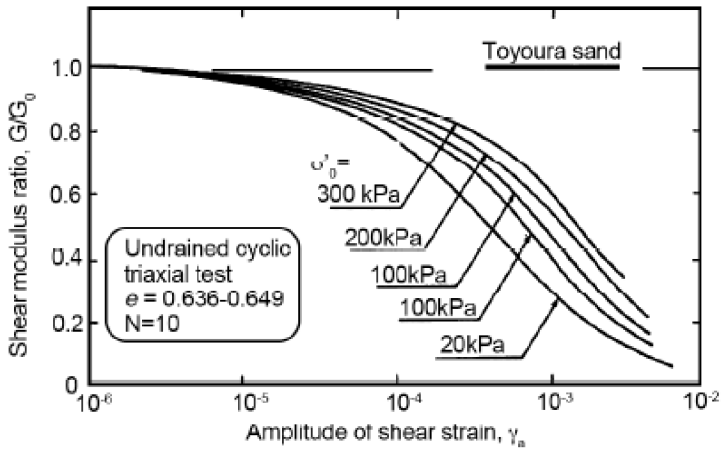

Figure 6: Medium strain hysteresis characteristics [29]

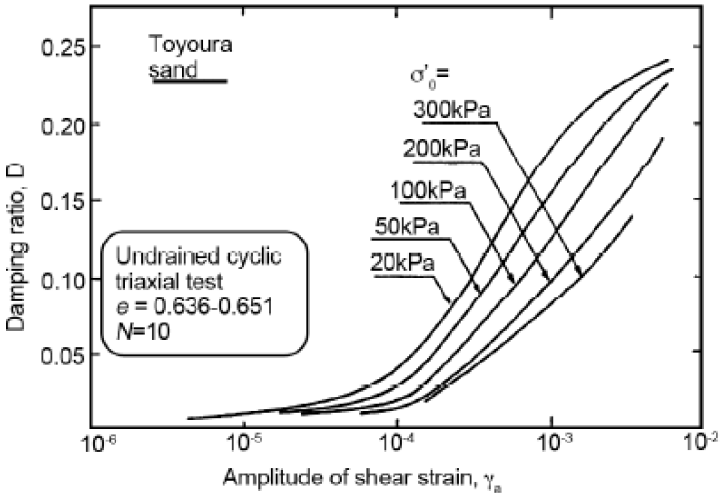

Figure 7: Medium strain characteristics [29]

The damping is dependent on the strain level and the frequency of the loading. The behaviour of the stiffness and the damping ratio can be found from the stress-strain diagram in figure 8.

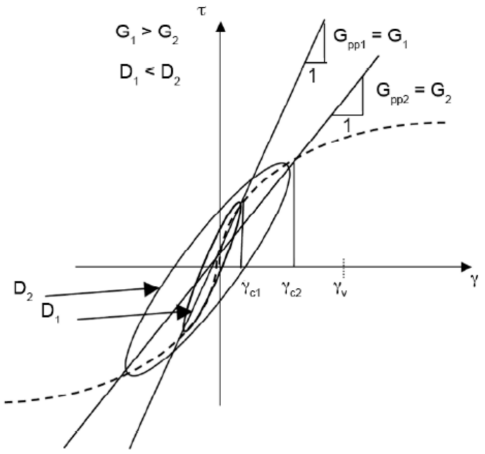

Figure 8: Medium strain hysteresis characteristics [29]

The behaviour changes for different strain levels, where the medium strain level is indicated in figure 9 between the two dotted lines. The modelling of the damping ratio with viscoelasticity is no longer valid and plasticity comes into play.

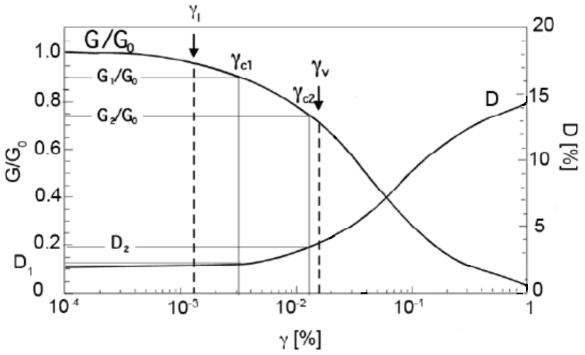

Figure 9: Medium strain characteristics [29]

For large strains there are hydromechanical effects like pore pressure build up and liquefaction. Failure modes occur due to the rearrangement of the soil particles and eventual loss of contact between the particles that form the soil skeleton. This mostly occurs for fine grained soils. These effects are left out of the scope.

To conclude, soil is strain level dependent. Both the damping ratio and stiffness are affected. Hydromechanical nonlinearities arise for high strain levels. For small strain levels an idealized linear model can be sufficiently accurate. Medium strain level models do better to include plasticity and soil stiffness nonlinearity. The soil dissipates energy by forming hysteresis loops. It is dependent on the type of soil which other nonlinearities affect the damping ratio and the stiffness. For course grained soils mostly the confinement pressure is important. For fine grained soils also the plasticity index and overconsolidation ratio have influence. Generally as the strain level increases, the damping ratio increases and the stiffness decreases.

3.5 Material Hardening

Soil plasticity can be modelled with different level of complexity. The inclusion of these effects is more realistic [30]. Three types of hardening can be distinguished with a different background for its cause and effects on the soil behaviour.

Volumetric Hardening

- Definition: Volumetric hardening refers to the change in the size or volume of the yield surface in stress space as a result of plastic deformation.
- Effect: Volumetric hardening influences the overall size of the yield surface, affecting the material's response to changes in hydrostatic stress or volume during plastic deformation.
- Cause: Volumetric hardening typically arises from changes in the material's bulk properties, such as density or volume, during plastic deformation.
- Example: Materials exhibiting volumetric hardening may undergo volumetric expansion or contraction as they deform plastically, leading to changes in the yield surface size in stress space.

Kinematic Hardening

- Definition: Kinematic hardening refers to the change in the shape or orientation of the yield surface in stress space as a result of plastic deformation.
- Effect: Kinematic hardening influences the shape or orientation of the yield surface, affecting the material's response to changes in the stress state or loading direction during plastic deformation.
- Cause: Kinematic hardening typically arises from changes in the material's internal structure or microstructure, such as dislocation accumulation or reorientation, during plastic deformation.
- Example: Materials exhibiting kinematic hardening may experience a translation or rotation of the yield surface in stress space as they deform plastically, leading to changes in the material's response to subsequent loading.

Isotropic Hardening

- Definition: Isotropic hardening refers to the uniform expansion or contraction of the yield surface in stress space around the current stress state as a result of plastic deformation.
- Effect: Isotropic hardening affects the overall size of the yield surface, similar to volumetric hardening, but without a direct correlation to changes in hydrostatic stress or volume.
- Cause: Isotropic hardening typically arises from changes in the material's yield stress with plastic deformation, leading to an increase or decrease in the size of the yield surface.
- Example: Materials exhibiting isotropic hardening may undergo a uniform expansion or contraction of the yield surface around the current stress state as they deform plastically, without significant changes in volume or internal structure.

In summary, while volumetric hardening is associated with changes in volume or bulk properties, kinematic hardening is related to changes in shape or orientation, and isotropic hardening involves uniform expansion or contraction of the yield surface. Each mechanism contributes to the material's response to plastic deformation under different loading conditions and influences its overall behavior.

3.6 Loads & Boundary conditions

3.6.1 Loads

Earthquake are non-periodic and have a wider frequency band [29]. The frequencies present in an earthquake signature are typically lower than 10Hz with the amount of cycles between 10-100. Representative earthquake signatures can be generated by statistical evaluation of previous measurements. Offshore wind turbines are also subjected to aerodynamic and hydrodynamic loads, which are not considered in this research. Also vertical accelerations related to buckling of the tower [31] are outside of the scope.

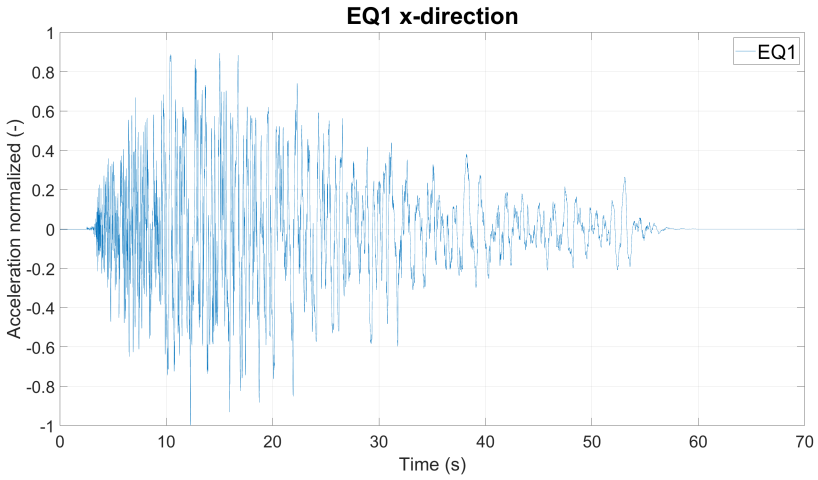

Figure 10: Earthquake 1 signature

3.7 Damping

Malekjafarian et al. reviewed foundation damping for monopile-founded OWTs [32]. An overview is given of all the sources of damping in an OWT. Each type of damping is defined, their significance to dynamic response is discussed. Each damping type has their modelling methods and challenges.

Structural Damping:

- **Definition:** Structural damping is the dissipation of energy along the structure when it vibrates, resulting from internal friction in the structural material or loose connections like bolted joints.
- **Contribution:** Damping values, as defined in standards for steel structures, are typically used. Values of damping ratio (ξ) as a percentage of critical damping range from 0.15% to 1.5%, depending on factors such as material type and structural configuration.
- **Modelling:** Structural damping is often modeled by applying the defined damping ratios from standards or recommended values for steel structures in numerical simulations.

Aerodynamic Damping:

- **Definition:** Aerodynamic damping occurs due to the interaction between the wind turbine and the air force acting on the structure.

- **Contribution:** Highly significant during operational conditions, contributing to the overall damping. However, during rotor-stop conditions, aerodynamic damping is negligible which may be problematic for fatigue as there is still wave loading.
- **Reported Values:** Researchers have reported values within the range of 4%–8% in the for-aft direction and 0.08%–1.43% in the side-side direction, depending on factors like wind speed, rotation speed, pitch angle, and yaw angle.
- **Modelling:** Analytical models are used to predict aerodynamic damping. These are often based on the interaction between the wind turbine and the airflow.

Hydrodynamic Damping:

- **Definition:** Hydrodynamic damping arises from water wave radiation and damping due to hydrodynamic drag.
- **Contribution:** The reported values vary between 0.07% and 0.23%, which is considerably lower than those of other damping sources.
- **Modelling:** Numerical simulations and hydrodynamic models are commonly used to capture the influence of wave radiation and drag on the structure.

Supplemental Damping:

- **Definition:** Supplemental damping is introduced to reduce dynamic responses and fatigue in the structure, often through the application of structural control techniques.
- **Example:** Tuned mass dampers may introduce a high amount of damping. For instance, a specific system presented introduces 1.36% damping for a particular offshore wind turbine.
- **Modelling:** Modelling methods for supplemental damping are relatively simple. They account for the mass and damping properties of the introduced dampers.

Foundation (Soil) Damping:

- **Definition:** Foundation damping includes contributions from radiation damping, pore-water dissipation (seepage) damping, and soil material damping (plasticity).
- **Importance:** Considered to have the second-largest contribution to the overall damping during operating conditions, after aerodynamic damping.
- **Challenges:** Soil material damping presents challenges in accurately determining damping ratios for monopiles.
- **Modelling:** Modelling of foundation damping often involves incorporating soil-structure interaction models and numerical methods to capture the dynamic response of the foundation under various loading conditions.

For the seismic analysis in this research, structural damping and numerical damping is applied to quantitatively simulate the behaviour found in reference models. Damping influences the behaviour of the model over time. The amount of free vibrations and the magnitude of those oscillations may be reduced. The maximum loads are influenced to a lesser extent. The research goal dictates the degree to which more careful consideration has to be done for the implementation of multiple damping mechanisms.

4 Methodology

The methodology for building the model is based on the findings in the literature review chapter and suited to the challenge brought forward in the problem statement. [Also the scope of the research is discussed in this chapter.]

The main body of this research is computational modelling. The goal is to build a realistic jacket-founded OWT FEM model with nonlinear soil. The simulations can be executed with this model and results can be evaluated to find the influence of SSI effects on the structural response. There is no model for a representative jacket-founded OWT to use as benchmark. That is why there are multiple models with climbing complexity. They shall be verified by comparing the results with external reference models of which unfortunately limited information is known.

It is explained how the models with all their parts which can be found in Figure 11 are built based on which theory with the considerations that come with it and verified that they work as desired. The jacket that is modelled has three legs.

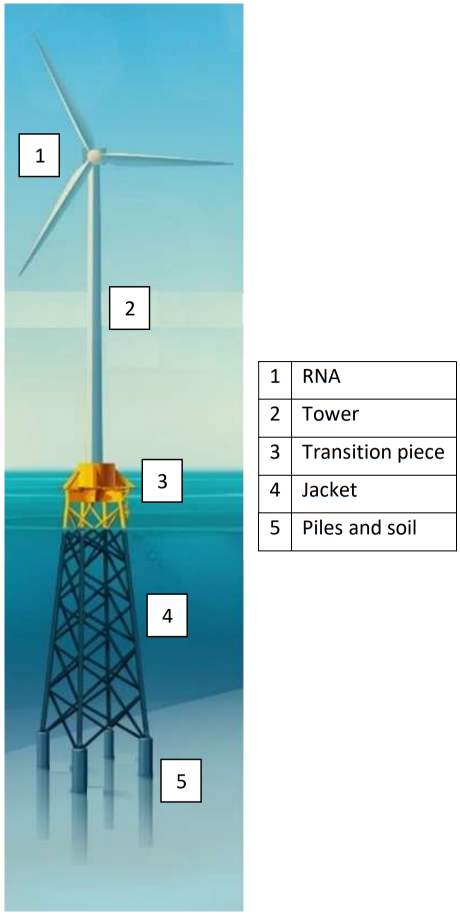

Figure 11: Parts of the structure [33]

4.1 Numerical modelling

This chapter describes all the computational modelling choices that have been made in order to model the OWT with the desired function.

In order to manifest a model that has the accessibility to the discussed calculation methods, a finite element program can be used. For this research Abaqus is used to obtain a solution to the equation of motion and to visualize the results. Abaqus is a finite element software developed by Dassault Systèmes. It is designed for among other things structural and nonlinear analysis for both static and dynamic problems. There is a user interface provided to create, analyze and visualize models.

The analysis that needs to be performed for this research can be done in three phases. Firstly a static simulation phase for the gravity that acts on the structure. The static equilibrium gives the initial conditions for any other loads that need to be considered. The other phases are related to the dynamics of the structure. One dynamic simulation phase calculates the eigenfrequencies and mode shapes of the unloaded and undeformed structure. The other simulation phase is a simulation of an earthquake in which the analysis captures the response of the system over time to a load with a time signature.

4.1.1 Analysis parameters

When performing a dynamic analysis, there are choices that can be made regarding the execution of the analysis [34]. The options come forth when an Explicit dynamic step is chosen.

The first choice is for the consideration of nonlinear geometry which is related to analyses where large displacements are expected to occur and influence the results. Nonlinear geometry is not taken into account, because relatively small displacements and no second order effect are expected to significantly influence the results.

The second choice is about the incrementation of the time step. The maximum number and the minimum time step size of increments can be controlled. The time step is automatically adjusted by Abaqus to ensure numerical stability. These parameters are chosen appropriately, because there is no specific interest in restricting computational time.

The third choice is about the matrix storage option. The matrix at hand are the stiffness and mass matrices. When these are symmetric, this is advantageous for the computational memory requirement. Abaqus is left to decide this choice for itself.

Then a solution technique has to be chosen. In order to find equilibrium at each time step for nonlinear problems, an iterative procedure is required. There are multiple popular iteration schemes. There are two variants available in Abaqus. There is the Modified Newton-Rhapson method which updates the stiffness only in the first iteration of the load increment and secondly the Full Newton-Rhapson method which updates the stiffness at every iteration of the load increment. Updating the stiffness by solving the matrix each iteration can be problematic for large finite element codes [35], but for the model in this research it is not a problem. The Full Newton-Rhapson method is used. Furthermore, to reach convergence there has to be an acceptable error set in order to not take up too much time with continuing iterations. The error should not influence the results significantly, but it may increase the speed of the calculation. Default convergence and solver tolerances are chosen.

The last choice that has to be made is for the time integration parameter. There is a parameter alpha, which relates to time integration parameters beta and gamma for both Newmark and HHT method. This parameter introduces numerical damping which is artificial. It is done in order to balance the numerical dissipation and stiffness which stabilizes the solution and controls oscillations. The default option for slight numerical damping is picked, which results in a value of $\alpha = -0.05$. It can also be performed without.

4.1.2 Equation of motion

In order to solve structural dynamics problems there is a typical equation that needs to be solved. The equation of motion, which describes the balance of external and internal forces.

$$\mathbf{M}\ddot{\mathbf{x}}(t) + \mathbf{C}\dot{\mathbf{x}}(t) + \mathbf{K}\mathbf{x}(t) = \mathbf{F}(t)$$

Where:
$\mathbf{M}$ is the mass matrix
$\mathbf{C}$ is the damping matrix
$\mathbf{K}$ is the stiffness matrix
$\mathbf{F}$ is the force vector
$\mathbf{x}(t)$ is the vector of unknowns

The vector of unknowns are the variables that are sought after when solving the equation. For example displacements or rotations of a certain node. For linear problems these variables are time dependent and the forcing can be too. The mass, damping and stiffness can be time dependent, but in that case the equation becomes nonlinear. To be time dependent means to change over time. This can happen thanks to constitutive relationships.

Depending on the type of forcing, there can be an analytical solution. In this case the integration can be performed analytically and the solution is exact. In the nonlinear case a numerical integration has to be performed. This is sensitive to the integration scheme and the time step size in order to find equilibrium in the formulated equation for each time step.

4.1.3 Element properties

The details about the finite elements and their computation are shown in table 1. The piles and the soil springs have certain overlap between the nodes. Connected parts of the structure share some nodes as well.

Model part	Elem type	DoFs (nodes x DoFs)	Interp. Scheme	Integration Scheme	Shape dimension	Topological dimension	Stress comps.	Shear deformation	Average size (m)	Total elements	Total nodes
Tower	Beam B31	6 (2x3)	Linear	1 point Gauss	1D	1D	Sxx	No	0.5	223	231
Jacket							Sxy		3.0	189	146
Piles									1.0	120	246
Soil springs elastic	Spring2	6 (2x3)	Linear		1D	1D	Sxx	No	1.0	246	492
Soil springs plastic	Truss T3D2	9 (3x3)	Linear	2 point Gauss	3D	2D	Sxx Sxy	No	1.0	246	492

Table 1: Element properties

4.2 Superstructure

The offshore wind turbine can be separated into two sections. The superstructure and the foundation. The superstructure includes everything above the jacket-tower interface. The foundation is everything below the interface and includes the soil.

4.2.1 Tower

The tower is likely the most realistically modelled part of the structure. The sections are connected rigidly due to the continuous use of elements. This is also the goal when constructing the tower. There is a design of the tower that is followed. The same tower as that of the reference project from SGRE is chosen. It is a tower that is designed for the largest latest turbine. The tower design does not specify the material characteristics. The density and elasticity are estimated and optimized to match the natural frequencies of the reference tower design.

In order to know if the model built is realistic and representative of a jacket-founded OWT, the systems properties are investigated. The eigenfrequencies of the system give indications about the expected response under certain loading conditions. For the linear system a transfer function can be found that connects the variables of displacement, velocity or acceleration to the response of a certain load at a certain point through the frequency response function which carries the amplitude for each frequency. For nonlinear systems this does not exist, because the response also depends on the displacement, velocity or acceleration at a certain time. However the output can be transformed to the frequency domain to be compared to the input loads frequency signature.

The representativity of the tower is verified by evaluating its properties as a free standing tower that is clamped at the bottom. The values are compared with reference jacket-founded OWTs from other jackets in the reference project.

4.2.2 RNA

The modelled RNA simulates the blades, rotor and nacelle. However, instead of attributing a geometry and discretizing the blades a simplified version of the RNA is adopted. The total mass of the components is combined into one mass and placed above the tower along its height axis at the level of the center of gravity of the RNA. In chapter 3.2.2 can be found that in seismic analysis it is common to simplify the RNA to a lumped mass and that adding inertia adds to the accuracy of the dynamic response. Only vertical eccentricity of the mass is considered. This distance is closed using elements with a very stiff material to simulate a rigid link. To simulate the response to accelerations and rotations of the blades an inertia is assigned for all three main rotational directions together with the mass. The inertia helps to approximate the correct eigenfrequencies of the system [19].

Not having elements for the blades makes it unable to get data of the response of the system at points along the blades. The dynamics of the blades in this model are unknown as well as the interaction of those dynamics with the rest of the system. This is done for the simplicity of the model and focus on global behaviour of the system and influence of soil-structure interaction for seismic analysis. The RNA is schematized as a lumped mass with inertia as can be found in Figure 16.

4.3 Superstructure verification

Firstly the superstructure comparison and evaluation. The structure in Figure 16 is considered and the tower is fixed at the bottom. Between the top of the tower and the RNA is a section modelled as a rigid link.

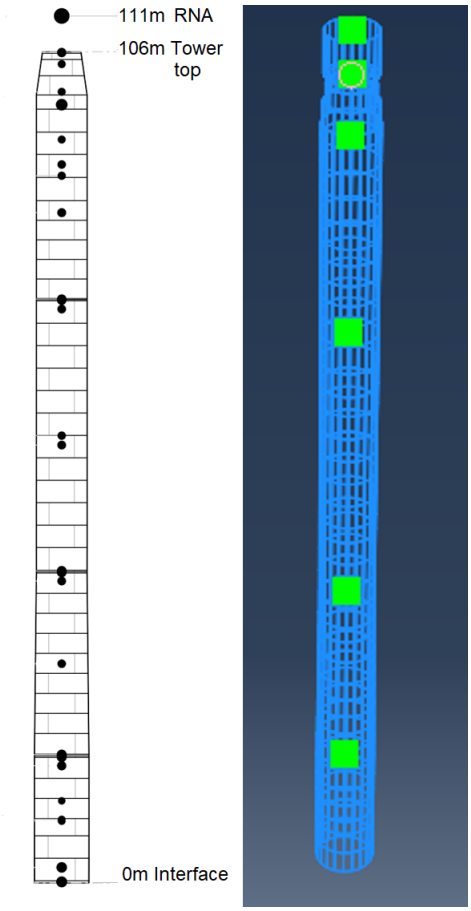

Figure 12: Superstructure only design

Figure 2 shows the eigenfrequencies for the built model and the difference compared to the reference model. In the final column can be found the difference between the eigenfrequencies of the models.

Tower only	Model eigen-frequency (Hz)	Difference with reference (%)
1st fore-aft	0.2291	3.5
1st side-side	0.2324	0.6
2nd fore-aft	1.6658	3
2nd side-side	1.3754	0.2
1st torsional	0.9291	1.4

Table 2: Eigenfrequencies tower reference comparison

4.4 Substructure

4.4.1 Jacket

The jacket design is based on a reference model of a DNV document which describes seismic analysis simulations with a 15MW wind turbine [36]. The jacket design is not optimized to the soil types considered or for the loads that are used. That is why it its properties are investigated by comparing different parts and combinations of the foundation and superstructure to reference projects. The dimensions of the jacket can be found in Figure 13. The jacket is three-legged and symmetrical, so only one face is shown.

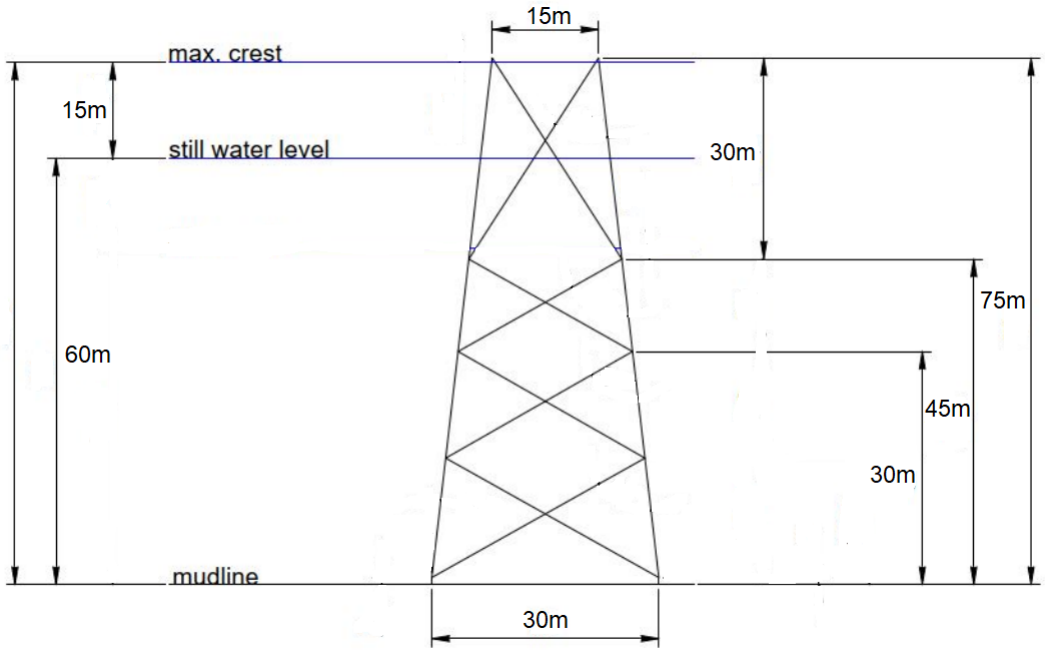

Figure 13: Jacket dimensions - Original [36]

4.4.2 Transition piece

As discussed in section 3.3.2 the goal of the transition piece is to add a rigid connection between the jacket and the tower [26]. It is not explicitly modelled. Instead it is simulated by increasing the stiffness of the sections on top of the jacket structure. The geometry of the braces on top of the jacket are increased in diameter. This is an essential modelling step to have the eigenfrequencies of the complete model match those of the reference models with the reference tower design. Additionally, a lumped mass equal to the transition piece mass is modelled at the jacket-tower interface.

4.4.3 Piles

The piles follow from the same as the jacket design. Important parameters are the embedment depth of 40 meter into the soil and the pile diameter of 3 meter using the same reference as the jacket model [36].

4.4.4 Soil

The soil model which is used consists of springs in two horizontal directions with a certain stiffness. The springs are distributed discretely over each meter of depth along the pile. P-y curves describe the force-displacement diagram of a soil spring. The p-y springs are based on certain characteristic soil parameters. The depth, shear modulus, effective unit weight, undrained shear strength, vertical restraint factor and the consolidation ratio ε_{50}. There are four soil models with differences in linearity and memory. In Table 3 can be found a description of each soil model.

Model	Nonlinearity	Stiffness input	Unloading	Reloading
A	Linear elastic	Equal to initial stiffness of the p-y curve	Always follows the initial stiffness of the p-y curve	Always follows the initial stiffness of the p-y curve
B	Nonlinear elastic	Equal to p-y curve	Always follows the p-y curve	Always follows the p-y curve
C	Nonlinear plastic	Partially equal to p-y curve	Follows initial stiffness of the p-y curve	Follows initial stiffness within previously set out envelope and resumes p-y curve stiffness outside of envelope
D	Nonlinear plastic	Only initially equal to p-y curve	Follows initial stiffness of the p-y curve	

Table 3: Characteristics soil models

To clarify the distinction between the models, the relation between the stiffness, unloading and reloading scheme is shown in Figure 15. The initial stiffness which is equal to that of Model A is indicated in all figures. For Model C and D, which include isotropic hardening plasticity, it is indicated how the hysteresis loop would evolve in two cycles. Model A is a linear elastic model. Model B is a model with nonlinear elastic model which follows the stiffness according to the p-y curves. Model C is a nonlinear plastic model and follows a different nonlinear stiffness to investigate the influence of more perfectly elastoplastic behaviour. Model D is supposedly the most realistic model with both nonlinear stiffness according to the p-y curves combined with isotropic hardening plasticity.

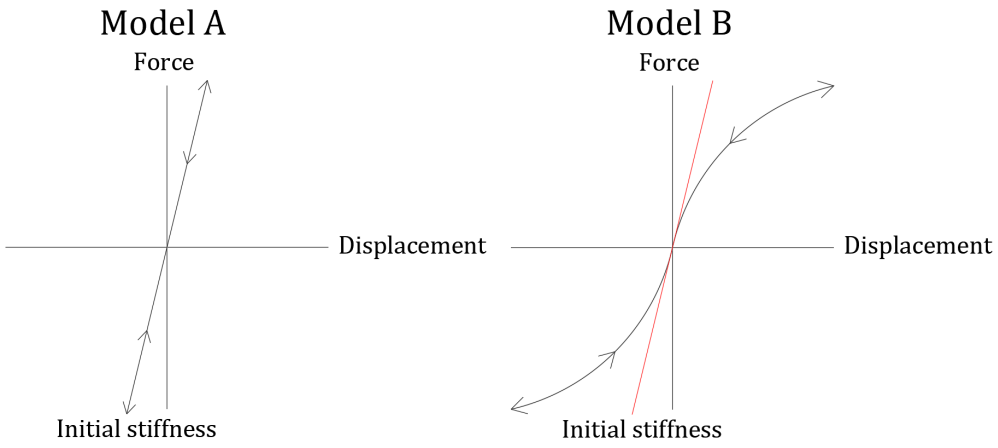

(a) Model A

(b) Model B

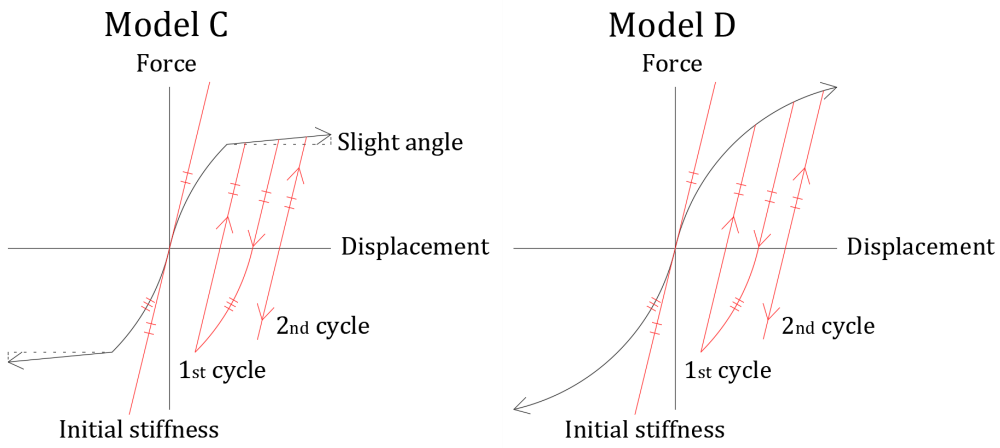

(a) Model C

(b) Model D

Figure 15: Different Soil Models A-D

4.5 Foundation verification

In the same way that the representativity of the tower design is verified, so can this be done for the foundation. The foundation by itself is analyzed with a fixed and free interface. The values are compared with reference jacket-founded OWTs from other jackets in the reference project. Not known about these projects are the parts of the foundation that concern the jacket design and the soil properties. The references are part of the same project, but they vary in jacket design and soil model of which the specifics are not known.

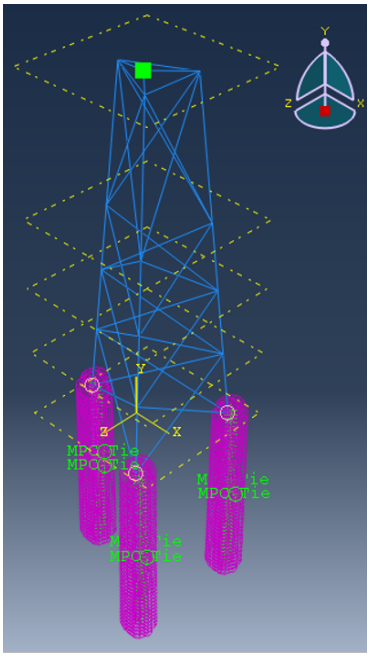

Figure 16: Foundation only design

Tables 4 and 5 shows the eigenfrequencies for the built model and the averaged eigenfrequencies of the reference models. The foundation is evaluated for a fixed and a free variation. This concerns the node at the interface between the jacket and the tower, indicated by the green square in figure 16. For the fixed variation all 6 DOFs of that node are fixed. In the free variation they are all free.

Free interface	Model eigen-frequency (Hz)	References average (Hz)	Difference with reference (%)
Mode nr. 1	1.1038	1.1062	0.2
2	1.2362	1.1065	11.7
3	2.6968	1.8260	47.7
4	3.619	2.6169	38.3
5	3.9348	2.6199	50.2
6	4.4373	3.6967	20.0
7	4.6861	3.7015	26.6
8	5.1112	4.1052	24.5
9	5.1311	4.1132	24.7
10	5.3377	4.4090	21.1

Table 4: Eigenfrequencies Free interface foundation reference

Fixed interface	Model eigen-frequency (Hz)	References average (Hz)	Difference with reference (%)
Mode nr. 1	3.5481	1.9147	85.3
2	3.8963	1.9258	102.3
3	4.2981	2.1868	96.6
4	4.5455	3.6743	23.7
5	5.0944	3.6787	38.5
6	5.1245	3.9481	29.8
7	5.1735	3.9612	30.6
8	5.4591	4.5840	19.1
9	6.2192	5.1530	20.7
10	6.3792	5.1836	23.1

Table 5: Eigenfrequencies Fixed interface foundation reference

The free eigenfrequencies are very similar to those of the reference models. The eigenfrequencies of the fixed model don't match as well. However, there can be seen a big jump in the eigenfrequencies between the reference model for both the fixed and free eigenfrequencies. It seems that the jump is larger for the built model. This can perhaps be explained by the ratio of the stiffness between the jacket and the soil. However, an exact pinpoint for the reason is not possible due to the unavailability of information about the reference models.

To check the structural safety of the design, the stresses in the jacket are analyzed for an earthquake that is leads to a representative ULS load. Stresses for most of the structure are within the elastic range of the material in case S355 is used. Some parts should be strengthened, but this is not expected to change the eigenfrequencies of the system much.

4.6 Soil springs verification

Another part of the model that should be investigated is the functionality of the soil springs to ensure the response is as desired and expected. The way to validate the soil springs is to look at a simple model. Three types of springs have to be validated, these are the elastic spring from Model A, nonlinear-elastic spring from Model B and plastic springs from Models C & D.

The springs from Abaqus themselves can be linear, where the only parameter required is the stiffness. They can also be nonlinear, in which case both the negative and the positive side of a Force-displacement curve have to be prescribed. They can freely move in the 3D space and give forces along the line with the nodes they are attached to or in the case of this research return forces only in one principal direction. The plastic springs have to be modelled using material plasticity [37]. Abaqus' "Engineering feature" springs are not suitable for this [38], so extension bars are used.

The curve of the p-y springs at mudline and at the bottom of the piles are defined in Figures 17 and 18. The curves are generated based on the API formulations for clay [39]. For this research, only part of the curve is effectively used. The effective curve is shown in Figure 35 for the reader to understand the type of effects that can be expected. The softening shown in Figures 17 and 18 does not occur in the analyses, because such displacement is not reached.

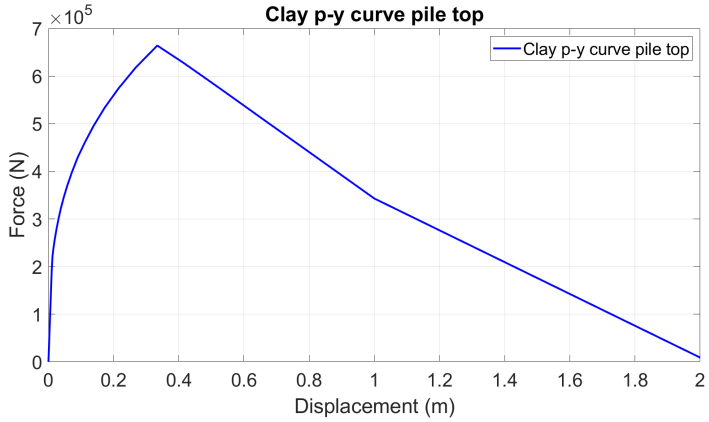

Figure 17: Clay p-y curve pile top

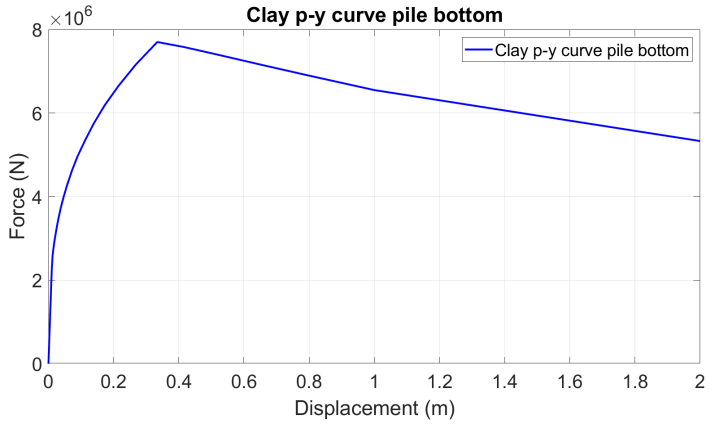

Figure 18: Clay p-y curve pile bottom

4.6.1 Model A elastic type spring

The linear-elastic spring from soil Model A can be verified using a dummy spring model shown in Figure 20 from the user interface in Abaqus. The purple entity is the spring which is specified to work only in x direction with the parameter and value $K = 1000$ for the stiffness. It is completely clamped at one side and loaded with a force dynamically on the other side. The force has an increasing amplitude over time.

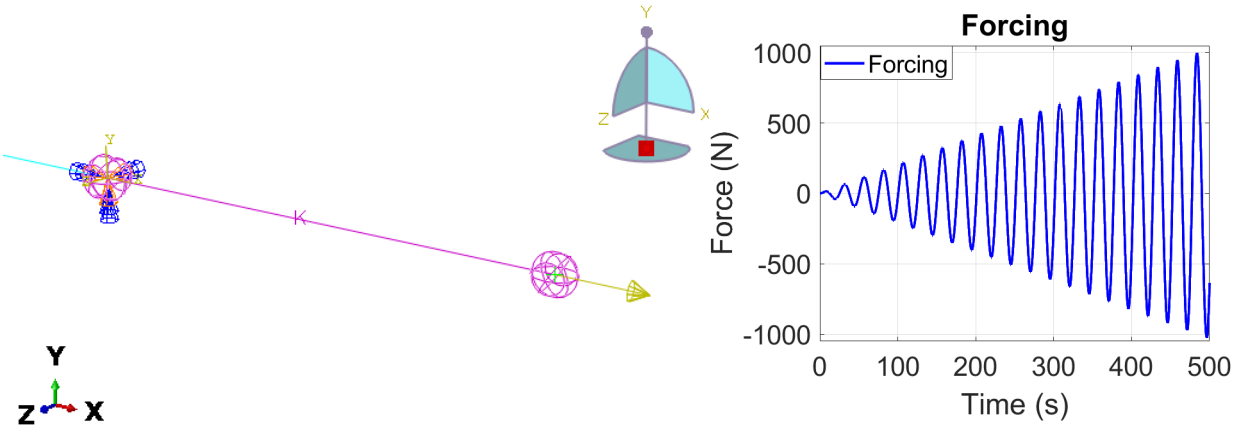

(a) Model A dummy spring

(b) Time dependent forcing amplitude

Figure 19: Model A dummy spring input

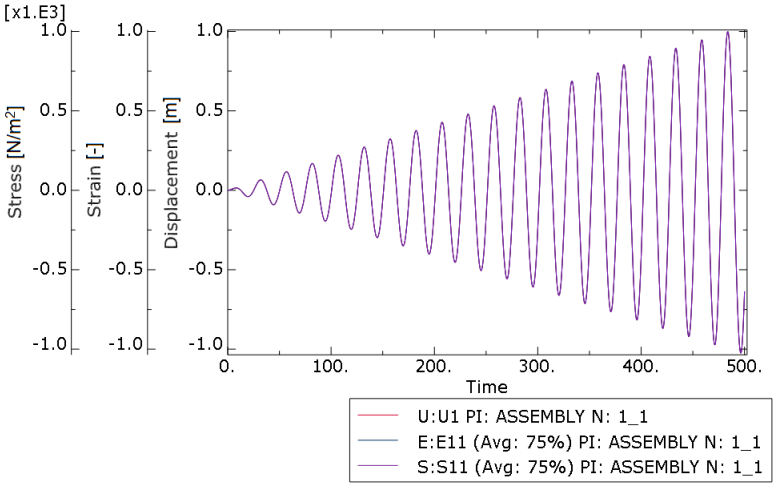

Figure 20: Model A spring results

In Figure 20 can be seen the way in which the stress $S : S11$, strain $E : E11$ and displacement $U : U1$ have a constant relationship. The similarity in these variables show the elasticity of the spring type used in Model A.

4.6.2 Model B nonlinear elastic type spring

The same output of springs used in Model A can also be shown for the Model B nonlinear-elastic type of springs. The Force-displacement relationship for a Model B type spring is prescribed for both the positive and negative displacements and is simplified in a dummy model to follow a bilinear path as found in Figure 21.

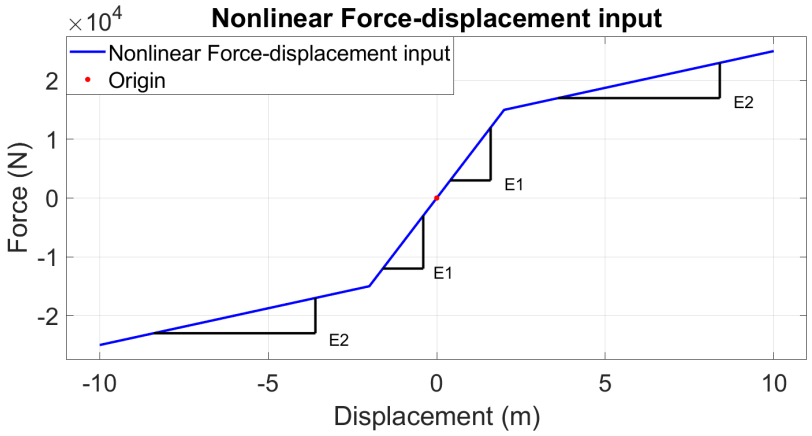

Figure 21: Model B Force-displacement

In the model used, two stiffness parameters can be recognized, $E1 = 7500N/m$ and $E2 = 1250N/m$. There is a kink at a positive and negative displacement of $2m$.

The results of testing the dummy nonlinear elastic spring are shown in Figure 22. The stress (force) can be found to be proportional to the prescribed force. The displacement and strain can be found to be proportional for the part where the force is still below the threshold of the initial branch of the force-displacement curve. After the threshold the displacement becomes larger quicker as the stiffness decreases for larger forces.

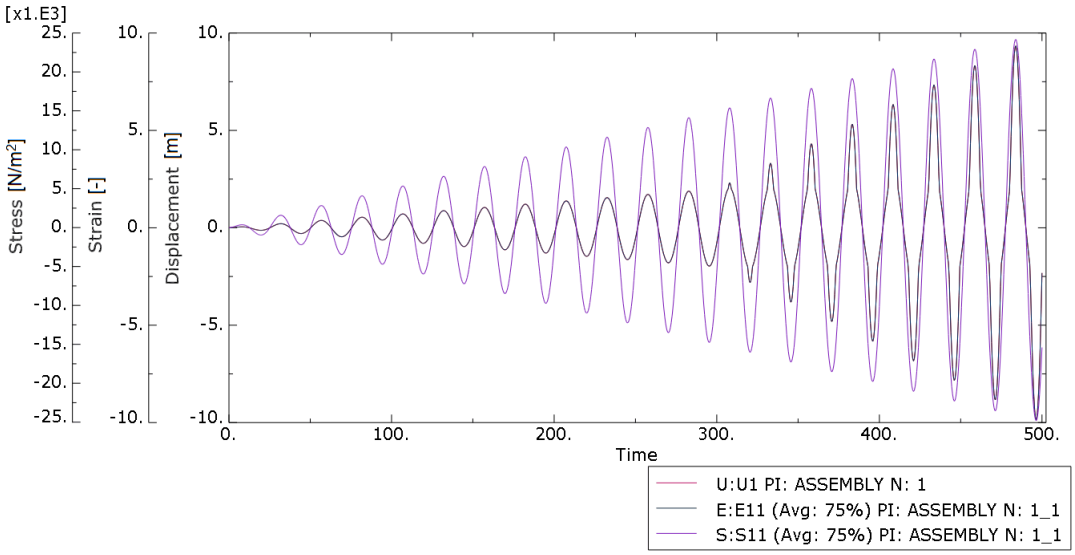

Figure 22: Model B spring results

4.6.3 Model C & D plastic type springs

Lastly the plastic springs used in Model C & D have to be validated. This is done with a dummy spring model subjected under a displacement controlled boundary with increasing amplitude over time. The spring is modelled using an extension bar that is restricted on one end and loaded at the other. The plasticity comes from the prescribed material properties.

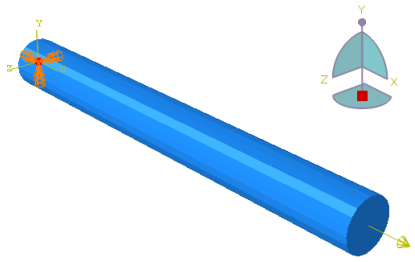

Figure 23: Model C & D springs

The loading and the material stress-strain relationship are described in Figures 24a and 24b.

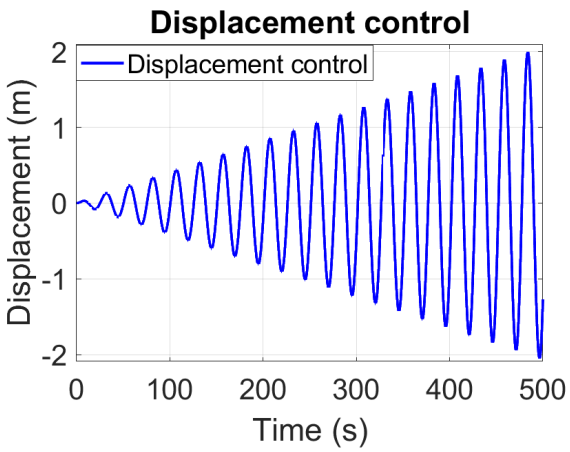

(a) Time dependent displacement control

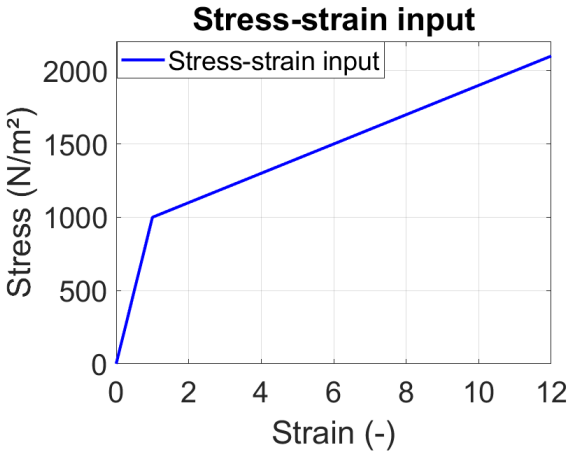

(b) Stress-strain relationship

Figure 24: Loading and material input plastic spring

The displacement control over time for the displacement (δ) shown in Figure 24a is given by equation 14.

$$\delta = 0.01 \cdot t \cdot \sin\left(0.25 \cdot t\right) \tag{14}$$

The input for Abaqus consists of the elastic and plastic stress-strain relationship as shown in Figure 24b. There is an elastic branch and a plastic branch to simulate isotropic hardening. The elastic limit is at a yield stress of $\sigma_y = 1000[MPa]$ after which the plastic branch starts. As plastic deformation occurs, the yield stress is updated. This mechanism counts for both positive and negative stress and strains. Unloading follows the initial elastic stiffness. Reloading follows the initial stiffness until the updated yield stress σ_y' is reached and then continues along the plastic branch to the next yield stress.

The isotropic hardening model describes the behavior of materials subjected to normal stresses, incorporating the effects of plastic deformation and hardening. The model consists of the following equations using the theory from [40]:

Yield Criterion The yield function is defined based on the normal stress (σ) and the yield stress (σ_y). As a side note the density of $5[kg/m^3]$ is used to avoid dynamic behaviour:

$$f(\sigma) = |\sigma - \sigma_y| - H \cdot |\varepsilon^p| \tag{15}$$

Where:

- $f(\sigma)$ is the yield function,
- σ is the normal stress,
- σ_y is the yield stress, starting at $1000[MPa]$
- H is the hardening modulus equal to $100[MPa]$
- ε^p is the plastic strain, starting at $\varepsilon = 1[-]$

Flow Rule The plastic strain increment ($\Delta\varepsilon^p$) is related to the stress increment ($\Delta\sigma$) through the isotropic hardening modulus (H):

$$\Delta\varepsilon^p = \frac{\Delta\sigma}{H} \tag{16}$$

This equation indicates that the plastic strain increment is directly proportional to the stress increment.

Isotropic Hardening The yield stress updates based on the accumulated plastic strain. It increases linearly with plastic strain:

$$\sigma_y' = \sigma_y + H \cdot |\varepsilon^p| \tag{17}$$

Stress-Strain Relationship The stress-strain relationship during plastic deformation can be obtained by integrating the flow rule and the isotropic hardening rule along the loading path. During unloading, the material follows the initial stiffness until it reaches the updated yield stress level. The unloading behavior is characterized by the material returning elastically to the yield surface corresponding to the updated yield stress. Upon reloading, the material follows a new loading path determined by the updated yield surface and the accumulated plastic strain.

Equations 15-17 collectively describe the behavior of materials undergoing isotropic hardening, capturing both the initial stiffness for unloading and the subsequent increase in yield stress with plastic deformation.

In Figure 25 can be found the manner of which the plasticity is activated in the soil springs for Model C & D. The plastic material behaviour is best shown in Figure 26 for Force-displacement .

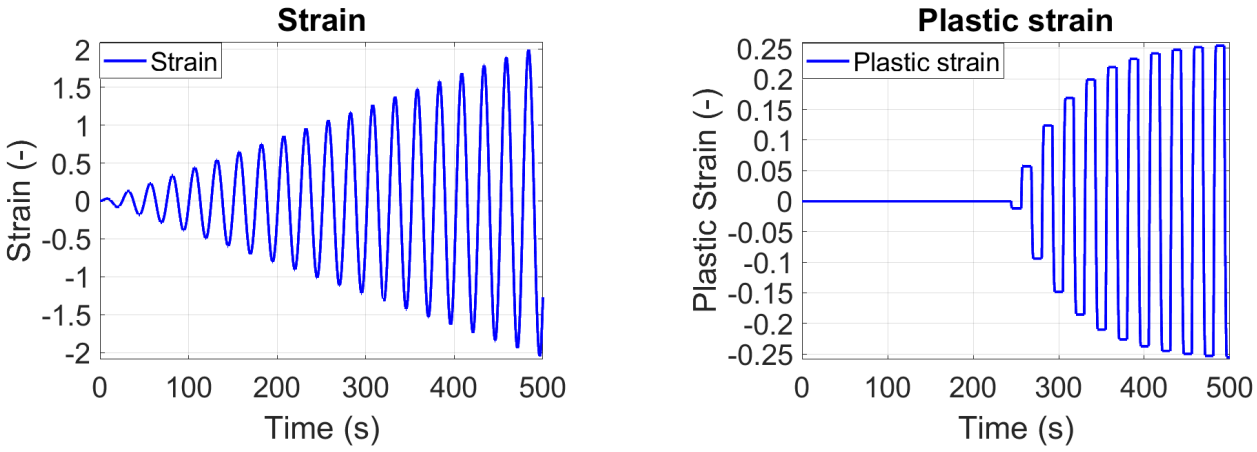

(a) Strain

(b) Plastic strain

Figure 25: Force and plastic strain of plastic spring

The expected behaviour is that the material reacts elastically until the plastic threshold is met. After this threshold, the force and displacement are no longer explicitly coupled. The maximum reaction force flattens through the stress-strain relationship and plateaus can be seen in the force graph. Because the force keeps increasing the plateaus become larger, but this is only because the stress-strain relationship is bi-linear and not perfectly plastic.

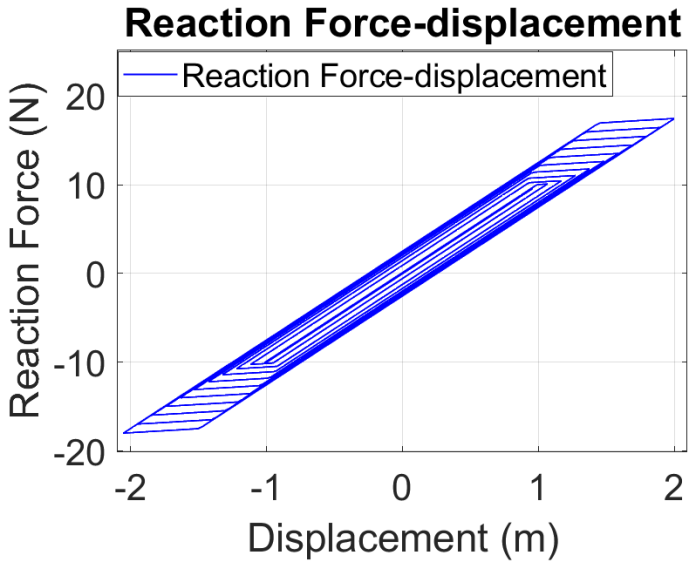

Figure 26: Force-displacement of plastic spring

When plasticity is reached the displacement keeps steadily increasing. The plastic strain increase becomes less, because the resistance is higher. More work is done with less additional . If the forcing were to continue an amplitude equal or lower than before, it would only result in elastic movement. This is the desired behaviour for the plastic soil model used in this research. Previously deformed soil will give less resistance to lower forcing and always plasticises more if the force goes past the previous maximum.

4.6.4 Complete model soil springs application

Now the springs can be applied to the complete model to test them with a complete simulation of an earthquake loading. The output is taken from a spring at the interface between the pile and the jacket leg (mudline) in x-direction. An earthquake acceleration load is applied on the soil-side node.

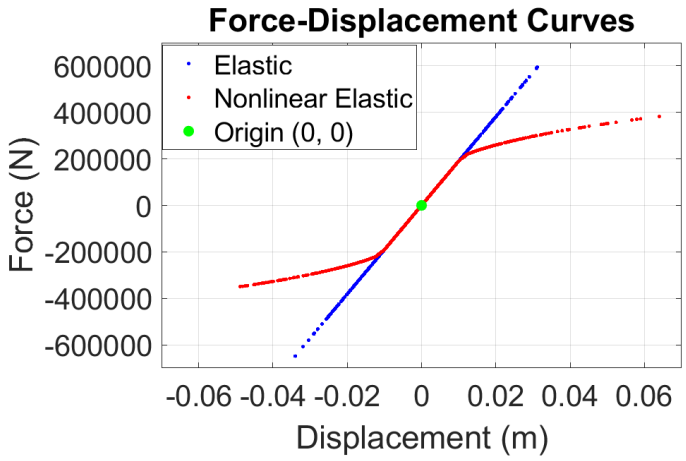

Figure 27: Model A & B Force-displacement output

To show how the soil-structure interaction develops over time, the force can be plotted against the displacement for each of the soil models. In Figure 27 are shown the results for Model A & B. Model A has one single stiffness for a specific spring and Model B has a decaying stiffness for higher displacements.

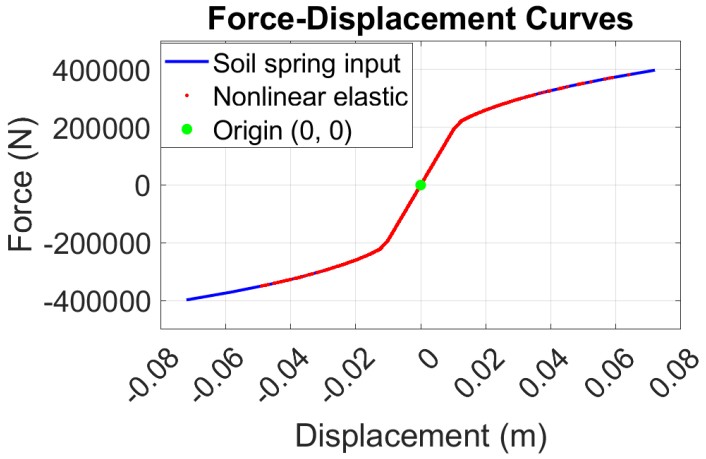

Figure 28: Input vs Nonlinear-elastic Force-displacement

The output can be compared to the input to verify the models. Part of the nonlinear input together with the output is shown in Figure 28. It can be seen that the stiffness is followed properly.

The results for Model C and Model D are shown in Figures 29 and 30 respectively.

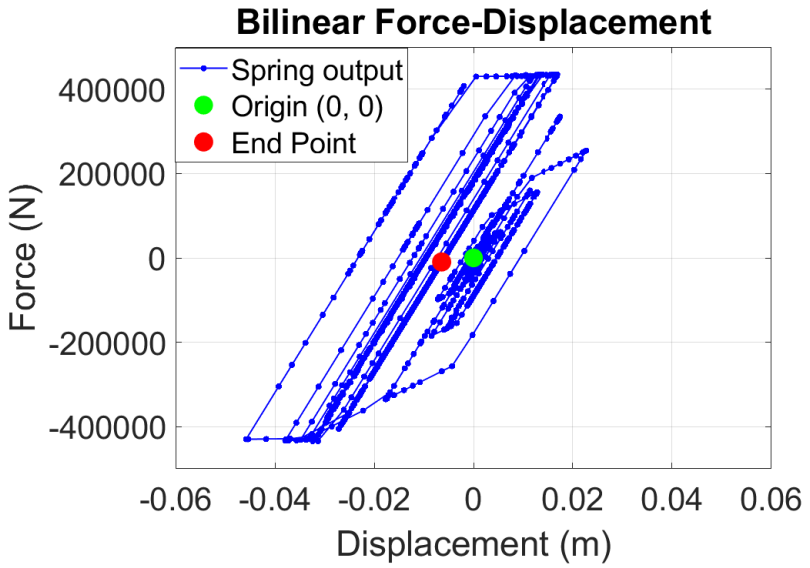

Figure 29: Model C Force vs Displacement

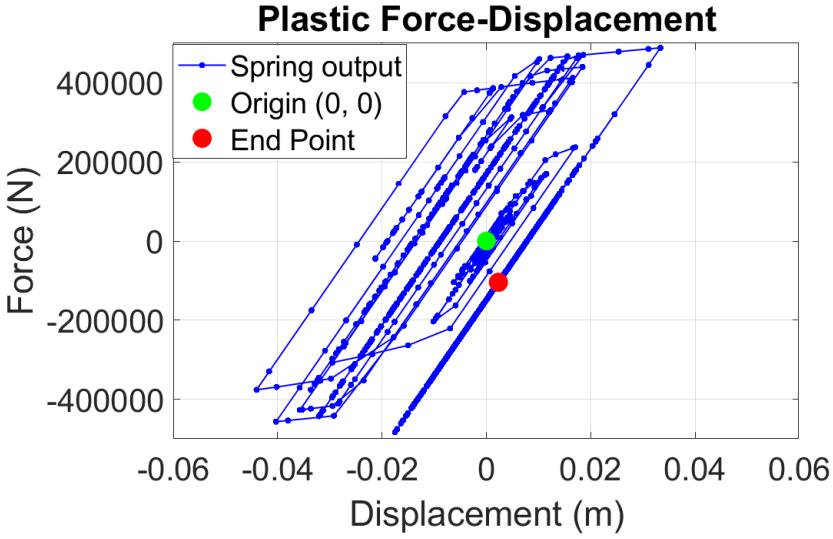

Figure 30: Model D Force vs Displacement

The results for Models C & D both show hysteresis loops. This indicates the dissipation of energy. However, energy is only dissipated whenever plasticity is activated thanks to isotropic hardening. After reaching the maximum displacement during a simulation, the soil won't plastify further and thus does not dissipate energy anymore for the oscillations that occur afterwards. The density of the data on the same line as the final point depicted as a red dot in Figure 30 of Model D shows that this has been in an elastic range for about the second half of the response.

4.6.5 Simulation example

The results of one of the simulations for a specific node at mudline is used to show the the behaviour between the force and the displacement in the spring. At mudline is where most of the nonlinearity is activated in the soil. The displacement here stands for the elongation of the extension bar or spring element. There is a force-displacement graph for each of the analyses with distinct characteristics. Figures 31 and 32 show the elastic and nonlinear-elastic evolution of the force and elongation in the spring during the analysis.

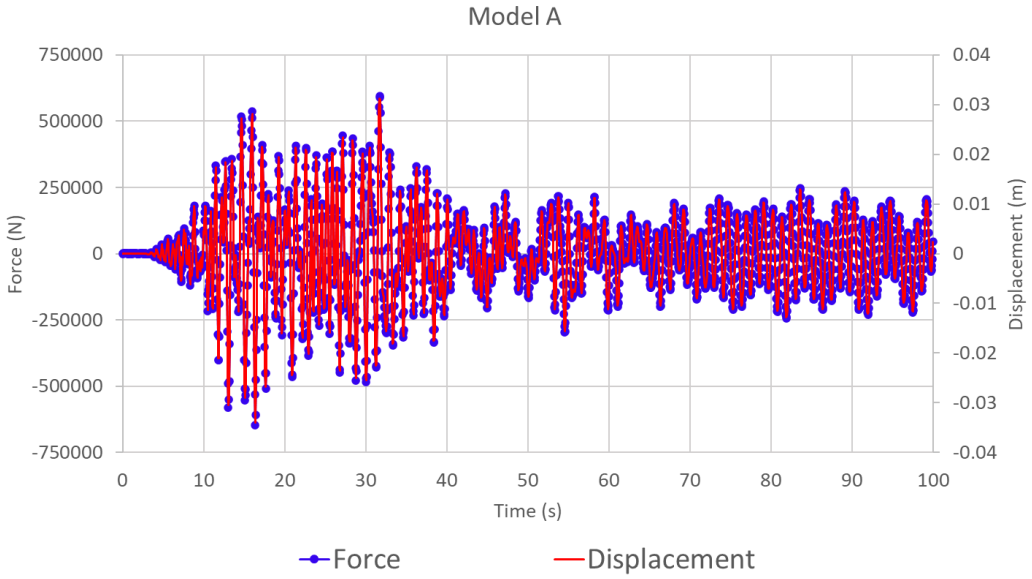

Figure 31: Model A Force (blue) & Displacement (red)

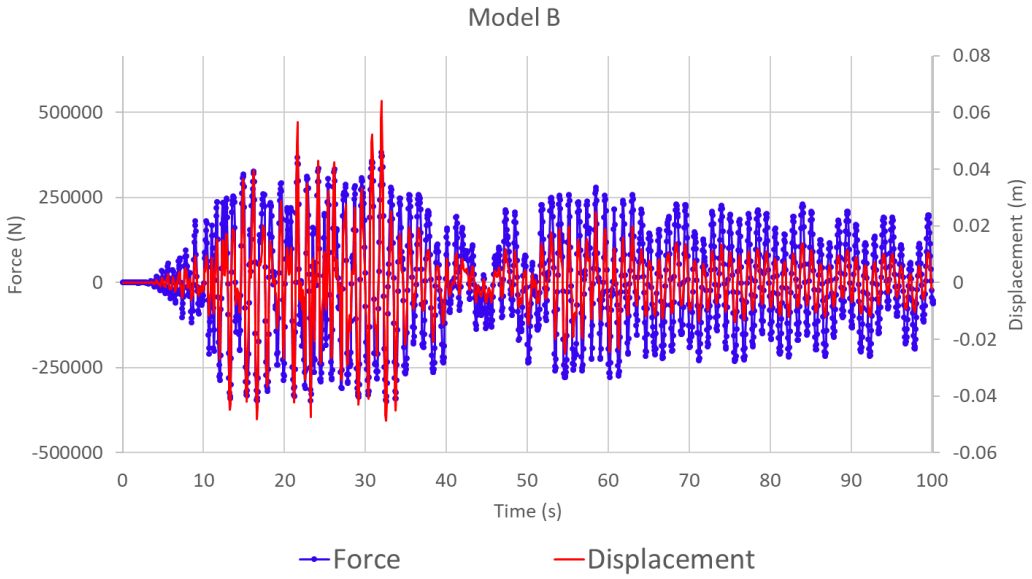

Figure 32: Model B Force (blue) & Displacement (red)

The relationship between the force and the displacement for Model A is that they are constantly similar and stay that way over time. For Model B the displacement shoots away for peaks, but it is simply following the prescribed force-displacement curve as proven in Figure 28. It has the same relationship as for Model A when it comes to smaller displacements that fall within the initial stiffness load level.

Then the results at mudline of the plastic models are shown in Figures 33 and 34 .

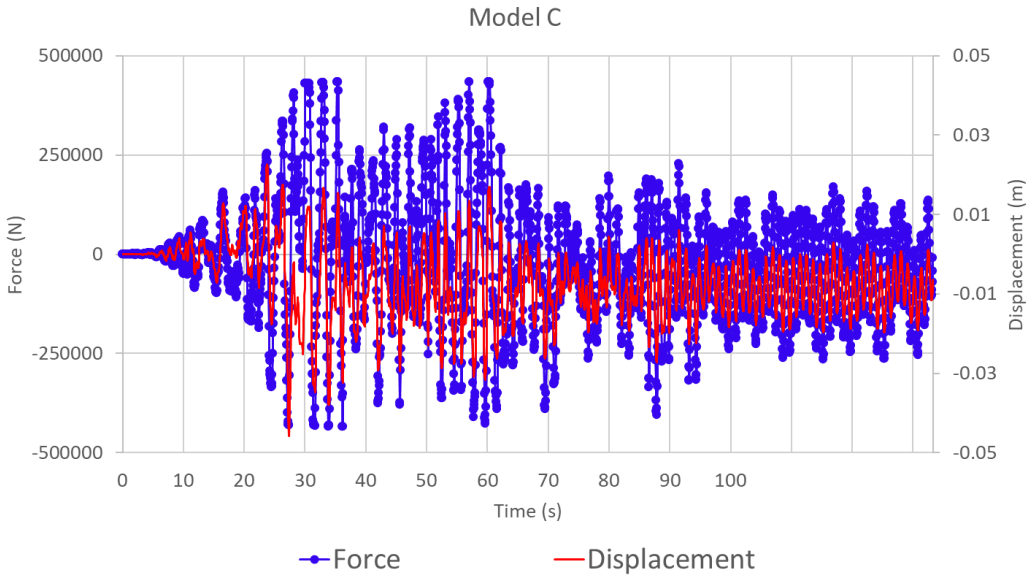

Figure 33: Model C Force (blue) & Displacement (red)

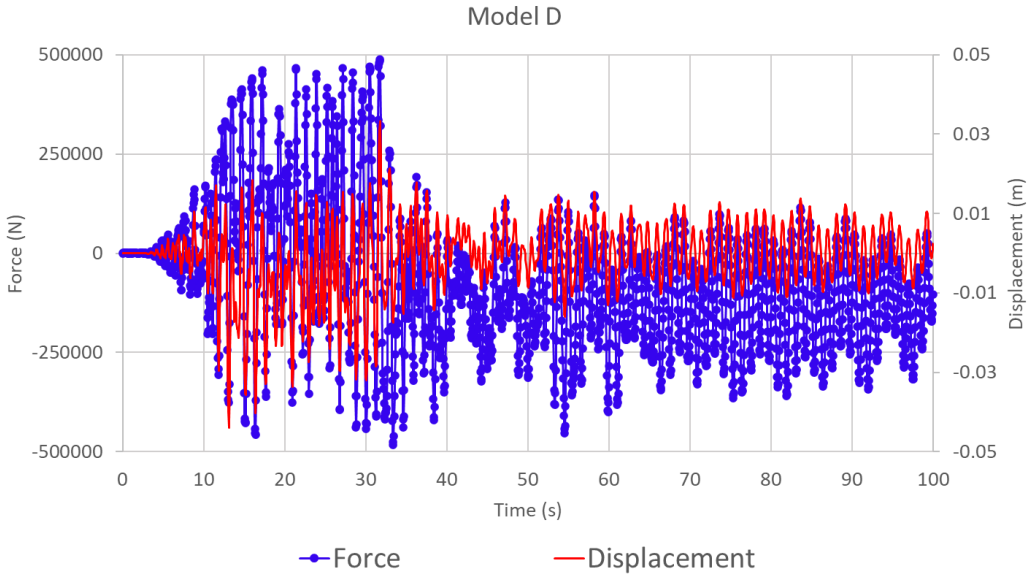

Figure 34: Model D Force (blue) & Displacement (red)

For the results of Models C & D in Figures 33 and 34 there are peaks in the force where there is an accompanying drift in the displacement. This is brought forward more in Model C than in Model D, because the change of stiffness is immediate past a certain point. Once some plasticity seems have been achieved, there is no longer a direct connection between the force and the displacement. However, after the maximum displacements have been passed, the system reacts elastic again. Thus showing similar movements between the force and the displacement in the second half of the simulation. The new elastic range can be found along the line of the end point in Figure 30. Also can be seen the permanent plastic deformation of the soil. The nonzero mean of the free vibrations of the force can be explained from the new equilibrium of the structure above with the drift in displacement of the soil. The remaining oscillations in the time response from 34 are also recognized in Figure 30 as data points along one line in the elastic range.

The response of Model D in Figure 34 shows a displacement near 0.04m. To get a better idea of the stiffness curve that is used for such magnitude of displacements, the effectively used p-y curves are shown in Figures 35 and 36.

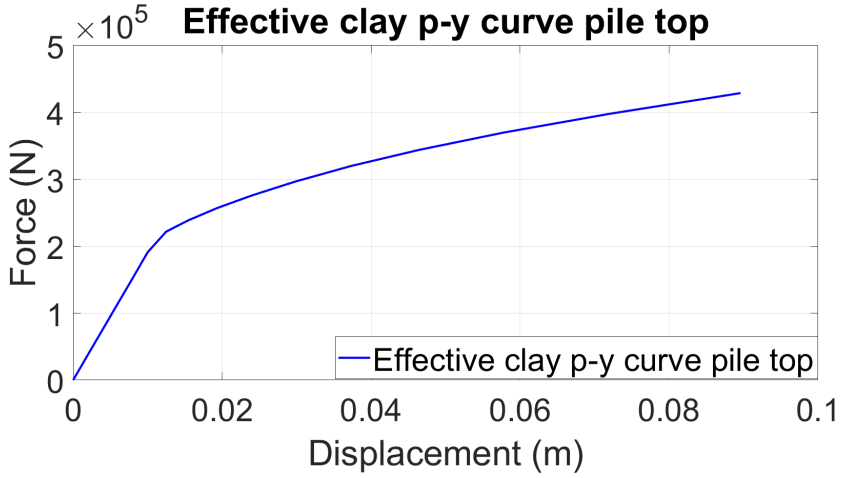

Figure 35: Effective clay p-y curve pile top till relevant displacement

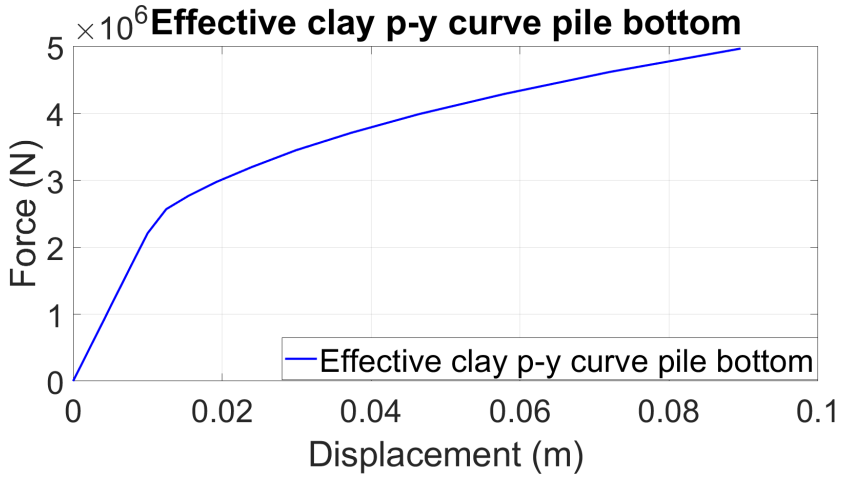

Figure 36: Effective clay p-y curve pile bottom till relevant displacement

4.7 Complete model verification

Lastly the complete model is evaluated, where the springs are integrated with the rest of the structure. Statically it is verified using a gravity load, which will also be present in the dynamic simulations as initial deformation conditions and loads. Then its dynamic properties are verified using reference models. Eigenfrequencies and magnitudes of forces are used to verify that the modelled OWT is representative.

4.7.1 Static

First the system is checked for statics by using a gravity load. Figures 37a and 37b show the deformation due to the gravity load scaled by a factor 500. Gravity is defined in the negative vertical direction following the Abaqus library for defining a gravity load [41].

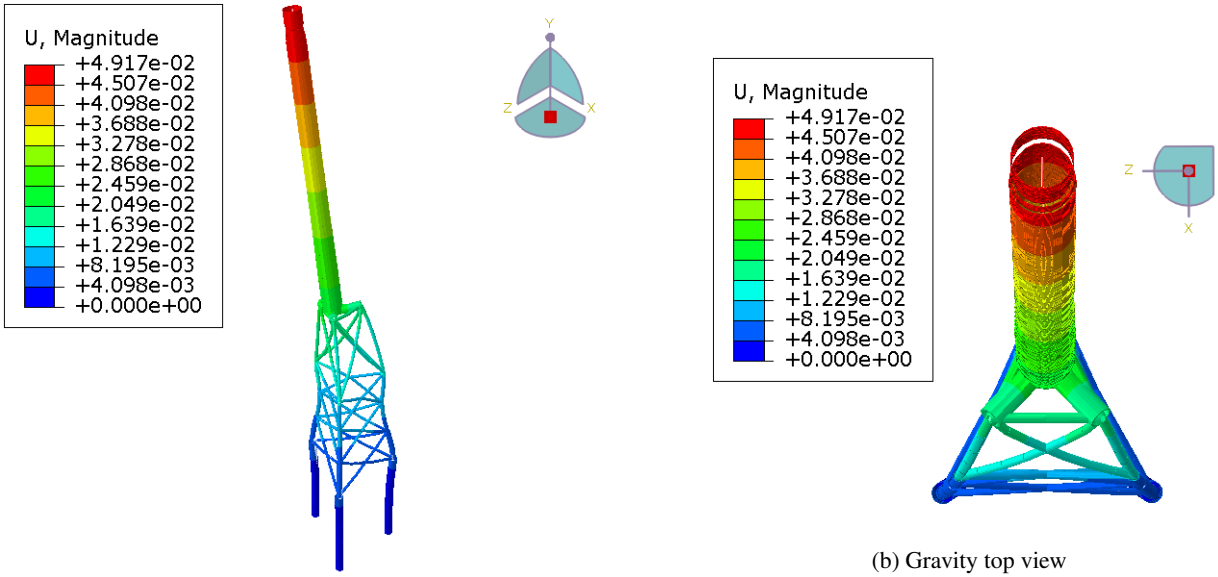

(a) Gravity load

(b) Gravity top view

Figure 37: Static model views

The gravity makes the tower bend somewhat towards one of the legs. The tower is not directly placed in the center of gravity of the triangle of the jacket top. The top of the jacket legs bend outwards while the bottom of the jacket legs move inwards. This seems to be due to the relatively high point load coming from the tower self weight at the transition from the tower to the jacket.

4.7.2 Dynamic

In order for the dynamic verification the modeshapes are evaluated to check the absence of rigid body modes and collaborate the typical modeshape names with the reference designs. There are three types of modeshapes that are typical and the frequencies can be found in table 38b. The tower dictates typical beam modeshapes and due to the level/extent of symmetry of the structure there are pairs that can be recognized. The first pair of modes found in Figures 39a and 39b are similar to the first mode of a clamped beam, where the jacket is not included. The second pair of modes found in Figures 40a and 40b are similar to the second mode of a clamped beam, but also includes movement of the jacket.

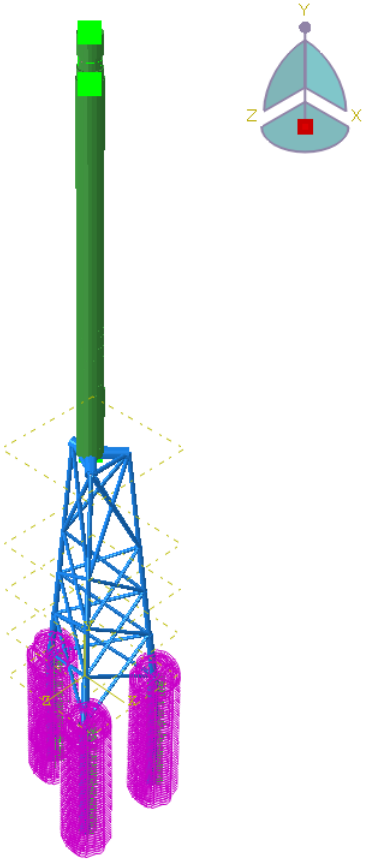

(a) Complete model design

Complete	Model eigen-frequency (Hz)	References average (Hz)	Difference with reference (%)
1st fore-aft	0.18885	0.19744	4.4
1st side-side	0.17553	0.19506	10.0
1st torsional	0.77788	0.79829	2.6
2nd fore-aft	0.91098	0.93339	2.4
2nd side-side	0.89634	0.89647	0.0
3rd fore-aft	1.5755	N/A	N/A
3rd side-side	1.6954	N/A	N/A

(b) Eigenfrequencies complete model reference comparison

Figure 38: Dynamic model verification

Table 38b shows the eigenfrequencies for the built model and the difference between the average of 7 reference models.

The eigenfrequencies from the complete model match very well those of the reference models. The modes shown are expected to dominate the response of the structure. The mode shapes look can be found in the following Figures 39, 40, 41.

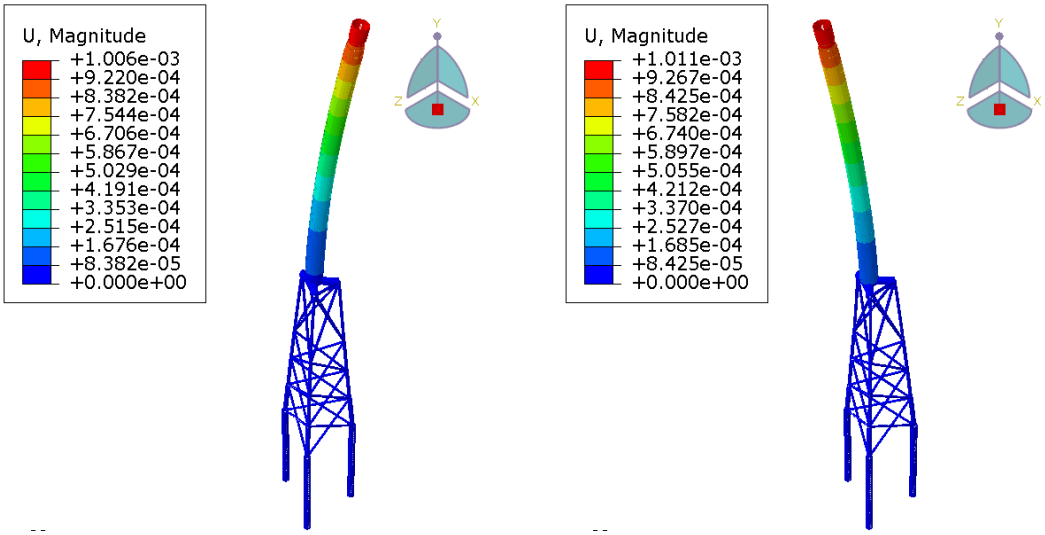

(a) Mode 1, 1st fore-aft

(b) Mode 2, 1st side-side

Figure 39: 1st set of bending modes

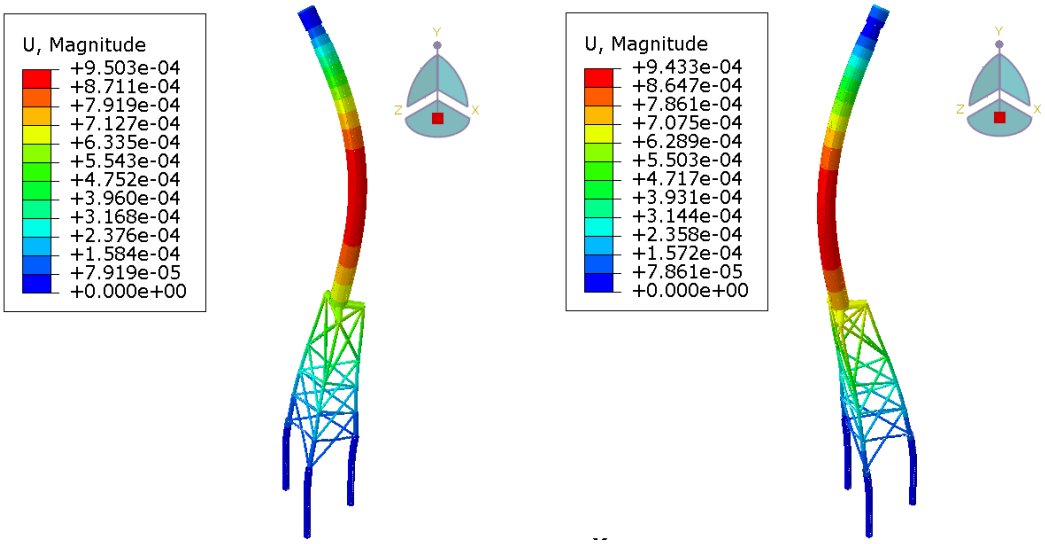

(a) Mode 3, 2nd fore-aft

(b) Mode 4, 2nd side-side

Figure 40: 2nd set of bending modes

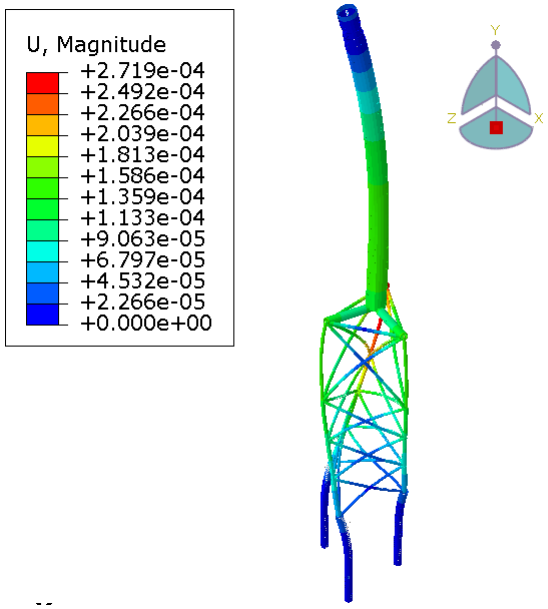

Figure 41: Mode 5, torsional

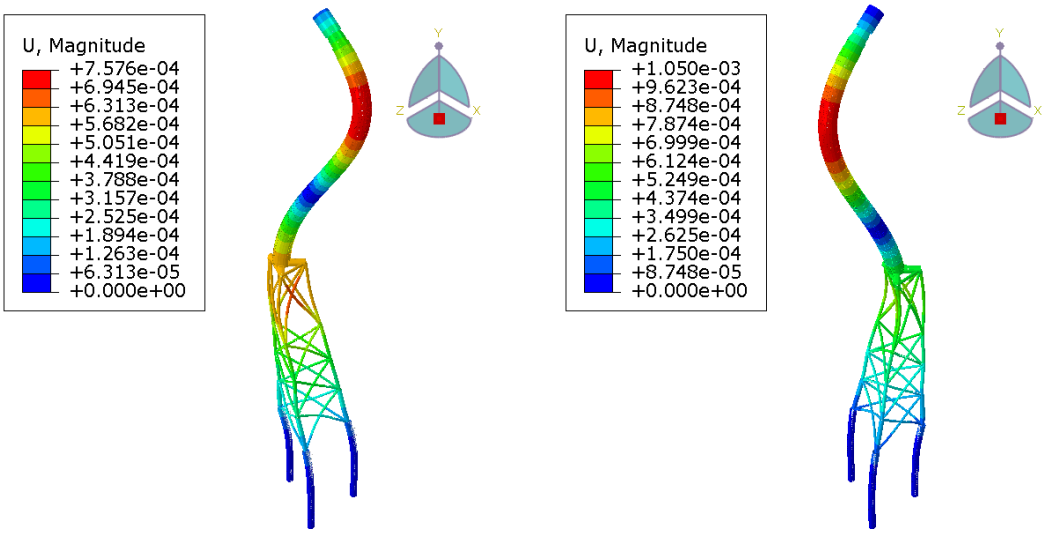

(a) Mode 6, 3rd fore-aft

(b) Mode 7, 3rd side-side

Figure 42: 3rd set of bending modes

In chapter 4.6 can be found in which ways the model will be altered to account for the different soil models. Analysis using a completed model has already been executed there to verify the soil models. With the knowledge of the eigenfrequencies the model is deemed representative and useful for further investigation on the soil-structure interaction effects.

4.8 Loads & Boundary conditions

4.8.1 Loads

The loading is simulated by accelerations attached to the horizontal directions of the soil springs that follow different earthquakes' signatures. The loading is chosen to be uniform over depth to reduce the complexity of the modelling process [9]. This simplification has impact on the response compared to more complex soil spring relationships. The motion is also prescribed synchronously on each of the three piles. This is allowed for the reason that the wavelength of the earthquake signatures are large enough so not to fit between the jacket legs distance of 30m. The earthquake signatures have different frequency content and the amplitude is tuned to scale them to a realistic design load.

The following input is one of seven earthquake signatures used and it is only in x direction. It should be disclosed that the original signature has been altered by leaving out the first 30 seconds to conserve computation time and output file size, but the acceleration for that part is negligible. It is also multiplied by a factor 3 to achieve a more realistic load level. This amplification is reasonable for finding ULS loads for the wind turbine life span and is similar to the reference project according to SGRE.

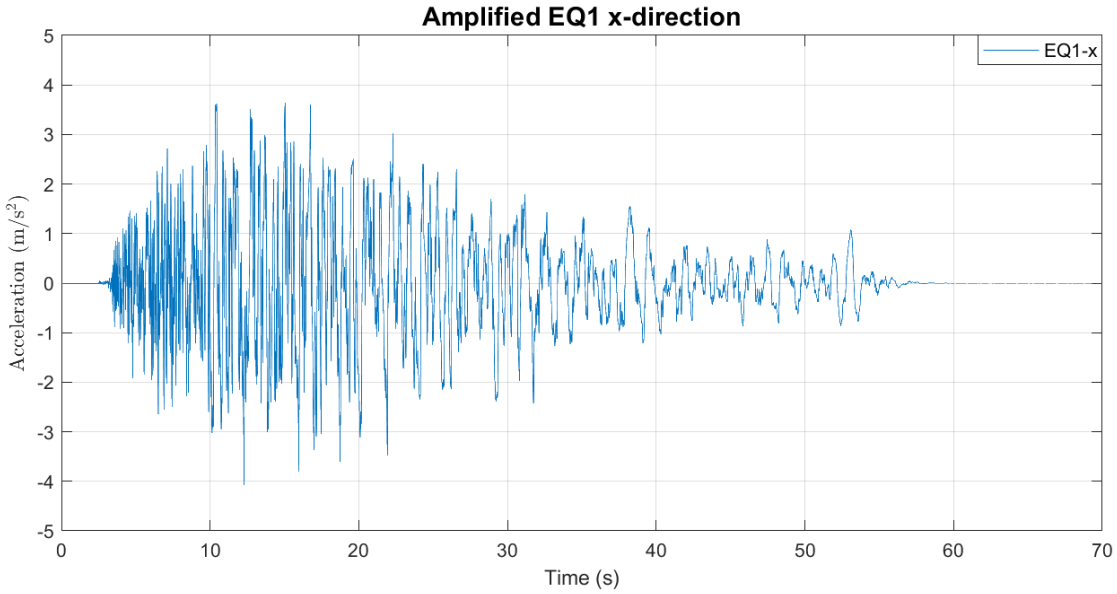

Figure 43: Earthquake 1 loading signature

4.8.2 Boundary conditions

The horizontal directions are loaded by the earthquake signals. Since the loading is only applied in two horizontal directions, the remaining vertical direction is kept unmoved. The boundary condition is applied at the bottom of the piles, which notably causes the weight of the structure to also be present in the piles. In Figure 44 can be found the vertical boundary conditions at the bottom of the piles and the acceleration loads on the attachment points of the soil-side of the springs.

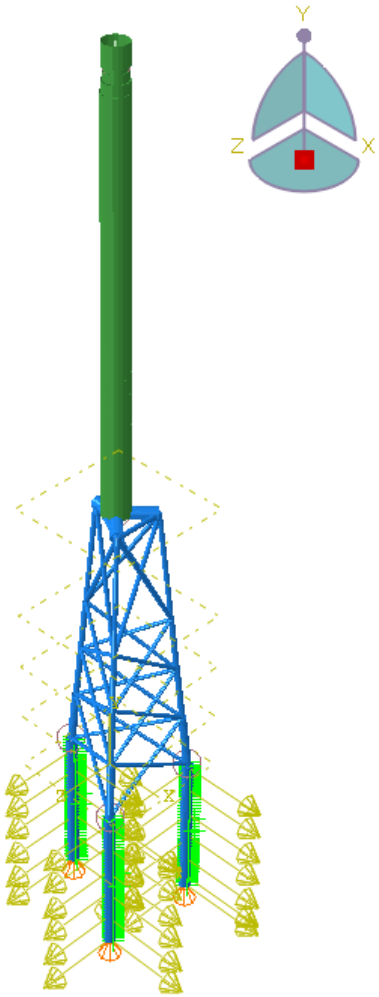

Figure 44: Boundary conditions & loads

4.9 Damping

There is structural damping in the system. Structural damping comes from movements between parts of the structure which in reality allow some dissipation through marginal movements at the joints. The parameters are calibrated using the eigenfrequencies of the superstructure. This can work because the first and second mode of the superstructure dominate the response to many of the earthquake signatures.

In equation (18) can be found the formula for the damping ratio for mode i that is calculated with circular frequency ω and Rayleigh parameters α_R and β_R.

$$\xi_i = \frac{\alpha_R}{2\omega_i} + \frac{\beta_R \omega_i}{2} \tag{18}$$

For the first and second mode of the reference project there is a percentage of damping that is expected for free oscillations.

Damping ratios ξ_i per mode i:

$$\xi_1 = 1.82 \ \ \%\text{logarithmic decrement}$$
$$\xi_2 = 5.59 \ \ \%\text{logarithmic decrement}$$

The logarithmic decrement is defined as the natural log of the ratio of the amplitudes of any two successive peaks. The natural frequencies of the two bending modes of the tower are as follows.

$$f_1 = 0.23$$
$$f_2 = 1.375$$

The circular frequency is used in formula 19. It can be calculated from the natural frequency.

$$w_i = f_i \cdot 2\pi \tag{19}$$

Equation (20) can be used to determine the Rayleigh parameters.

$$\begin{bmatrix} \frac{1}{2\omega_1} & \frac{\omega_1}{2} \\ \frac{1}{2\omega_2} & \frac{\omega_2}{2} \end{bmatrix} \begin{bmatrix} \alpha_R \\ \beta_R \end{bmatrix} = \begin{bmatrix} \xi_1 \\ \xi_2 \end{bmatrix} \tag{20}$$

The calculated Rayleigh parameters are then calculated as $\alpha_R = 0.00473$ and $\beta_R = 0.00174$. These are applied in all structural materials, excluding the soil spring materials.

Another type of damping is used in some of the soil models. Models that include plasticity have damping through physically nonlinear behaviour. The used p-y springs have an initial stiffness related to a 0.0001m displacement. Any more displacement than this means that plasticity occurs. The unloading stiffness is equal to the initial stiffness. This causes energy dissipation any time a larger displacement occurs. Radiation damping of the soil and hydrodynamic damping are not explicitly included in the model. Numerical damping is included in the model. The degree of damping has been discussed in 4.1.1.

5 Results

In this section the results are discussed obtained from simulations involving four model types with seven earthquake signatures each. The goal is to represent the data in a digestible manner. Therefore a specific selection of output variables are used. The research is focused on finding ULS design loads, which are represented by displacements and forces. Additionally the response of the system and its dependence on the soil model type is of interest. The variables of interest for ULS design loads are the section moments at the jacket-tower interface and at the tower top. These locations are shown in figure 45. The RNA location is at the top of the rigid link. Below the rigid link is the tower top. The Interface location is between the jacket and the tower. The Mudline spring location is the x direction spring at the transition from the jacket leg to the pile at the positive x and z coordinate.

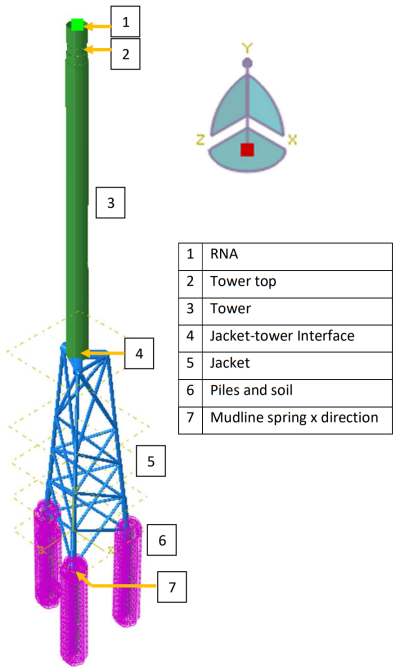

Figure 45: Variables location indication

The data shown in this chapter considers one direction for the displacements and the section moment, because this direction has the highest peak values. The direction is named U1, which coincides with the x direction. The section moment is named SM1 and represents the first principal stress, which is the maximum normal stress magnitude at a given point. The direction of the first principal stress is along the axis where this maximum normal stress occurs.

The data for the maxima is normalized by setting Model D as a reference as it is deemed the most realistic model. This is corroborated by chapter 3.4 about the soil characteristics. Other figures are normalized by the maximum peak of the shown variable. Differences in results between model types are investigated and explained. There are general patterns and exceptional data found which lead to the conclusion of the research.

In order to exemplify the general pattern, data from an arbitrary earthquake is used to investigate the output variables and dynamics of the system. The exceptional data that is elaborated represents an observation on one single earthquake and analysis type. This is classified as a case of resonance.

5.1 Displacements

Displacements at specific locations in the structure shown in Figure 45 are used to investigate part of the structural response. Figure 46 shows the maximum values across the soil models for the Interface displacement. Compared to Model D, Model C generally has lower maxima and Models A & B have higher maxima. In Figure 47 for the Maximum U1 RNA there is a similar trend, but the % difference is relatively small.

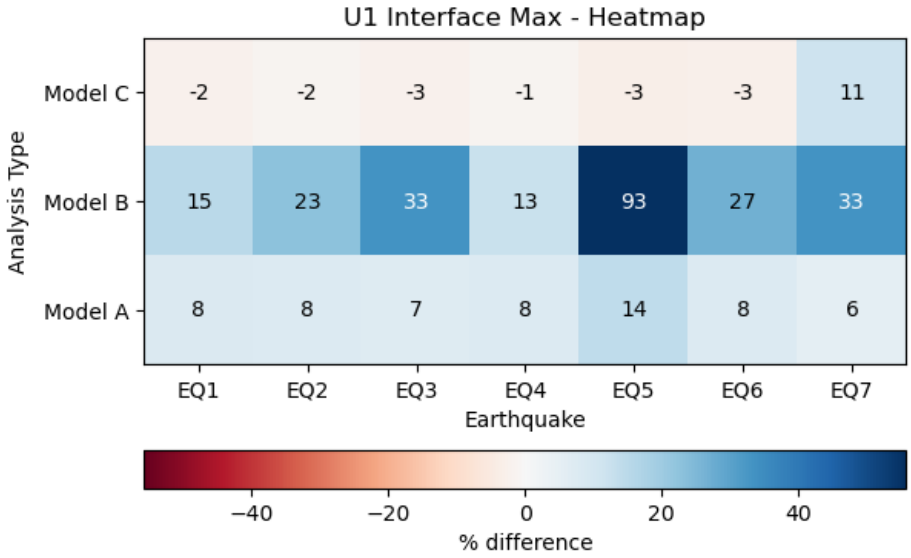

Figure 46: U1 Interface Max difference with respect to Model D

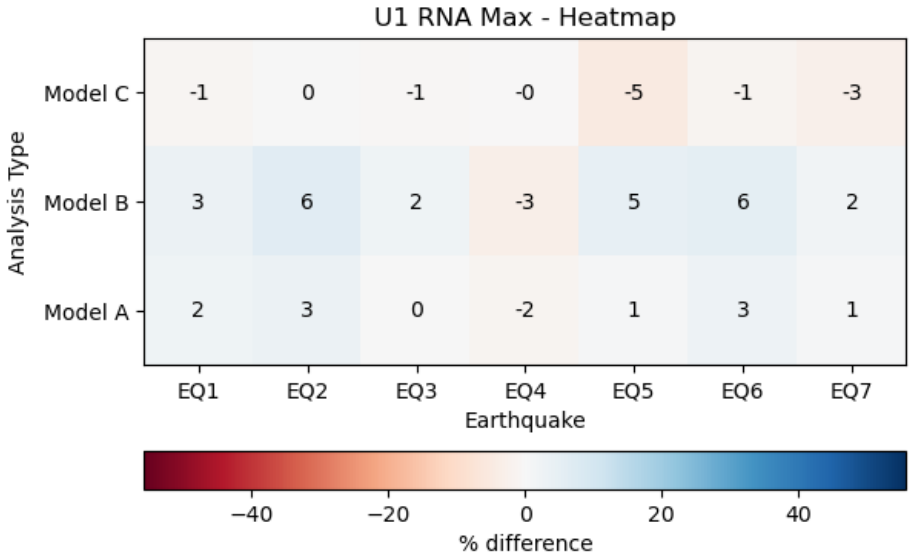

Figure 47: U1 RNA Max difference with respect to Model D

Data from an arbitrary earthquake is used to investigate dynamics of the system. The signature from earthquake loading signature EQ1 is used. In Figure 43 can be found the time domain and in Figure 48 the frequency domain of the earthquake signature. Additionally the important eigenvalues of the system are represented both together with the earthquake and in Table 6. The selected eigenfrequencies have the most significant contribution to the total response for the displacement and section moment variables.

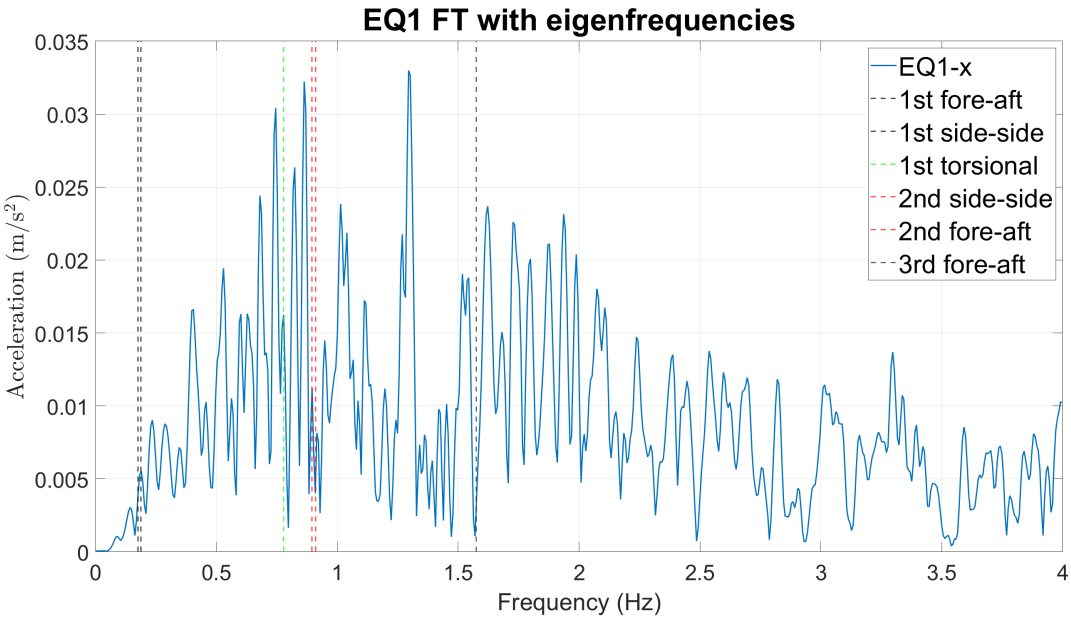

Figure 48: EQ1 FT including important eigenvalues

Complete	Model eigen-frequency (Hz)
1st fore-aft	0.18885
1st side-side	0.17553
1st torsional	0.77788
2nd fore-aft	0.91098
2nd side-side	0.89634
3rd fore-aft	1.5755
3rd side-side	1.6954

Table 6: Eigenfrequencies model

The time history together with the Fourier transform of the Interface and the RNA displacement give valuable information about the structural response and the eigenfrequencies that govern them.

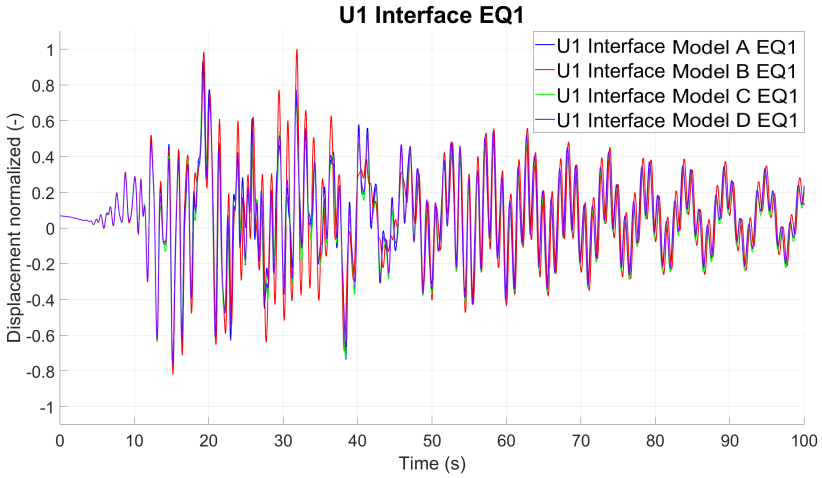

Figure 49: U1 Interface EQ1

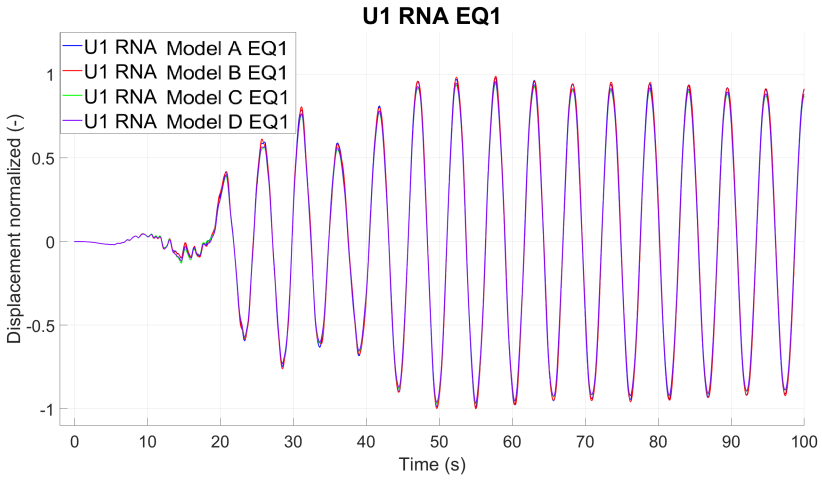

Figure 50: U1 RNA EQ1

The RNA and Interface displacement response are governed by specific frequencies. The Interface displacement peaks are found to oscillate in higher frequencies than those of the RNA. The dominant RNA displacement frequency is close to the first fore-aft mode at 0.19Hz and the Interface displacement frequency is close to the 2nd fore-aft mode at 0.91Hz. The influence of a different soil model also becomes apparent. Model B gives higher peak values, which can be recognized from the heat maps figures 46 and 47. Differences in peaks due to a different soil model are more pronounced in the Interface response than in the RNA response.

To complement the insight into the RNA and Interface displacements, also the frequency domain of their response is shown. The Fourier transform is exact for linear systems, but depending on the degree of nonlinearity it can provide valuable insight.

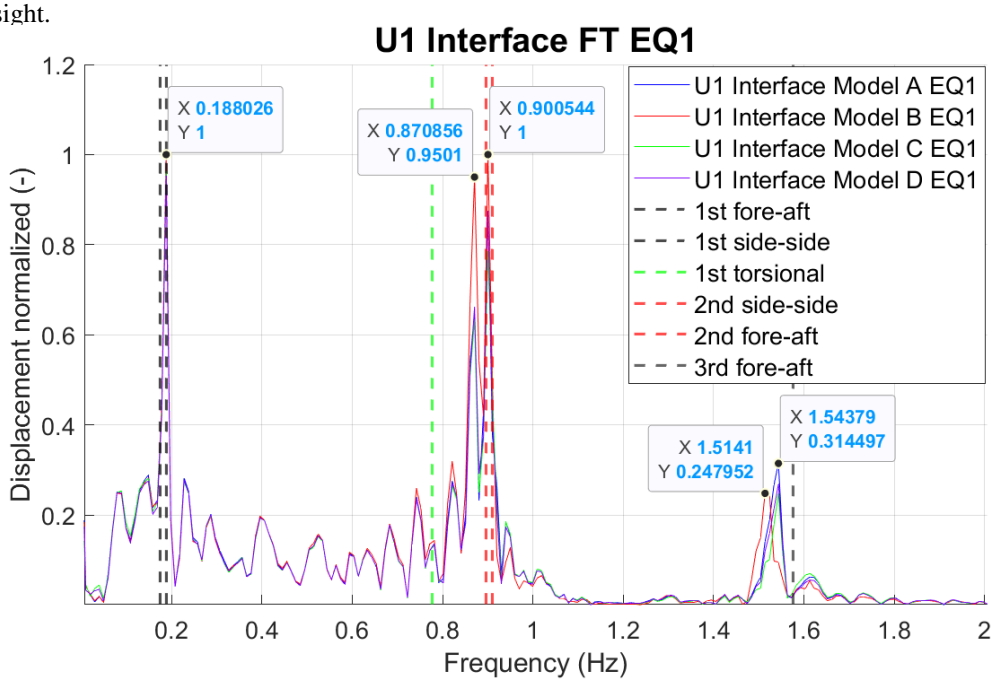

Figure 51: U1 Interface EQ1 FT

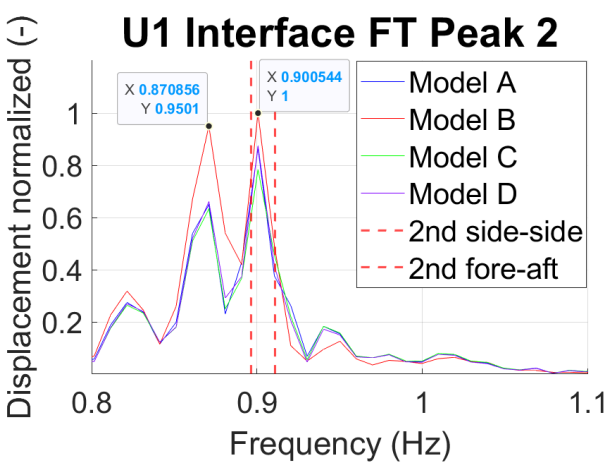

(a) U1 Interface EQ1 FT Peak 2

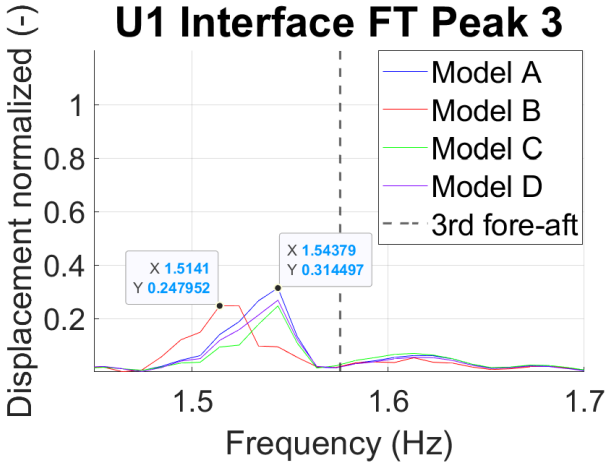

(b) U1 Interface EQ1 FT Peak 3

Figure 52: U1 Interface EQ1 FT Peaks

In Figure 51 can be seen the Fourier transform of the output data of the x direction displacement of the Interface for EQ1. Figure 52 is a zoomed version of the two peaks to show the difference between the models more clearly. The eigenfrequencies of the system are also indicated. The time domain motions are similar, so there is overlap of the frequencies across soil models. Near the first and second tower bending modes Model B has greater peaks. These can also be found in the time domain response shown in Figure 49. Peaks of the Model B response are prone to appear at slightly lower frequencies than the other models. This may be due to softening of the system stiffness via the nonlinear springs. The Interface displacement response is affected by all three tower bending modes of which the 2nd set of tower bending modes has the greatest influence on the time domain amplitude.

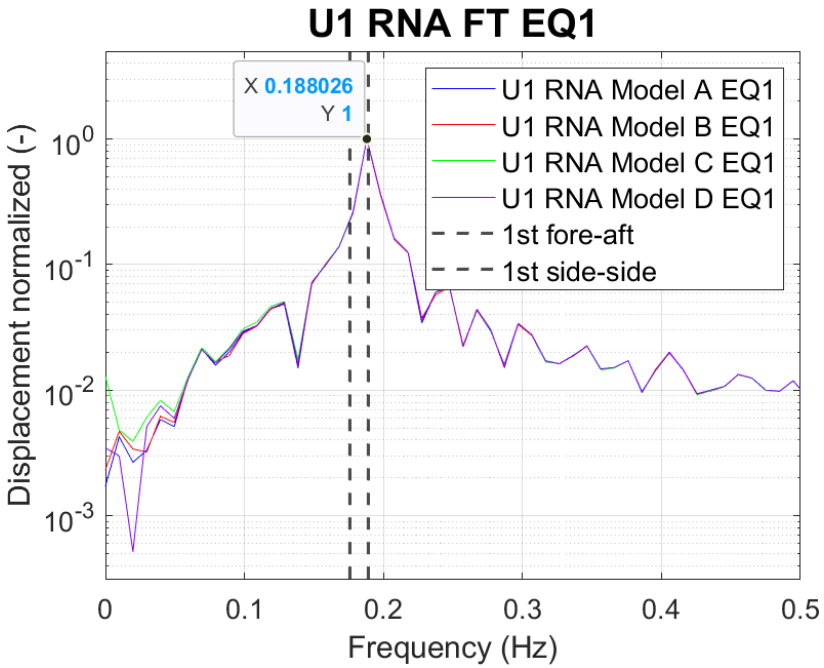

Figure 53: U1 RNA EQ1 FT

In Figure 53 can be seen the Fourier transform of the output data of the x direction displacement of the RNA for EQ1. The eigenfrequencies of the system are also added to the figure. The time domain motions are similar both in frequency and amplitude, which results in significant overlap across soil models. The Nonlinear elastic model has slightly greater peaks which can be found also in the time domain response shown before in Figure 50. The RNA displacement response is governed by the 1st set of tower bending modes.

The RNA displacement does not seem affected by a different soil model as much as the Interface displacement. Differences between displacements across different soil models originate from the activation of nonlinearity. The more nonlinearity, the greater the difference. The elongation of the soil springs from oscillations at these frequencies give an indication of the activation of nonlinear effects. The time history and Fourier transform of the soil springs force and elongation show the magnitude of the nonlinearity taking place.

The influence of the soil model to the displacement response variables is investigated. Since the soil spring characteristics are the only varying entity, it makes sense to look at their response. The time history together with the Fourier transform of the soil springs' forces and elongations are used to gain valuable information. The output from the spring at mudline is used, because it experiences the most elongation.

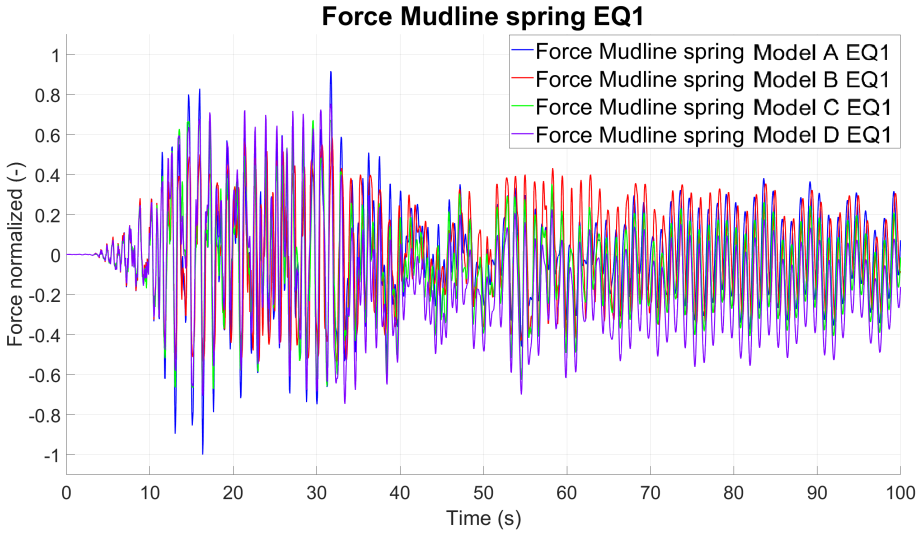

Figure 54: Mudline spring force EQ1

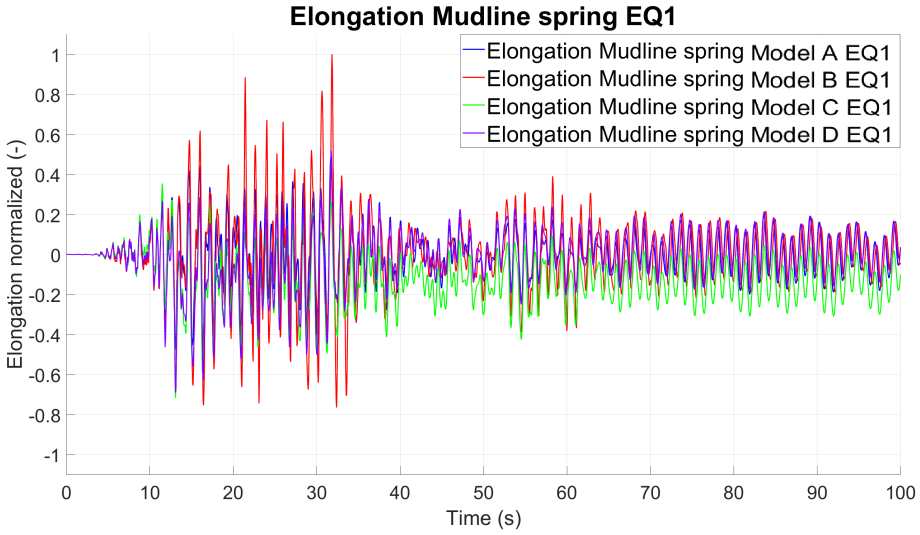

Figure 55: Mudline spring elongation EQ1

In Figures 54 and 55 the influence of each soil model becomes apparent. Differences are present in the peaks and free vibrations. In Figure 54 the spring force peaks are highest for Model A and lowest for Model B. In Figure 55 the elongation peaks are the highest for Model B and lowest for Model A. Models C & D are in between for both the spring force and elongation. Plasticity introduces a drift in both spring elongation and spring force. The persisting force is from the new equilibrium of the soil with the elastic jacket legs and structure above due to the drift in elongation of the soil. This drift is present in both Models C & D due to permanent plastic deformation.

The soil springs have transformed the loading on the structure. The output frequencies of the forcing passed on by the springs are affected due to softening of the spring stiffness. The loading amplitude is affected by the transformation which causes significant difference in the response. In Figure 56 can be found the Fourier Transform of the spring force.

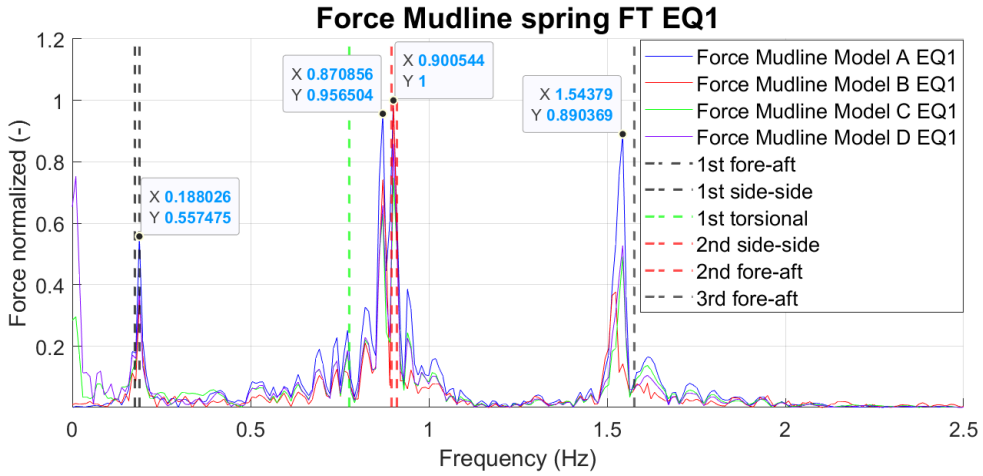

Figure 56: Mudline spring force EQ1 FT

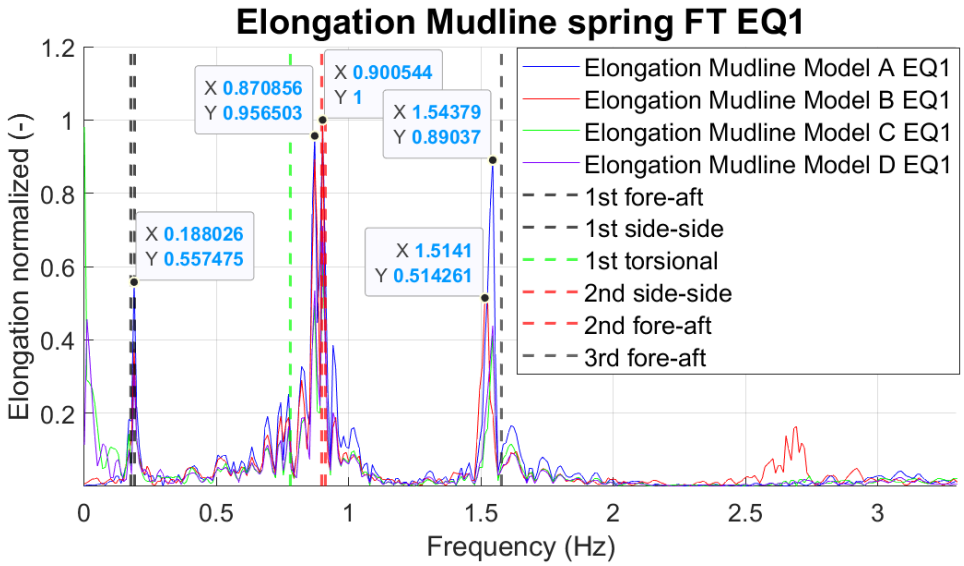

Figure 57: Mudline spring elongation EQ1 FT

Figures 56 and 57 show the overall Fourier Transform of the mudline spring force and elongation in which three frequency peaks can be distinguished. In Figures 58, 59 and 60 can be found a zoomed in version of the three peaks to show the difference between the models.

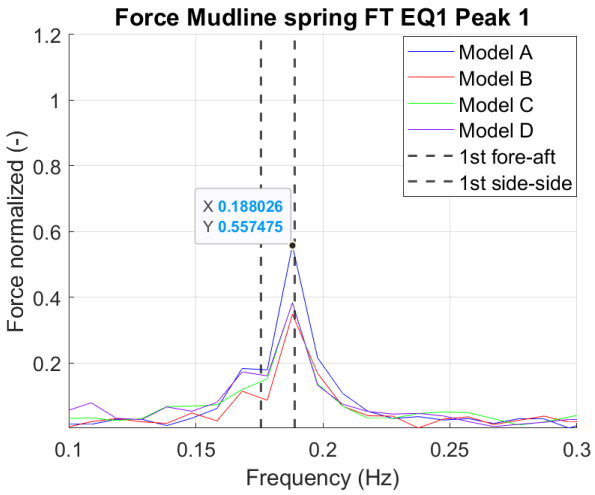

(a) Mudline spring force EQ1 FT Peak 1

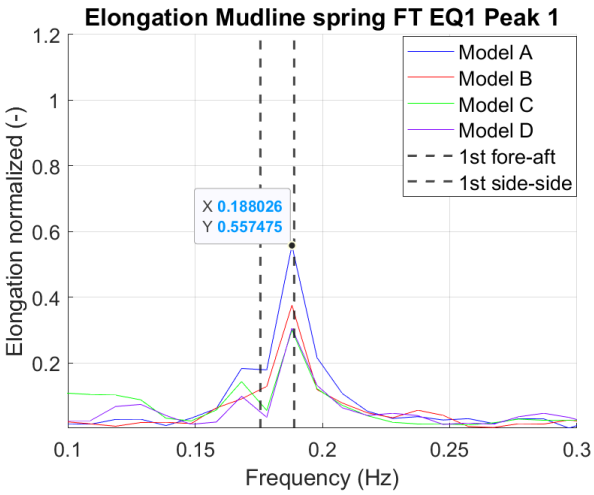

(b) Mudline spring elongation EQ1 FT Peak 1

Figure 58: Mudline spring force and elongation Peak 1

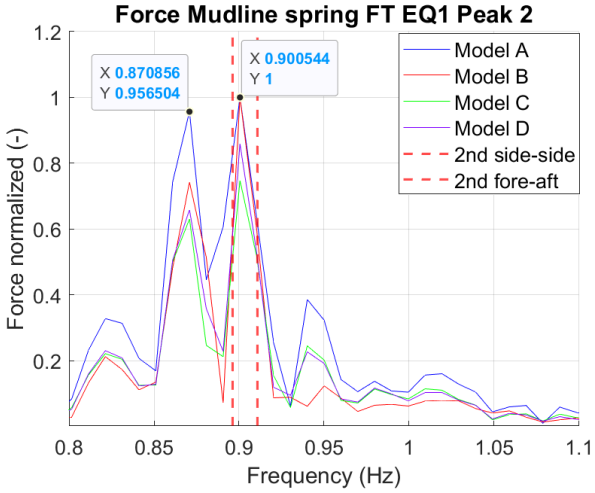

(a) Mudline spring force EQ1 FT Peak 2

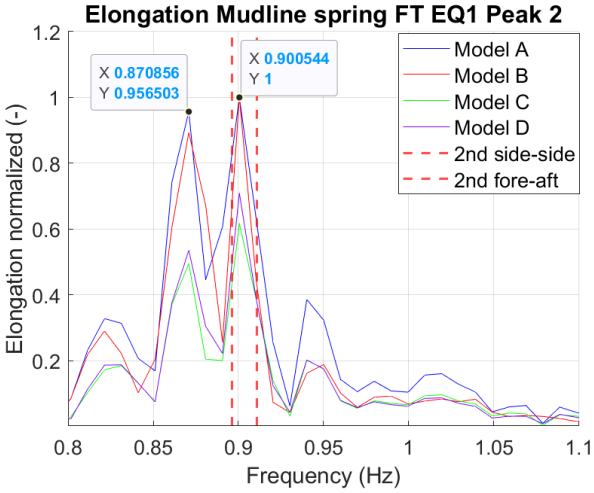

(b) Mudline spring elongation EQ1 FT Peak 2

Figure 59: Mudline spring force and elongation Peak 2

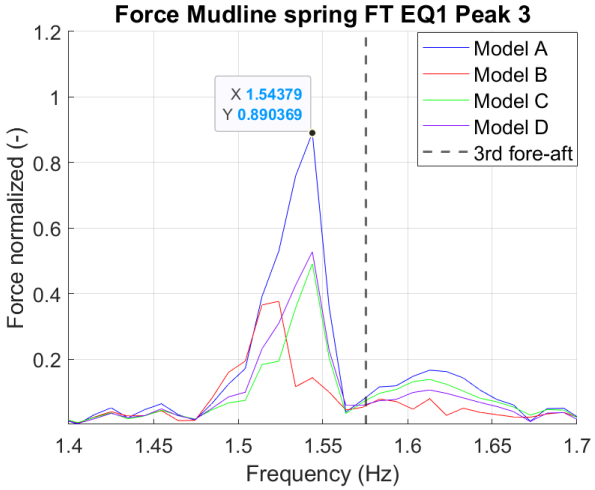

(a) Mudline spring force EQ1 FT Peak 3

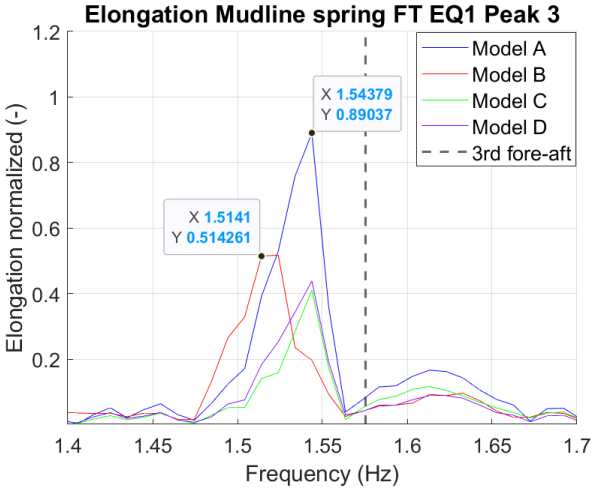

(b) Mudline spring elongation EQ1 FT Peak 3

Figure 60: Mudline spring force and elongation Peak 3

In Figures 54 and 55 can be found that Model C and D have similar behaviour to Model A, but the amplitude of the oscillations for the mudline spring force and elongation are smaller. This is due to the plasticity that occurs at increasing deformation. The spring force at mudline for Model B is lower than that of Model A as can be found in Figures 54 and 56. The spring elongation at mudline for Model B is higher than the other models as can be found in Figures 55 and 57. This phenomenon can be explained by the change in modeshapes while the soil stiffness softens. Deformation in the soil may lead to more Interface and RNA displacement in the mode shapes. Thus for the same frequencies and lower forces, the displacement response may be greater.

There is a general pattern for the Interface displacement. The nonlinear elastic Model B response has consistently higher peaks, which can be found in Figure 46. The Interface displacement has the greatest peaks and correspond to a frequency of around 0.9Hz and 0.87Hz. While there is no eigenfrequency specifically at 0.87Hz, it is very prevalent in the response. Known from Model B is the softening of the stiffness, resulting in a range of eigenfrequencies rather than specific ones.

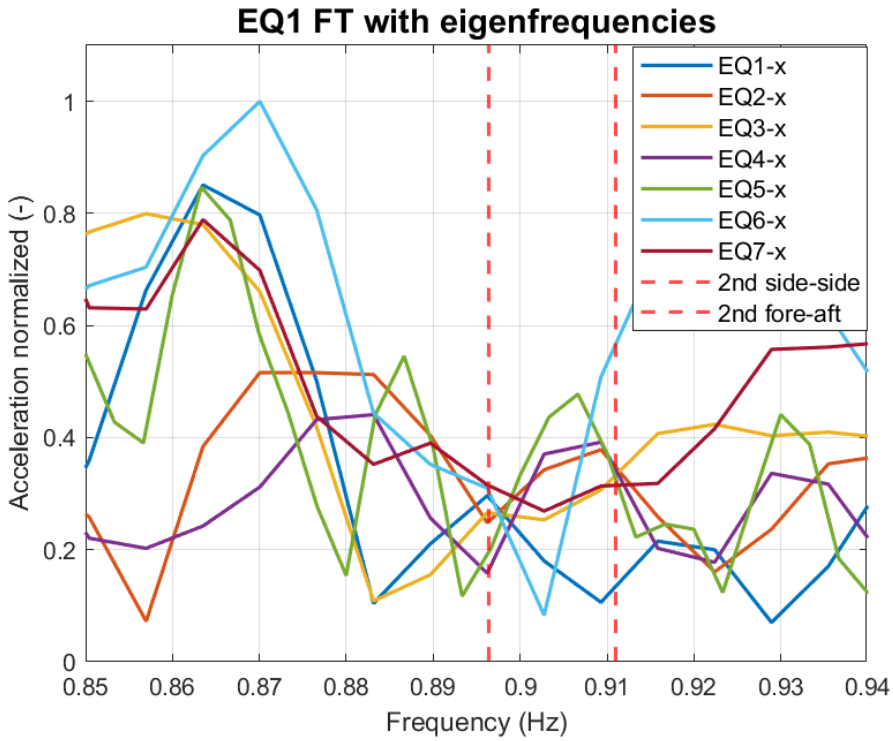

Figure 61: Fourier transform all EQs - 2nd mode frequency range

In Figure 61 it can be found that the reason for the higher peaks in the Interface displacement of Model B is an increase in the loading as its stiffness softens. The figure shows the frequency domain of all 7 earthquake loading signatures in x direction. The eigenfrequency of elastic Model A is around 0.9Hz for the 2nd set of tower bending modes. The earthquake signatures all have an increase in amplitude ranging from 0.9Hz to 0.87Hz. Earthquakes 2 and 4 don't have as much increase and subsequently also have lower maxima of U1 Interface. Due to the softening of the p-y stiffness curves, Model B is excited more. As the stiffness softens, the eigenfrequencies decrease to a range where the loading has more energy.

The contribution to the total response of the eigenfrequencies around 0.9Hz for the Interface displacement can be recognized by the peaks in Figure 49. However, the general pattern that the RNA displacement is not influenced significantly by the soil model has to be investigated. The magnitude from oscillations of the elongation of the soil spring around the governing RNA displacement frequency can be used to find activation of nonlinearity. The contribution to the total Mudline spring elongation response from the governing RNA frequency oscillations can be found by performing the Fourier transform of the soil spring elongation for frequencies < 0.2Hz. These frequencies are compared to the total Mudline spring Elongation response in Figure 62.

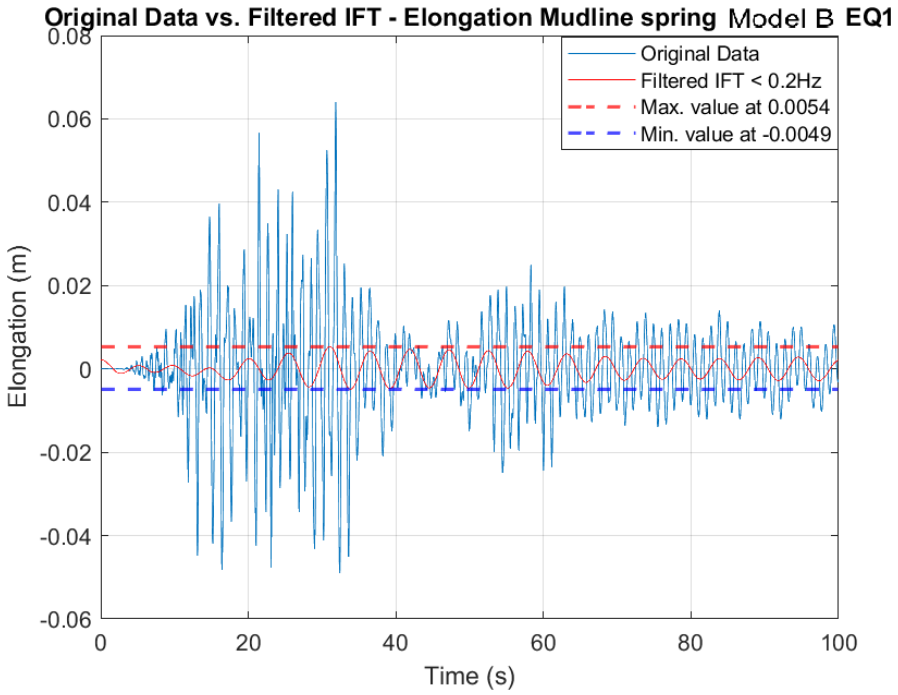

Figure 62: Elongation mudline spring total response & contribution < 0.2Hz - elastic model EQ1

In Figure 62 can be seen that the contribution of the RNA frequency is relatively small compared to the highest peaks. For the free vibrations the contribution is relatively greater. This shows that differences in RNA displacement between the soil models occur mostly due to overlap of the Mudline spring Elongation peaks of the governing frequency for the Interface displacement of around 0.9Hz. The summation of these two sum up to be sufficient deformation for nonlinearity, which transforms the force. Nonlinearity is activated for a spring elongation of 0.01m, which can be found in Figure 35 in Chapter 4.6.4. The contribution of frequencies below 0.2Hz don't go above 0.0054m.

5.2 Section moments

Section moments at specific locations in the structure shown in Figure 45 are used to investigate part of the structural response. Figure 64 shows that for the Maximum SM1 Interface, Model C generally has lower maxima and Models A & B have higher maxima compared to Model D.

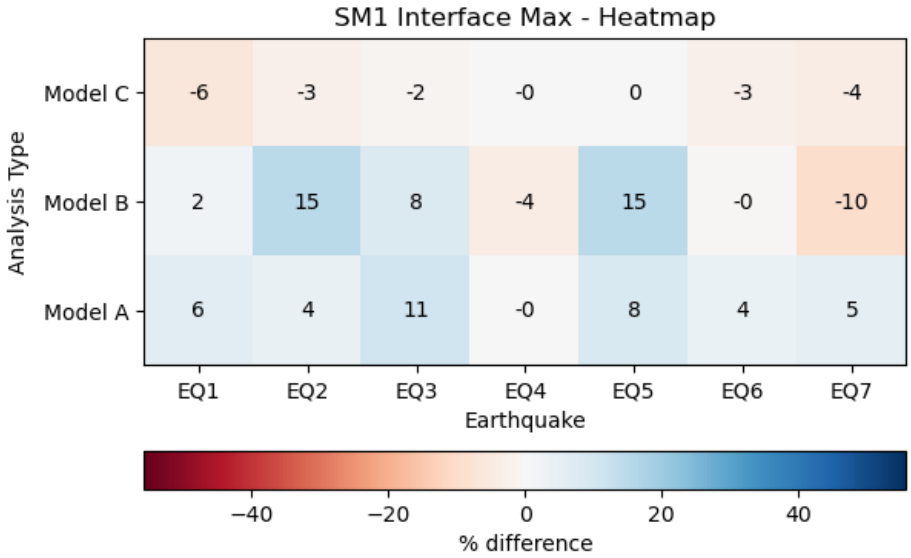

Figure 63: SM1 Interface Max difference with respect to Model D

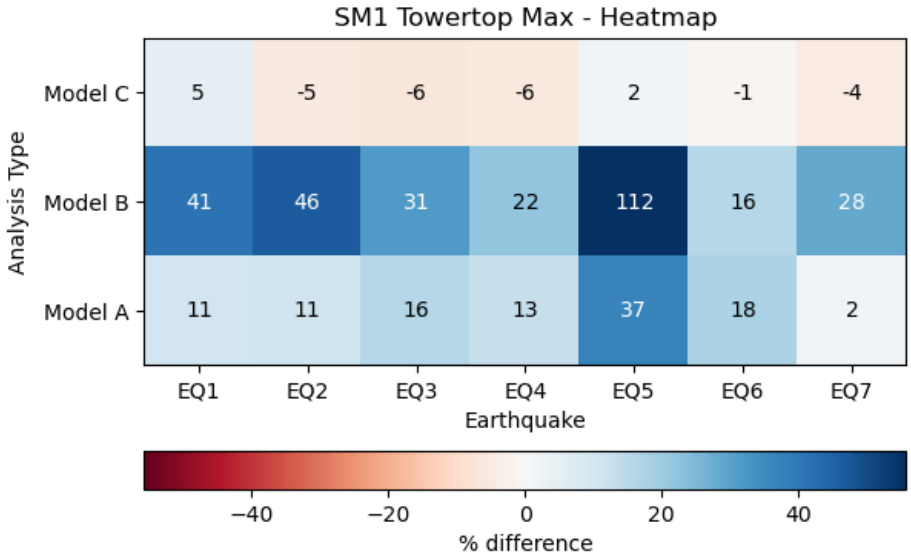

Figure 64: SM1 Tower top Max difference with respect to Model D

To find out more about the contribution of modes to the section moment, the Fourier transform of the variables can be used.

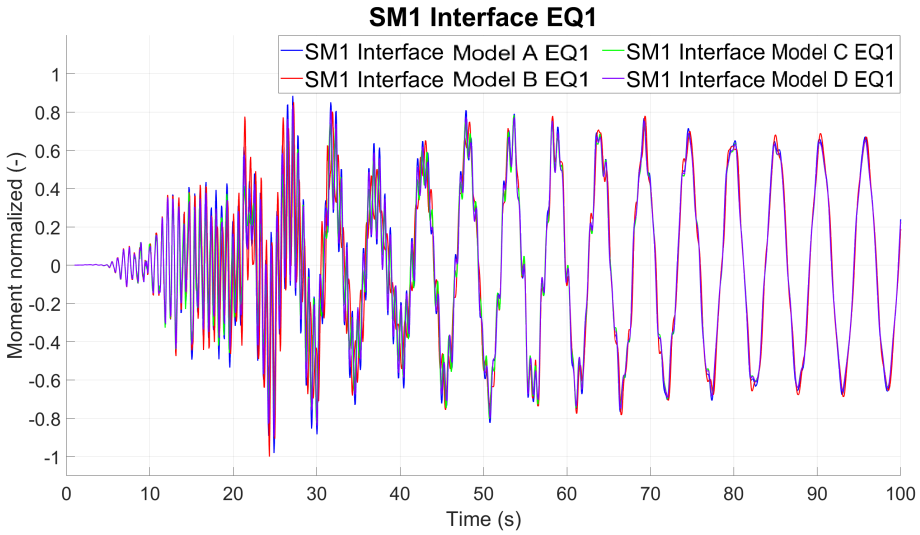

Figure 65: SM1 Interface EQ1

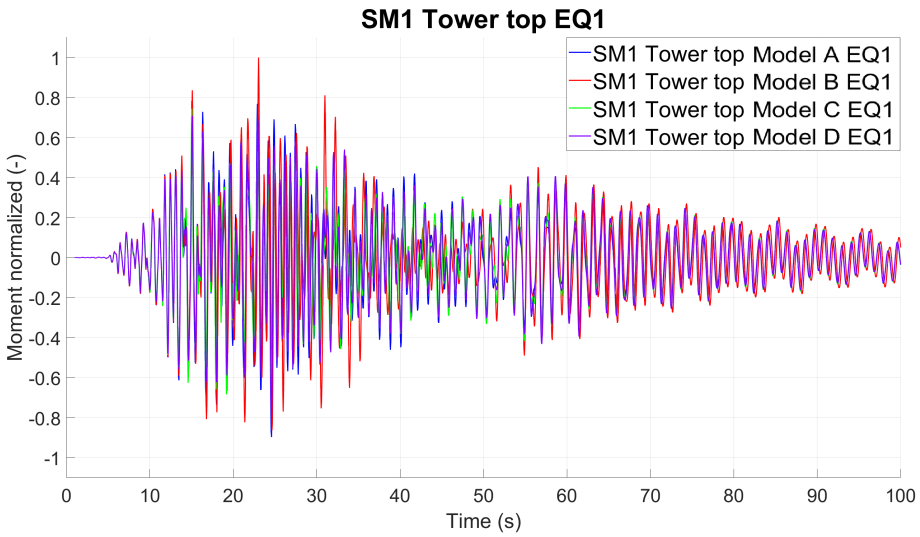

Figure 66: SM1 Tower top EQ1

In Figure 65 and 66 can be found the normalized time history of the output data of the section moment about the x axis of the Interface and Tower top for EQ1. For the Interface section moment, there is a lesser significant difference in peaks between the models. For the Tower top section moment, the difference in peaks is more pronounced and Model B has the greatest peaks.

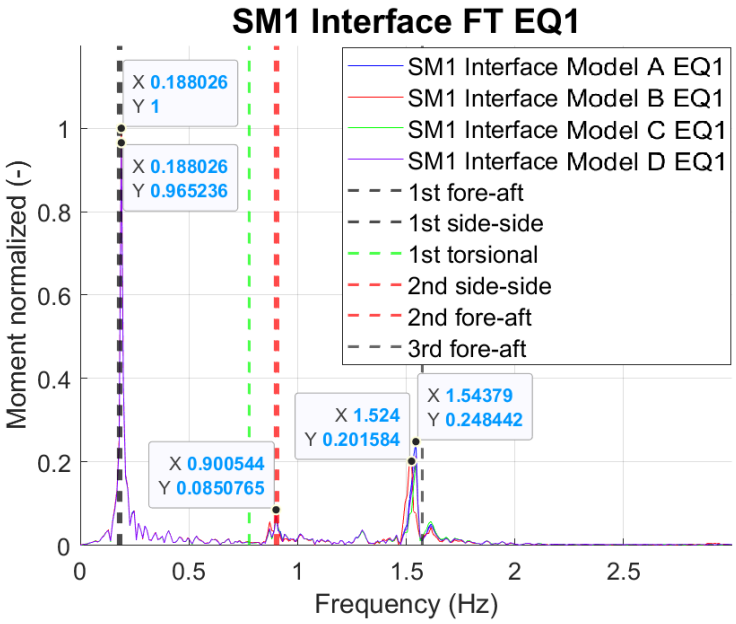

Figure 67: SM1 Interface EQ1 FT

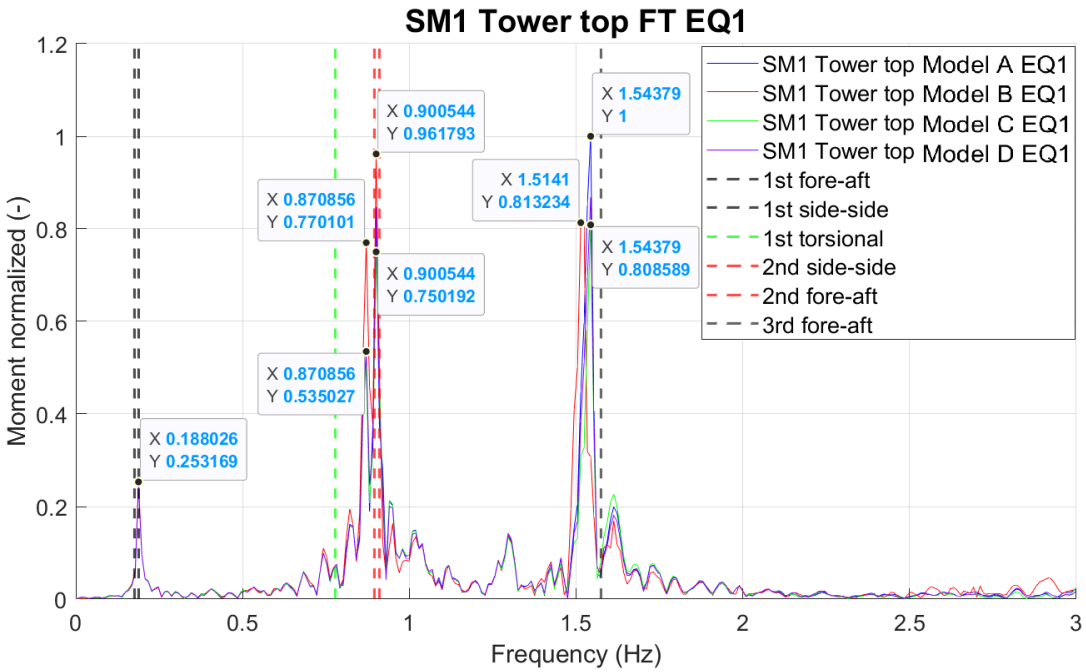

Figure 68: SM1 Tower top EQ1 FT

In Figure 67 and 68 can be found the Fourier transform of the output data of the section moment about the x axis of the Interface and Tower top for EQ1. The eigenfrequencies of the system are also added to the figures. There is only a slight difference between soil models. Model B has peaks at lower frequencies due to the softening of the soil model and dominates two peaks at 0.87Hz and 0.9Hz. Models C & D are bound to respond similarly to Model A through the falling back to the initial stiffness for unloading and reloading.

The displacements and section moments can be compared through their Fourier transforms. In Figures 51 and 53, the third tower bending moment is more significantly present than in Figures 67 and 68. The explanation for this is in the physics of the system and it shows that the section moments give valuable information. Bending moments are related to the curvature in the tower. The modes related to curvature at the Tower top are predominantly the second and third tower bending modes found in found in Figures 69b and 69c. The modes related to curvature at the Interface are the first and the third tower bending modes found in Figures 69a and 69c. This is corroborated by the Fourier transforms of the section moments. In Figure 67 the second tower bending mode is less significantly present and in Figure 68 the first tower bending mode is less significantly present.

The contribution of the 3rd tower bending mode is the cause for the greater differences in the maxima between the displacements (46, 47) and section moment (63, 64). The 3rd tower bending mode frequency is forced with more energy than the 1st tower bending mode and thus contributes more to the elongation of the soil springs. This activates more nonlinearity in the system.

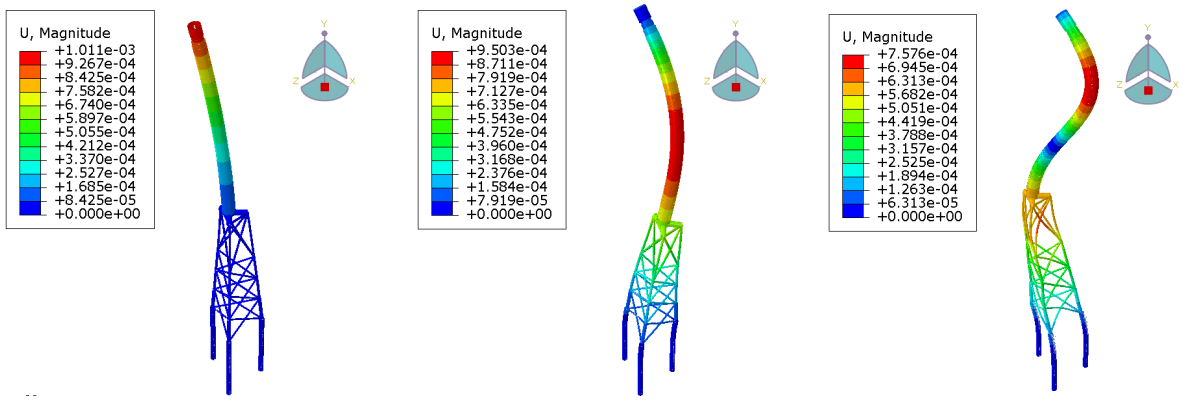

(a) Mode 1, 1st fore-aft (b) Mode 3, 2nd fore-aft (c) Mode 6, 3rd fore-aft

Figure 69: x direction tower bending modes

5.3 Resonance case

In Figures 46 and 64 can be seen that there is significant outlier for the Nonlinear analysis for earthquake signature 5, where the value for U1 is 93% higher and SM1 is 112% higher with respect to the plastic case. To learn how this occurs the dynamics are investigated using the Fourier transform. Since the interface is moving it makes sense to look at modes that have such characteristic in its mode shape. The 2nd fore-aft mode in Figure 40a which occurs at a frequency of 0.91Hz has a moving jacket-tower interface. The frequency response may shift during the Nonlinear elastic analysis due to the input p-y curve which decreases the stiffness of the soil with elongation of the springs. Since the stiffness becomes lower, the eigenfrequency should become lower. Figure 70 shows the time response of the jacket-tower interface node in x direction. The spectrum in Figure 71 shows the FT of the nonlinear output.

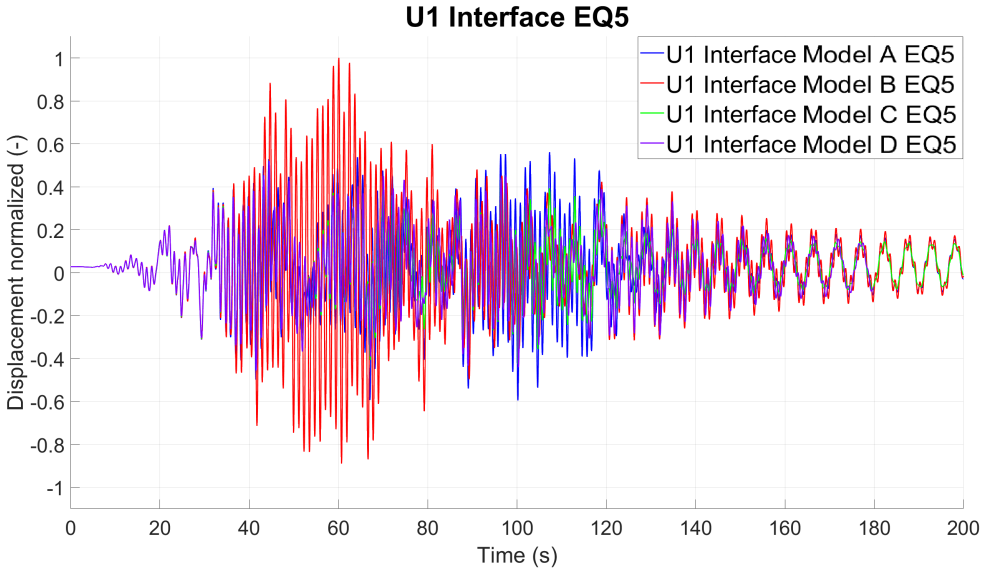

Figure 70: U1 Interface Nonlinear EQ5

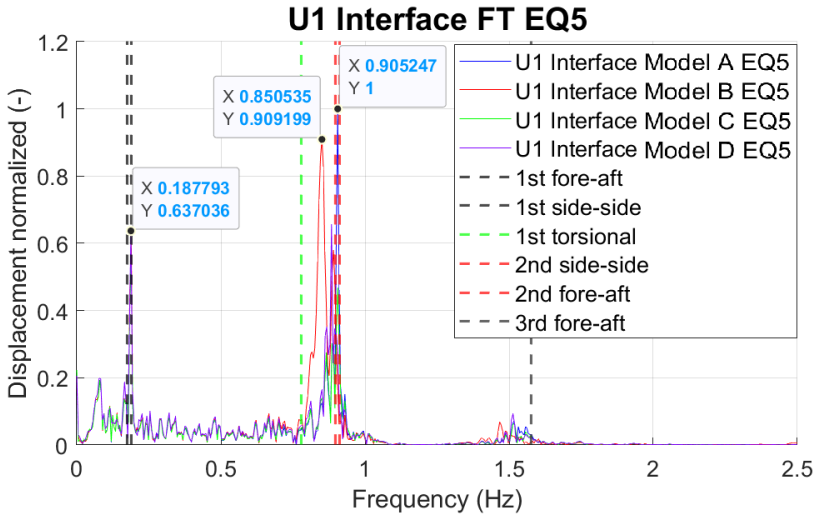

Figure 71: U1 Interface Nonlinear EQ5 FT

In Figure 71 a bifurcated peak can be found for Model B in the frequency range of 0.8-0.9Hz. The distribution of energy shows that there are many frequencies with a significant amplitude contributing to the total response. It can be noted that for nonlinear response there is a range of frequencies present in the response due to the change in stiffness, while for Model A they are more narrow peaks. It is now the question if the input motion also has peaks at these frequencies that may have caused this exceptional response.

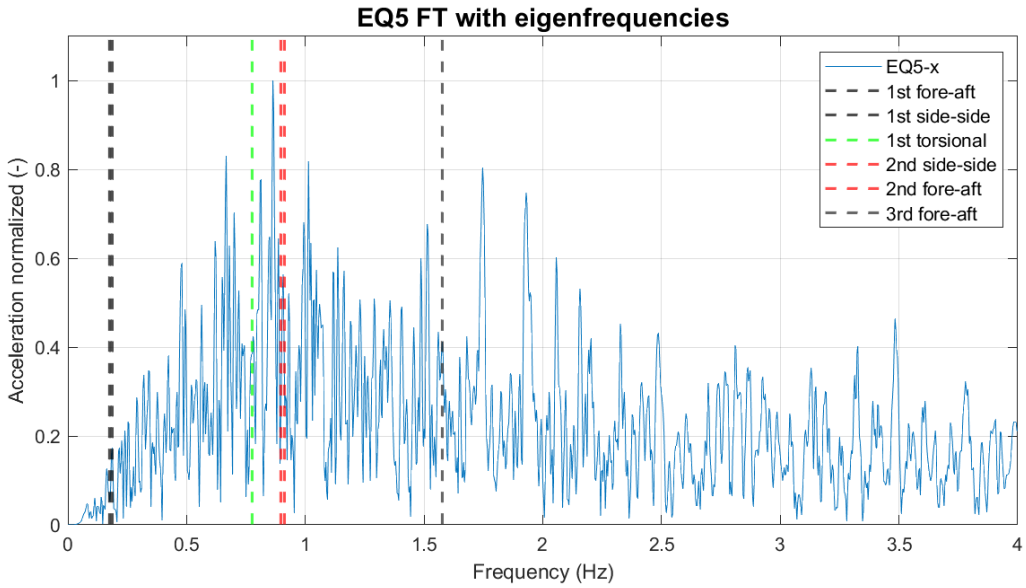

Figure 72: FT EQ5 x direction

In figure 72 can be found the frequency domain of the input motion of earthquake 5 together with the important eigenvalues of the system. Its highest peak is at 0.86Hz with more peaks around the maximum. This indicates that Model B has received much more energy than the other models.

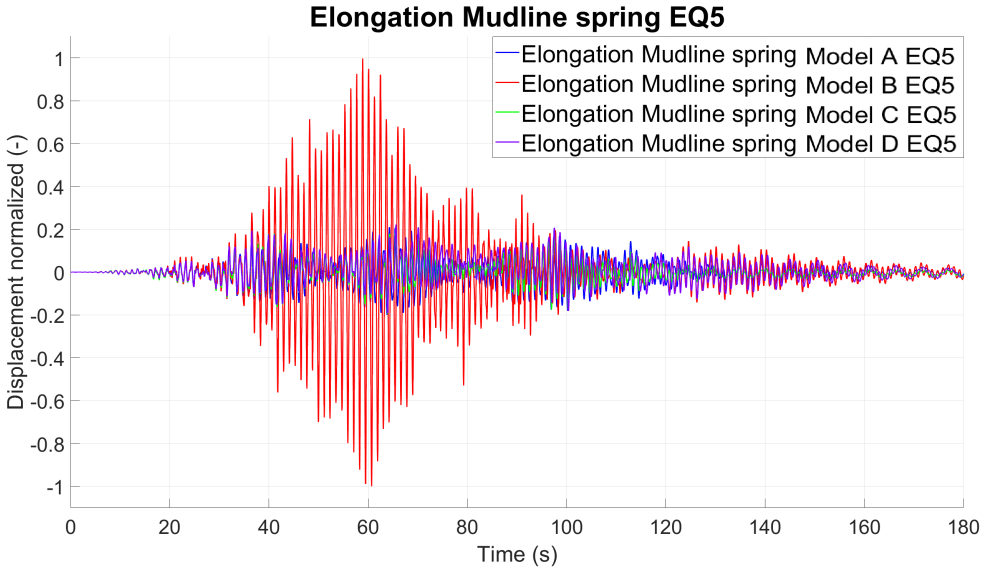

Figure 73: Mudline spring elongation EQ5

In Figure 73 can be found the Elongation of the mudline spring for all models. Out of all analyses, the spring elongation at mudline of the Nonlinear analysis of earthquake 5 is the highest at 0.3m. Other simulations have a maximum around 0.08m elongation. The oscillations of the Nonlinear response have a frequency of around 0.8-0.89Hz. Due to the circumstances of the loading signature, there is a resonance build up for the displacement and section moment output variables.

6 Conclusion

6.1 Sub-question 1: Current modelling approaches

Sub-question 1. What are the current approaches for modeling representative OWTs?

This sub-question seeks to create an overview of the existing methodologies and techniques that are used for the modeling of offshore wind turbines, highlighting the limitations and shortcomings of current practices. It is answered by the general overview of the computational modelling of OWTs in the Literature Review chapter 3. The design choices for the models used in this research are posed in the Methodology chapter 4.

The found methodologies for the current practice of modelling OWTs consist of a fully integrated method and a reduced method. In order to verify that the structure is safe, these two methods can be used to efficiently evaluate global failure modes and structural behaviour. More elaborate methods lend themselves for local failures, while simplifications may not significantly affect global dynamic behaviour. The Superelement method may be used to reduce the size of the matrix that has to be solved in case of dynamic analysis of the whole structure. This can be applied to any linear elastic part of a model as long as there is discretion with the amount of reduction. The main benefit from using reductions and simplifications is that the required computational power and time is less.

The computational model for this research holds many choices related to simplifications that influence how well the model approaches real physics. The obtained data is therefore an approximation. The simplifications are regarding the finite element type, geometry of the structure, connection of parts, soil model and the loading. In Figure 45 can be found the computational modelling representation of the three legged jacket-founded OWT.

For the evaluation of the design loads it is found that the jacket founded OWT can be modelled using beam elements since the structure is relatively slender. This counts for the the tower, jacket and piles. The blades could be modelled as beam elements as well, but in this case are reduced to a lumped mass which represents the RNA, together with additional rotational inertia. The mass is placed above the tower with a rigid link eccentric to the tower along the yaw axis. All beam elements are kinematically constrained, which couples the rotations and displacements at the connection of the beam elements.

The soil is another complex entity as far as physics goes. In order to capture the stiffness, the soil is represented by discretized springs along the pile. It is possible to do this for all three principal directions, but in this case only horizontal stiffness is modelled.

Representative horizontal acceleration signatures of seven different earthquake signals are used. The loading is uniform over the depth and synchronous for the three jacket legs. Only two of the seven signatures have a vertical component. The accelerations are applied in the two horizontal directions only. The vertical loading is mostly interesting for the jacket-tower interface punching, but is left out for this research due to the focus on soil nonlinearity. Therefore the only other boundary condition is the vertical displacement, which is set to zero at the pile bottom. An arbitrary loading and the boundary conditions are shown in Figures 44 and 43.

6.2 Sub-question 2: Modelling a representative OWT with nonlinear soil

Sub-question 2. How can a representative OWT be modeled with nonlinear soil?

Secondly sub-question 2 is answered by giving a general overview of ways to model soil in the Literature Review Chapter 3. In the Methodology Chapter 4 the different soil models are elaborated and the computational application is verified. Here, the focus will shift towards the computational modelling of an offshore wind turbine with the incorporation of nonlinear soil behavior. This aims to capture the dynamic and complex interactions of the OWT with surrounding soil.

The different soil models that are considered are Model A-D. The characteristics of these models are shown in Figures 3 and 15. The stiffness is based on a p-y curve that is generated based on the soil type and embedment length of the piles based on the API formulations for clay. The soil considered is clay and the parameters which dictate the p-y curve are shear modulus, effective unit weight, undrained shear strength, vertical restraint factor and the grain size distribution ε_{50}. The stiffness curve changes with depth.

The stiffness curve is nonlinear and is adopted exactly in the Nonlinear elastic springs of model B. The springs of Model A use the initial stiffness of the nonlinear curve. Model D follows the same p-y curve as that of Model B. Model C follows the p-y curve initially, but has a horizontal branch at a certain displacement. This is to investigate the limit case of a more elastoplastic model and find out about the effects of plasticity on the system behaviour. Model C & D have plastic behaviour, where they fall back to the initial stiffness for unloading. The Force-displacement relationship for Models A & B can be found from a simulation. This is shown in Figure 27. The verification between the input and the output of the springs is shown in Figure 28. Model D two realistic soil characteristics according to the literature review in chapter 3.4. It includes an accurate nonlinear stiffness relationship and also an energy dissipation mechanism under cyclic loading.

During a simulation the Force-displacement relationship for Models A & B is constant or as is prescribed. That of Models C & D is irregular when plasticity is reached, because the stiffness falls back to the initial stiffness after reaching a greater peak than has been reached before. This can be seen in Figure 30, where there is a dense concentration of points which are on a straight line around the end point due to a constant stiffness after reaching the maximum displacement.

6.3 Sub-question 3: Comparison of OWT response for linear and nonlinear soil models

Sub-question 3. What is the difference in response between a jacket-founded OWT model with a linear and nonlinear soil model?

Lastly sub-question 3 is answered by evaluating the output of the simulations from the different models subjected to the set of earthquake signatures in Chapter 5. The behavior of linear and nonlinear soil-structure interaction models are compared to understand the influence of increasing the complexity of the soil model. Model D has been taken as the reference model, but the realism of this model is nuanced. Plasticity and nonlinear stiffness are more realistic, but using isotropic hardening for plasticity yields a narrow frequency response range. This does not represent the softening response properly. Kinematic hardening is preferred instead to simulate the soil more realistically. Such hardening considers a nonlinear unloading path and also memory of the initial loading path at reloading.

Results from simulations include forces, displacements and dynamic characteristics of the system like modeshapes and response frequency content evaluation. The forces show the ULS loads in the structure and the influence of the soil models on the loading. The displacements at the jacket-tower interface and RNA are of interest. The behaviour of the system concerns the dynamics and the physics. These include the structural response, eigenfrequencies and modeshapes. These attributes indicate how a system may respond to environmental loads at specific frequencies and locations. These can be found for a linear system and give an indication for the nonlinear system depending on the significance of the nonlinearities. With the performed analyses the influence of the soil model to the response of the system can be investigated.

The soil models influence on the variables of interest can be evaluated using results from Chapter 5. Figures 46 and 47 show the comparison between the displacements at two locations in the structure across soil models and Figures 63 and 64 for section moments. There is a distinction to be made for general patterns and exceptions in the data. Exceptions arise from coincidental matching of parameters which may cause amplification in response. The frequency spectrum of the loads and softening of the stiffness due to nonlinearity are the cause. Results are influenced significantly by the frequency content of the earthquake loading signatures.

6.3.1 General patterns

The variables of interest are displacements and section moments of which two of each have been selected. The location of these variables in the structure is indicated in Figure 45. The two displacement locations are the jacket-tower interface and the RNA. The two section moments are at jacket-tower interface and at tower top. The direction is named U1, which coincides with the x direction. The section moment is named SM1, which is around the z axis (note that this is the vertical axis). The influence of the soil model to these variables is of interest to the research. To give a simple overview of the many combinations between the seven different input loads and four soil models, the maximum values are collected and shown in Figures 46 and 47. To investigate the behaviour of the structure and soil more in depth, data from EQ1 is collected. This loading gives a general idea of what results an arbitrary simulation would manifest.

There are some general pattern that give insight into the inner workings of the model. Firstly the models that include plasticity have lower maxima for both the displacements (Figures 46 & 47) and section moments (Figures 63 & 64) of the Interface and RNA or Tower top. The differences in section moments maxima are more significant than for the displacements. Displacements of the jacket-tower interface is governed by the first two bending modes as seen in Figure 51 and the RNA displacement only shows the first bending mode as seen in Figure 53. Section moments also have a contribution from the third bending mode as seen in Figures 67 and 68. This mode is present due to the curvature of the tower modeshapes, which is related to bending and moments. The contribution of the first mode is higher than the third mode, even though the loading is more significant for the frequency of the third mode than the first mode. The difference in maxima across soil models is related to the forces and elongation in the soil springs. Model C has the lowest maxima of all models. Nonlinearity in the soil springs influences the forces on the structure, which results in a change of amplitude and frequencies of the output. Plasticity dissipates energy out of the system, which influences the loading build up and frequencies of the output.

Secondly the Model B has significantly higher maxima across all loads compared to the other models. This is related to the frequency spectrum of the seven earthquake loads and the nonlinearity in the model. In Figure 61 can be found that the power of the earthquakes increases as the frequency goes down from 0.9Hz to 0.87Hz. There are eigenvalues of the linear system at 0.9Hz. This frequency contributes the most to the Interface response as can be seen

in Figure 49. The nonlinear spring input causes softening of the stiffness for increasing deformations. The softening lowers the models eigenfrequencies and covers a range of frequencies that are subjected to higher loads. Thus the Interface displacement of Model B is excited more than the other models.

In Figures 51 and 53 can be found the frequency spectrum of the output displacement variables. The Interface displacement is governed by the first three tower bending modes. The mode at 0.9Hz contributes most to the magnitude of the response. The RNA displacement is governed only by the first bending mode at 0.19Hz.

In Figures 56 and 57 can be found the frequency spectrum of the Mudline soil spring force and elongation. Both spectra are governed by the three tower bending modes. The mode at 0.9Hz contributes most to the magnitude of the response. The contribution of the mode at 0.19Hz to the Mudline spring elongation is shown in Figure 62. It is found to be insufficient to activate nonlinear effects by itself, but some nonlinearity may occur when there is overlap with peaks of other frequencies. This explains the relatively small differences in the RNA maxima across the soil models.

In Figures 67 and 68 can be found the frequency spectrum of the output section moment variables. The frequency content of section moments is related to the curvature of the mode shapes at the location of interest. The Interface section moment is governed by the first and third tower bending modes at 0.19Hz and 1.57Hz. The Tower top section moment is governed by the second and third tower bending modes at 0.9Hz and 1.57Hz. The curvature of the modeshapes can be inferred from Figures 69.

There are two effects of nonlinearity which can make it so that even with less energy put into the system, the resulting values are higher. Firstly, it has to be considered that the earthquake load signatures vary a lot in the frequency domain due to narrow peaks. Softening stiffness of nonlinear models can make the response move along the frequency spectrum. Secondly, nonlinearity introduces coupled modes that lead to higher peak values for the variables of interest along the height of the structure, because the stiffness locally at the soil is lower and thus is the modeshape displacement.

This generates a lot of uncertainty about how to model representative structures using simplified models, because there can be a varying response for different models that are supposed to represent the same system. These can be combated by taking a careful look at the eigenfrequencies of the system and the input loading. Resonance is possible for any of the models, but the influence of plasticity to Model C and D does make the linear Model A seem more conservative.

That being said, introducing plasticity to the model reduces the amount of resonance that can be built up. In case the loading frequency spectrum was more smooth, Model A and B would have a more similar response. There are much more realistic soil models to be considered that follow different unloading and reloading schemes. These models would introduce even more dissipation of energy. The nonlinear stiffness is realistic, but including plasticity significantly increases the realism of the model. When a fully integrated model is built, taking the soil from Model D is preferable over Model C. This is more realistic, because the initial P-y curve is followed.

6.3.2 Resonance case

Outliers of the displacements and section moments are found in Model B for the case of EQ5. Model B responds at a range of frequencies due to the nonlinear change in stiffness. The frequency spectrum of the loading has a peak for lower frequencies than the initial eigenfrequencies. The combination of a frequency load peak and softening stiffness are the cause for higher loads and make it stand out from the other soil models. These results are found to be circumstantial and are a reminder that such cases can occur under certain circumstances.

The data indicates that the softening behaviour of Model B combined with the highly varying loading peaks makes the different models difficult to compare. The sensitivity to the softening should be further investigated with different types of loading. The plastic models fall back to the initial stiffness upon unloading, so it responds less in a range of frequencies and more to the same frequency as Model A. More representative plastic soil models may give better insight to the softening effects combined with plasticity. The activation of multiple frequencies due to nonlinear stiffness should occur also for the models that include plasticity, but does not with this setup. Kinematic hardening instead of isotropic hardening can make the unloading also nonlinear, which makes the response more similar to that of the nonlinear elastic model.

7 Recommendations

The plastic Models C & D used in this research follow a linear stiffness for unloading due to isotropic hardening. This narrows down the frequency response range, which makes the response less comparable to nonlinear elastic Model B and more similar to linear Model A. In order to make the plastic models more realistic by having a response that occupies a wider frequency range, both the loading and unloading paths can be made nonlinear by making use of kinematic hardening. This change to the plastic soil model can contribute to a more accurate understanding of the influence of nonlinearities on structural dynamics.

Additionally, a thorough examination of the applied loading frequency spectrum is required. Dealing with loads with highly irregular frequency peaks can make the analysis more sensitive to the loading. Nonlinear and linear models may reach resonance on their own while they should represent the same system. This results in greater differences between analyses. That is why careful consideration of the loading spectrum smoothness can increase understanding of the influence of a nonlinear soil model and softening effects.

For a better understanding of the forces within the structure, it is advisable to investigate the velocity and acceleration data. These parameters can provide valuable insights into the dynamic behavior of the system. Also the loads within the structure at different locations can give a better indication of modal influence and governing design parameters.

The use of uniform motions may force the structure unrealistically. The explicit modelling of the foundation can be exploited by introducing non-uniform motions over the depth of the piles. This way the influence of the interaction between the soil and the pile flexibility can be included.

Furthermore, there is potential for an in-depth investigation into the RNA model, with a specific focus on incorporating dynamic interactions between the tower and the blades. This additional consideration can contribute to a more accurate representation of the real-world conditions and improve the overall fidelity of the computational model.

Lastly, it is worth exploring the impact of pre-loading on the structure during the production phase. In combination with the earthquake, higher loads may occur and introduce additional nonlinearity. Earlier activation of plasticity may affect maximum loads in the structure. Understanding and accounting for this normative situation can significantly enhance the estimation of design loads.

References

[1] L. VALIGRA, "Bangor daily news: Maine's offshore wind plan will take years to execute," 2023, Accessed: 22-11-2023. [Online]. Available: https://spectrumlocalnews.com/me/maine/news/2023/02/24/maine-s-offshore-wind-plan-will-take-years-to-execute.

[2] X. Wu, Y. Hu, Y. Li, *et al.*, "Foundations of offshore wind turbines: A review," *Renewable and Sustainable Energy Reviews*, vol. 104, pp. 379–393, 2019, ISSN: 1364-0321. DOI: https://doi.org/10.1016/j.rser.2019.01.012. [Online]. Available: https://www.sciencedirect.com/science/article/pii/S1364032119300127.

[3] WindEurope, "Offshore wind in europe key trends and statistics 2019," 2020. [Online]. Available: https://windeurope.org/wp-content/uploads/files/about-wind/statistics/WindEurope-Annual-Offshore-Statistics-2019.pdf.

[4] S. G. R. Energy, "Integrated load calculations for complex foundations," 2022.

[5] E. Tsudik, *Analysis of structures on elastic foundations*. J. Ross Publishing, 2012.

[6] R. Damiani, "JacketSE: An Offshore Wind Turbine Jacket Sizing Tool; Theory Manual and Sample Usage with Preliminary Validation," National Renewable Energy Lab.(NREL), Golden, CO (United States), Tech. Rep., 2016.

[7] P. Van der Valk and S. Voormeeren, "An overview of modeling approaches for complex offshore wind turbine support structures," *Proceedings of the ISMA2012-USD2012, Leuven, Belgium*, pp. 17–19, 2012.

[8] DNV, "Design of offshore wind turbine structures," 2014.

[9] DNV, "Seismic design of wind power plants," 2021.

[10] S. Funatake, "Development of clustering strategy to optimize the design of rna and support structure in offshore wind farm under seismic conditions," 2021.

[11] P. Van der Valk and S. Voormeeren, "An overview of modeling approaches for complex offshore wind turbine support structures," *Proceedings of the ISMA2012-USD2012, Leuven, Belgium*, pp. 17–19, 2012.

[12] N. Bazeos, G. Hatzigeorgiou, I. Hondros, H. Karamaneas, D. Karabalis, and D. Beskos, "Static, seismic and stability analyses of a prototype wind turbine steel tower," *Engineering structures*, vol. 24, no. 8, pp. 1015–1025, 2002.

[13] I. Lavassas, G. Nikolaidis, P. Zervas, E. Efthimiou, I. Doudoumis, and C. Baniotopoulos, "Analysis and design of the prototype of a steel 1-mw wind turbine tower," *Engineering structures*, vol. 25, no. 8, pp. 1097–1106, 2003.

[14] T. Bouman, "A winkler model for the seismic analysis of monopile foundations-an exploratory study on the modelling of soil-structure interaction during earthquakes," M.S. thesis, NTNU, 2018.

[15] T. Gentils, L. Wang, and A. Kolios, "Integrated structural optimisation of offshore wind turbine support structures based on finite element analysis and genetic algorithm," *Applied energy*, vol. 199, pp. 187–204, 2017.

[16] A. Ali, R. De Risi, A. Sextos, K. Goda, and Z. Chang, "Seismic vulnerability of offshore wind turbines to pulse and non-pulse records," *Earthquake Engineering & Structural Dynamics*, vol. 49, no. 1, pp. 24–50, 2020.

[17] A. Ali, R. De Risi, and A. Sextos, "Seismic assessment of wind turbines: How crucial is rotor-nacelle-assembly numerical modeling?" *Soil Dynamics and Earthquake Engineering*, vol. 141, p. 106 483, 2021.

[18] R. De Risi, S. Bhattacharya, and K. Goda, "Seismic performance assessment of monopile-supported offshore wind turbines using unscaled natural earthquake records," *Soil Dynamics and Earthquake Engineering*, vol. 109, pp. 154–172, 2018.

[19] I. Prowell, M. Veletzos, A. Elgamal, and J. Restrepo, "Experimental and numerical seismic response of a 65 kw wind turbine," *Journal of Earthquake Engineering*, vol. 13, no. 8, pp. 1172–1190, 2009.

[20] R. R. Damiani, H. Song, A. N. Robertson, and J. M. Jonkman, "Assessing the importance of nonlinearities in the development of a substructure model for the wind turbine cae tool fast," in *International Conference on Offshore ; Mechanics and Arctic Engineering*, American Society of Mechanical Engineers, vol. 55423, 2013, V008T09A093.

[21] Q. Zhao, S. Dong, and Q. Wang, "Seismic response of skewed integral abutment bridges under near-fault ground motions, including soil–structure interaction," *Applied Sciences*, vol. 11, no. 7, p. 3217, 2021.

[22] K. H. Chew, E. Ng, K. Tai, M. Muskulus, and D. Zwick, "Offshore wind turbine jacket substructure: A comparison study between four-legged and three-legged designs," *J. Ocean Wind Energy*, vol. 1, no. 2, pp. 74–81, 2014.

[23] K. Argyriadis and M. Klose, "Analysis of offshore wind turbines with jacket structures," in *ISOPE International; Ocean and Polar Engineering Conference*, ISOPE, 2007, ISOPE–I.

[24] J. Dubois, M. Muskulus, and P. Schaumann, "Advanced representation of tubular joints in jacket models for offshore wind turbine simulation," *Energy Procedia*, vol. 35, pp. 234–243, 2013.

[25] M. L. Larsen, V. Arora, M. Lützen, R. R. Pedersen, and E. Putnam, "Fatigue life estimation of the weld joint in k-node of the offshore jacket structure using stochastic finite element analysis," *Marine Structures*, vol. 78, p. 103 020, 2021.

[26] Y.-S. Lee, J. A. González, J. H. Lee, Y. I. Kim, K. Park, and S. Han, "Structural topology optimization of the transition piece for an offshore wind turbine with jacket foundation," *Renewable energy*, vol. 85, pp. 1214–1225, 2016.

[27] A. MAKRYKOSTA, "Soil-monopile interaction: From elastic to elastoplastic soil reaction modelling under quasi-static monotonic loading," 2023.

[28] A. Pecker, "Soil behaviour under cyclic loading," in *Advanced Earthquake Engineering Analysis*, Springer, 2007, pp. 1–13.

[29] F. Pisanò, "Cie5340-18 soil dynamics - cyclic/dynamic soil behaviour," 2020.

[30] A. Puzrin and J. Burland, "Kinematic hardening plasticity formulation of small strain behaviour of soils," *International Journal for Numerical and Analytical Methods in Geomechanics*, vol. 24, no. 9, pp. 753–781, 2000.

[31] N. Veritas, "Guidelines for design of wind turbines det norske veritas," *Wind Energy*, 2002.

[32] A. Malekjafarian, S. Jalilvand, P. Doherty, and D. Igoe, "Foundation damping for monopile supported offshore wind turbines: A review," *Marine Structures*, vol. 77, p. 102 937, 2021.

[33] M. Pham, "Offshore wind turbine foundations," Feb. 2022, MSc.PM; B.Eng.

[34] D. Simulia, "14.11.1 configuring a dynamic, implicit procedure," 2014. [Online]. Available: `http://130.149.89.49:2080/v6.13/books/usi/default.htm?startat=pt03ch14s11s01.html#usi-sim-configure-dynamicimplicit`.

[35] D. Simulia, "14.11.1 configuring a dynamic, implicit procedure," 2014. [Online]. Available: http://130.149.89.49:2080/v6.13/books/stm/default.htm?startat=ch02s02ath14.html#stm-anl-nonlinearsol.

[36] M. M. Mroczek, S. R. Arwade, and M. A. Lackner, "Design optimization of offshore wind jacket piles by assessing support structure orientation relative to metocean conditions," *Wind Energy Science Discussions*, vol. 2023, pp. 1–17, 2023.

[37] D. Simulia, "10.2 plasticity in ductile materials," 2014. [Online]. Available: http://130.149.89.49:2080/v6.14/books/gsa/default.htm?startat=ch10s02.html.

[38] D. Simulia, "32.1.1 spring," 2014. [Online]. Available: http://130.149.89.49:2080/v6.13/books/usb/default.htm?startat=pt06ch32s01alm37.html#usb-elm-espring.

[39] DNV/Risø, *Guidelines for Design of Wind Turbines*. 2002, ISBN: 87-550-2870-5.

[40] A. Puzrin, *Constitutive modelling in geomechanics: introduction*. Springer Science & Business Media, 2012.

[41] D. Simulia, "16.9.9 defining a gravity load," 2014. [Online]. Available: http://130.149.89.49:2080/v6.13/books/usi/default.htm?startat=pt03ch16s09hlb09.html.